Constitutive Modeling of Particulate Media-Structure Interfaces

Final Report on

AFOSR Parent Grant No: MIPR-93-0031
(Jointly funded by NSF and AFOSR)

and

AASERT Grant No: F49620-94-1-0325

UNIVERSITY OF
WISCONSIN
MADISON

Geotechnical Engineering Program
Department of Civil & Environmental Engineering
University of Wisconsin-Madison
Madison, Wisconsin 53706

REPORT DOCUMENTATION PAGE

Form Approved
OMB No. 0704-0188

1. AGENCY USE ONLY *(Leave blank)*	2. REPORT DATE	3. REPORT TYPE AND DATES COVERED
	14 August 2000	07/01/94 - 06/30/98

4. TITLE AND SUBTITLE
CONSTITUTIVE MODELING OF PARTICULAR MEDIA-STRUCTURE INTERFACE

5. FUNDING NUMBERS
F49620-94-1-0325

6. AUTHOR(S)
P.J. Boscher
T.B. Edil
M.E. Plesha

7. PERFORMING ORGANIZATION NAME(S) AND ADDRESS(ES)
BOARD OF REGENTS OF THE UNIVERSITY OF WISCONSIN
System 750 University Avenue
Madison, WI 53703

8. PERFORMING ORGANIZATION REPORT NUMBER

9. SPONSORING/MONITORING AGENCY NAME(S) AND ADDRESS(ES)
AIR FORCE OFFICE OF SCIENTIFIC RESEARCH
801 N. Randolph St.
Arlington VA 22203

10. SPONSORING/MONITORING AGENCY REPORT NUMBER
AFOSR

11. SUPPLEMENTARY NOTES

12a. DISTRIBUTION AVAILABILITY STATEMENT
UNLIMITED

12b. DISTRIBUTION CODE

13. ABSTRACT *(Maximum 200 words)*

The interaction of soil and structure is a problem that has challenged designers for centuries. Empirical relationships have been used to estimate the shear resistance between various materials and soil however this approach is limited to generic soils and interface materials, in addition these empirical relationships do not predict the deformation behavior at these interfaces. Proper characterization of interface behavior depends on the formulation of accurate constitutive relationships of interfaces.

To build accurate constitutive relationships, measurements are required from a variety of interfaces or an accurate model is required which can accurately predict interface behavior. We have employed several tools to understand the interaction relationships including: laboratory testing, discrete element modeling, and theoretical modeling. From these tools we have determined that interface zones are characterized by local slip occurring over a fairly narrow zone. The thickness of the zone is related to the size and shape of the particles, the roughness of the structural material, the normal stress, and rate of shear. Other related factors are the original relative density of the soil and the toughness of the soil particles. These later two factors also influence the grain lateral and rotational displacements and the amount of particle damage or degradation.

14. SUBJECT TERMS	15. NUMBER OF PAGES
SOIL-STRUCTURE INTERACTION, CONSTITUTIVE MODEL, DISCRETE ELEMENT MODEL	16. PRICE CODE

17. SECURITY CLASSIFICATION OF REPORT	18. SECURITY CLASSIFICATION OF THIS PAGE	19. SECURITY CLASSIFICATION OF ABSTRACT	20. LIMITATION OF ABSTRACT
		UU	

ABSTRACT

The interaction of soil and structure is a problem that has challenged designers for centuries. Empirical relationships have been used to estimate the shear resistance between various materials and soil however this approach is limited to generic soils and interface materials. In addition these empirical relationships do not predict the deformation behavior at these interfaces. Proper characterization of interface behavior depends on the formulation of accurate constitutive relationships of interfaces.

To build accurate constitutive relationships, measurements are required from a variety of interfaces or an accurate model is required which can accurately predict interface behavior. We have employed several tools to understand the interaction relationships including: laboratory testing, discrete element modeling, and theoretical modeling. From these tools we have determined that interface zones are characterized by local slip occurring over a fairly narrow zone. The thickness of the zone is related to the size and shape of the particles, the roughness of the structural material, the normal stress, and rate of shear. Other related factors are the original relative density of the soil and the toughness of the soil particles. These later two factors influence the grain lateral and rotational displacements and the amount of particle damage or degradation.

We have worked to calibrate the numerical modeling method with experimental techniques incorporating visual methods. These methods have enabled us to make direct measurement of the micro-structural behavior at the soil-structure interface. From this data, we have generalized the interface behavior and have built theoretical models to represent this behavior.

THIS
PAGE
IS
MISSING
IN
ORIGINAL
DOCUMENT

i

1. Section One, Introduction

1.1 Background and Motivation

The objectives of the project are to advance the understanding of interface zone behavior based on micro-structural studies and to develop a quantitative theory and a constitutive law that captures the physics of the interface zone behavior. The interface zone is defined as the area of soil from a structural surface to the point where the soil is no longer affected by shearing. Examples of structural surfaces are piles, sheet piles, ground anchors, soil nails, and ground penetrometers such as split spoons or cone penetrometers.

The project encompasses the study and modeling of a granular soil-to-solid surface interface by a series of laboratory experiments and computer simulations. The first step is to conduct micro-structural laboratory experiments to quantify the interface zone behavior. The second step is to supplement and generalize the observations in laboratory experiments by using numerical (discrete element) simulations of interface experiments. The third step in the project is to develop a constitutive interface model based on data collected in the first step. The final step in the project is the verification of the interface constitutive model by using numerical analysis and large scale physical model testing.

Section 2 presents the results from the micro-structural experiments. Section 3 describes the outcomes from the numerical modeling. Section 4 provides the constitutive interface model. Section 5 presents the summary and conclusions drawn from this project.

2. Section Two, Micro-Structural Laboratory Experiments

The goal for this section is to experimentally determine the micro-mechanical shear behavior of granular soil against a solid surface through image processing and direct shear testing and provide the physical properties of the interface shear zone as a function of various system variables.

2.1 Image Processing Literature Review

Imaging techniques have been extensively used in engineering research. Cross-correlation techniques have often been used to determine vector fields in seeded flow fields. Kumura and Takamori, (1986) developed a cross-correlation technique to obtain the instantaneous velocity vector distributions in a two-dimensional flow field. In their experiment, a seeded flow field around a vertical cylinder was imaged. Water containing white "seeds" distributed somewhat uniformly was imaged as it flowed around an obstruction (vertical cylinder) in the flow stream. These images were then processed and analyzed using the cross-correlation technique. For this application, the white "seeds" against a black background were easily detectable by the image processing techniques. Kumura and Takamori were able to obtain a velocity vector distribution over almost the entire flow field without interpolation. Further, changes in velocity vectors were clearly observable.

Donohoe *et al.*, (1991) developed a system to track individual sand particles in a cylinder after stress was applied by a mechanical press. The sand grains were filmed through a sapphire window as they moved and rotated after being subjected to the compressive strain or uniaxial load. To track particles using Donohoe's computer software, the user displays the first frame of the filmed sequence and identifies the centroid of various particles of interest. Using edge detection and boundary completion, the software locates the particle in subsequent frames and the particle's movement is recorded. Common drawbacks to this method are the relatively high degree of user interaction, the difficulty of identifying individual particles, and the ambiguity involved in edge detection

Macari, *et al.* (1997), completed further image analysis within geotechnical engineering applications. Macari *et al.* propose digital imaging and analysis as an alternative to the conventional procedure for determining the volume change of a soil specimen in a triaxial test. Volume change during a triaxial test is presently measured by the amount of pore fluid that flows into or out of a saturated specimen. Macari *et al.* propose to measure volume change by capturing images of the soil sample at various stages of shear. From these images, the outline of the soil specimen is determined by edge detection. Volume change is then calculated by mapping the two-dimensional image to a three-dimensional solid. According to Macari *et al.*, this method offers a viable alternative to conventional methods, especially for dry or partially saturated soil specimens where accurate pore fluid measurement is not possible.

The research that is most closely related to this project is that done at the University of Michigan under the direction of Dr. Roman Hryciw. The research done at Michigan parallels this research in that it is interested in particle motion of sands during shear, and the use of image processing to characterize this motion. Hryciw and Irsyam,(1993) used a video camera to characterize the behavior of shearing sand particles in the vicinity of rigid ribs attached to an interface. A Plexiglas walled direct shear box was constructed to allow visual

observation of grain movements during testing. Interfaces with ribs ranging in height from 0.6 mm to 2.5 mm were placed at the bottom of the shear box. Soil particles were manually tracked from a video taken of the area of sand between the ribs. In order to visually follow individual sand particles throughout shear testing, certain grains were colored with dye. Ottawa and Glazier Way sands were used as test sands. These sands represent extremes in roundness and angularity; Ottawa sand is considered rounded, while Glazier sand is more angular. Sands were sheared at relative densities of 30-40%, representing a loose state and 85-95% representing a dense state. Various tests were performed to determine the effects of rib spacing, rib geometry, grain size, and grain shape at normal stresses of 15.5 kPa or 50 kPa. Rib spacings of 33, 25.2, and 5.1 mm were also studied. For wide rib spacing (33 mm), a full passive zone was produced, while for narrower spacings (25.2 mm) only a partial passive zone could develop. At a rib spacing of 5.1 mm, all passive resistance disappears and the ribbed plate behaves as a rough surface (Hryciw and Irsyam, 1993). Two rib geometries were studied, square ribs and trapezoidal ribs. The geometry of the trapezoidal ribs caused sand grains to slip past the rib, resulting in no passive zone development (as was observed for the square rib). The absence of a passive zone indicates that trapezoidal ribs act as a roughened surface during shear (Hryciw and Irsyam, 1993). This is supported by the observation of a shear zone above the ribs. A smooth plate with no ribs, on the other hand, caused no shear zone development. For the smooth plate geometry, the grains slid along the interface surface. Grain shape effects were limited to the magnitude of the vertical displacement.

The majority of the work in Michigan has been done using the computer visualization system that was assembled at the University of New Mexico by Dr. Gregory Donohoe. Instrumental to this computer visualization system is the software called "Particle Tracker", or "Tracker". Tracker is considered a stand alone application that was developed using Khoros, an open software product which is used for information processing and data visualization (Hryciw, 1994).

Tracker follows selected sand grains in a sequence of images by segmenting individual particles in a grayscale image using edge detection. The edge detection method used by Tracker proved unreliable for segmenting individual particles in experiments performed on Ottawa sand. An additional problem associated with Tracker is the limited number of particles that are tracked. An image may contain over 200 soil particles, but Tracker is able to follow only 10 to 15 of them. One of the goals of this thesis is to obtain the displacement vector distribution for a much higher percentage of soil particles.

Raschke and Hryciw (1996) developed the second generation version of Tracker, called "Particle Tracer" or Tracer. Tracer is similar to Tracker, in that it attempts to follow individual soil particles from image to successive image, but Tracer uses a slightly different method. Rather than using edge-detection, like Tracker, Tracer uses a thresholding technique. This thresholding technique combined with altered lighting and image scene characteristics allow Tracer to identify and follow a number of selected sand grains throughout an image sequence.

Threshoiding is the process of selecting all the grayscale pixels that are within a given threshold value or range. For example, in order to delineate black objects in an image with a white background, the threshold range would be chosen to encompass the pixels of the black object, and not the background. By doing this, the software can identify the objects by searching for and selecting all pixels that defined the boundaries of the object. This operation is complicated significantly when objects (sand particles) do not have a definitive

boundary when compared to surrounding pixels. Figure 2-3 and Figure 2-4 in the next section illustrate this problem. The images are of Ottawa and Franklin Falls sand respectively. The image of Ottawa sand displays rather good contrast for a material that is semi-translucent, but the particle contrast is low compared to that of Franklin Falls sand. The lighting in Figure 2-3 has been manipulated to achieve this high a level of contrast. Still, the contrast of the Ottawa sand is not sufficient to allow successful thresholding. Since thresholding is usually not sufficient to delineate particles, Raschke and Hryciw (1996) aid Tracer by coloring certain sand grains with a fluorescent dye, and filming the experiment under ultra-violet light. Using this technique, the selected particles or tracer particles are much brighter than the surrounding particles and can successfully be segmented using a thresholding operation.

The goal of the research performed to complete this thesis parallels that done by Raschke and Hryciw, but deviates in its approach. Our research approach does not include the use of a thresholding technique like Tracer. Instead, a block-based matching algorithm is used to detect motion within the image scene. This matching algorithm is superior to Tracer in that it indirectly measures motion vectors over the entire image, rather than selected tracer particles. Additionally, our research does not rely on the alteration of the particle surface (florescent dying) to detect motion. The alteration of particle surfaces could affect the shearing properties of the soil by changing the friction angle or resistance to shear. Without this alteration, it can be assumed that the observed soil behavior is closer to *in situ* as possible.

2.2 Methods and Materials

2.2.1 Introduction

Direct shear tests were performed on two sands against structural surfaces of various roughness, at two different constant normal stresses. The seven structural surfaces in total, included a smooth steel plate and a range of 3M©'s industrial grade belt sanding papers. The direct shear tests were conducted as a constant stress test at two different normal stresses, 35 and 138 kPa. The shear force was applied using a standard direct shear machine with a modified shear box designed for interface testing. Throughout the test, a Sony© CCD digital video camera module captured images of the interface. Load cells and LVDTs measured the loading magnitudes and displacements respectively of the sand specimen.

2.2.2 Ottawa Sand and Granusil® Sand

2.2.2.1 Introduction

The two sands chosen for the interface testing were Ottawa sand and Granusil® sand. The sands were chosen based on their extreme values of angularity in addition to both being quartz-based sands. Ottawa sand is a very round sand (Edil *et al*, 1975) and Granusil® is an angular sand. Figure 2-1 shows a digital image of both Ottawa and Granusil® sand. The coarsest sand used was P20 – R30 and is on the left of the figure. P60 – R100 was the finest sand and is shown on the right portion of the figure. P20 – R30 means the sand grains pass through the #20 sieve and are retained on the #30 sieve.

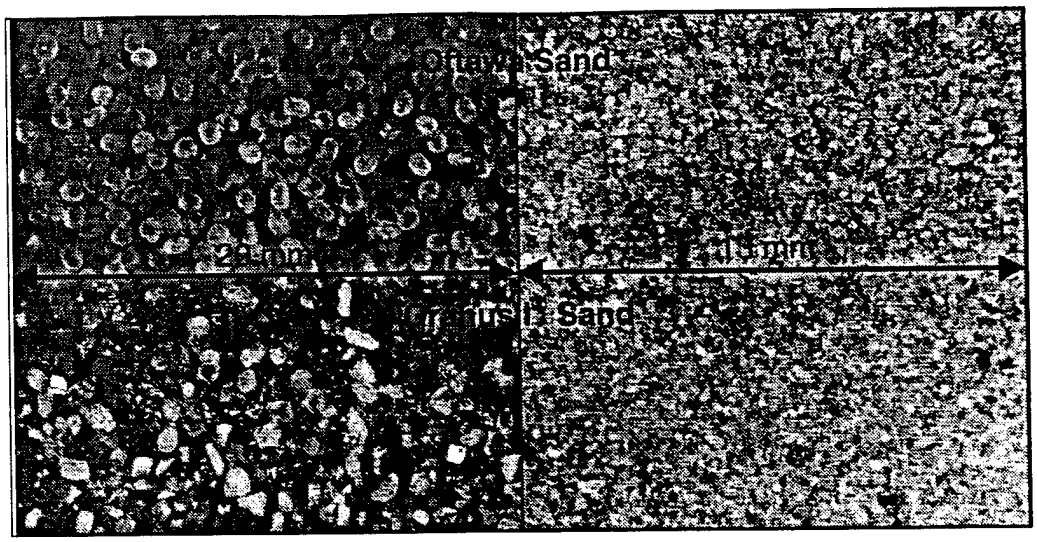

Figure 2-1 Digital Images of Ottawa and Granusil® Sand

Prior to interface testing the sands were sieved to obtain uniform grain sizes. The specific grain sizes were chosen corresponding to a range of the roughness of the selected surfaces. For selecting the roughness of the various papers, the papers were viewed through an optical microscope with a micrometer on the stage. Using focal distances, the amplitude of the particles on the papers was approximated. The range of surface roughness was chosen to fit within the range of $\frac{1}{2}D < \lambda < 4D$ where λ is the mean amplitude of the particles on the surface, and D is the mean diameter of the sand particles. Table 2-1 shows the selection criteria for the first stage of testing.

Table 2-1 Initial Surface Selection Criteria based on sand sizes

Sand Sieve Sizes	Average Sand Grain Diameter (mm)	Amplitude of particles on surface by optical microscope (mm)	Paper # (defined by 3M© manufacturing)
P20 – R30	0.725	0.70	P24
P30 – R40	0.5125	0.36	P50
P40 – R60	0.3375	0.23	P80
P60 – R100	0.20	0.10	P120

Following interface testing on the four surfaces, data was interpreted and the testing program was extended to include 3 more surfaces to better understand the transition from smooth to a rough surface. The surfaces added included a smooth steel plate and P180 and P240 grit papers. More thorough descriptions of these surfaces are included in Section 2.2.4.4.

After the sand sizes were determined, and prior to conducting the shear tests, index properties of the test sands were conducted to characterize the sand. The properties included minimum and maximum densities, specific gravity, grain shape, and strength parameters.

2.2.2.2 Maximum, Minimum and Relative Densities

2.2.2.2.1 Introduction

Density is a quantitative term to express the mass of the sample in a given unit volume. Relative density is the term used to quantitatively describe the state a sample is in with respect to the maximum and minimum densities of a material. As the relative density increases the amount of air in the pores of a sample decreases. The relationship between maximum, minimum and relative density is as follows (Holtz and Kovacs, 1981). Table 2-2 is a qualitative description of relative density. All tests conducted for this research were at 90% relative density.

$$D_r = \frac{1/\rho_{d\min} - 1/\rho_d}{1/\rho_{d\min} - 1/\rho_{d\max}} \times 100(\%) \qquad 3.1$$

This relation can also be expressed in terms of maximum and minimum void ratios.

$$D_r = \frac{e_{\max} - e}{e_{\max} - e_{\min}} \times 100(\%) \qquad 3.2$$

Table 2-2 Qualitative Description of Relative Density (Das, 1994)

Dr (%)	Description of Soil Deposit
0-15	Very Loose
15-50	Loose
50-70	Medium
70-85	Dense
85-100	Very Dense

The maximum density is the closest packing arrangement the particles can achieve, and the minimum density is the loosest packing arrangement. This corresponds to the minimum and maximum void ratios respectively. For example, if a layer of equal-sized spheres is placed on top of another layer of spheres such that each sphere is touching one sphere from the adjacent layer, the density is at a minimum, and the void ratio is at a maximum. Furthermore, if a layer of equal-sized spheres is place on top of another layer such that each sphere is touching four spheres from the adjacent layer, the density is at a maximum, and the void ratio is at a minimum. For granular soil deposits, the relative densities depend on several natural factors such as: depositional environment, stress history and shear history. Variations in the grain sizes of a soil mass always increases the density of the packing arrangement by decreasing the void ratio of the material (Holtz and Kovacs, 1981).

Testing to obtain the maximum and minimum densities of a soil is usually conducted using ASTM standards D 4253 and D 4254 for relative density. The data obtained for this research used two alternate methods, the Rain-Through-Air method for maximum density

and the Elephant Trunk method for minimum density. These methods are believed repeatable and accurate, and are often used at the University of Wisconsin – Madison. For this research both methods were compared against the standard methods. The results of this are included in Section 2.2.2.2.5. The vibrating table was not used for all determinations of maximum density, due to a lack of volume of the test sands. The bulk Ottawa sand was tested on the vibrating table described in ASTM D 4253 and compared to the results of the Rain-Through-Air method. ASTM D 4253 Test Method C for minimum density was also compared to the Elephant Trunk method with the bulk grade of Ottawa sand. No significant difference in the results was found for either of these two methods. Descriptions of the tests follow.

2.2.2.2.2 Elephant Trunk Method for Minimum Density Determination

The Elephant Trunk method for minimum density is conducted by filling a 2.5-cm diameter PVC tube with sand placed inside of a 1000 ml graduated cylinder. The outside diameter of the PVC tube should be just slightly smaller than the inside diameter of the graduated cylinder. The PVC tube is then slowly and carefully pulled out letting the sand flow out of the tube into the graduated cylinder. This gentle or low-energy stacking method allows grains to stop rolling in a meta-stable packed condition. Once the graduated cylinder is filled around 500 ml, the filling is stopped, the volume is read, and the mass of the sand is determined. Dividing the mass by the volume yields the minimum density.

2.2.2.2.3 Rain-Through-Air Method for Maximum Density Determination

The Rain-Through-Air method for calculating maximum density is simple, fast and accurate for uniform sands. The test uses a 2.5-cm diameter PVC tube with a 1 mm screen near one end and a distance of approximately 30 cm from the other end. The tube is fixed to a stand at a height just above the height of the graduated cylinder. Small amounts of sand are then slowly poured into the top of the PVC tube. As the sand pluviates or "rains-through-air", the fall of the sand is uniformly distributed throughout the inside of the tube by the fixed screen. The sand grains fall into a close-packed arrangement. The weight and volume are once again recorded and the maximum density is then determined. Figure 2-2 shows diagrams of the Elephant Trunk and Rain-Through-Air method for minimum and maximum density.

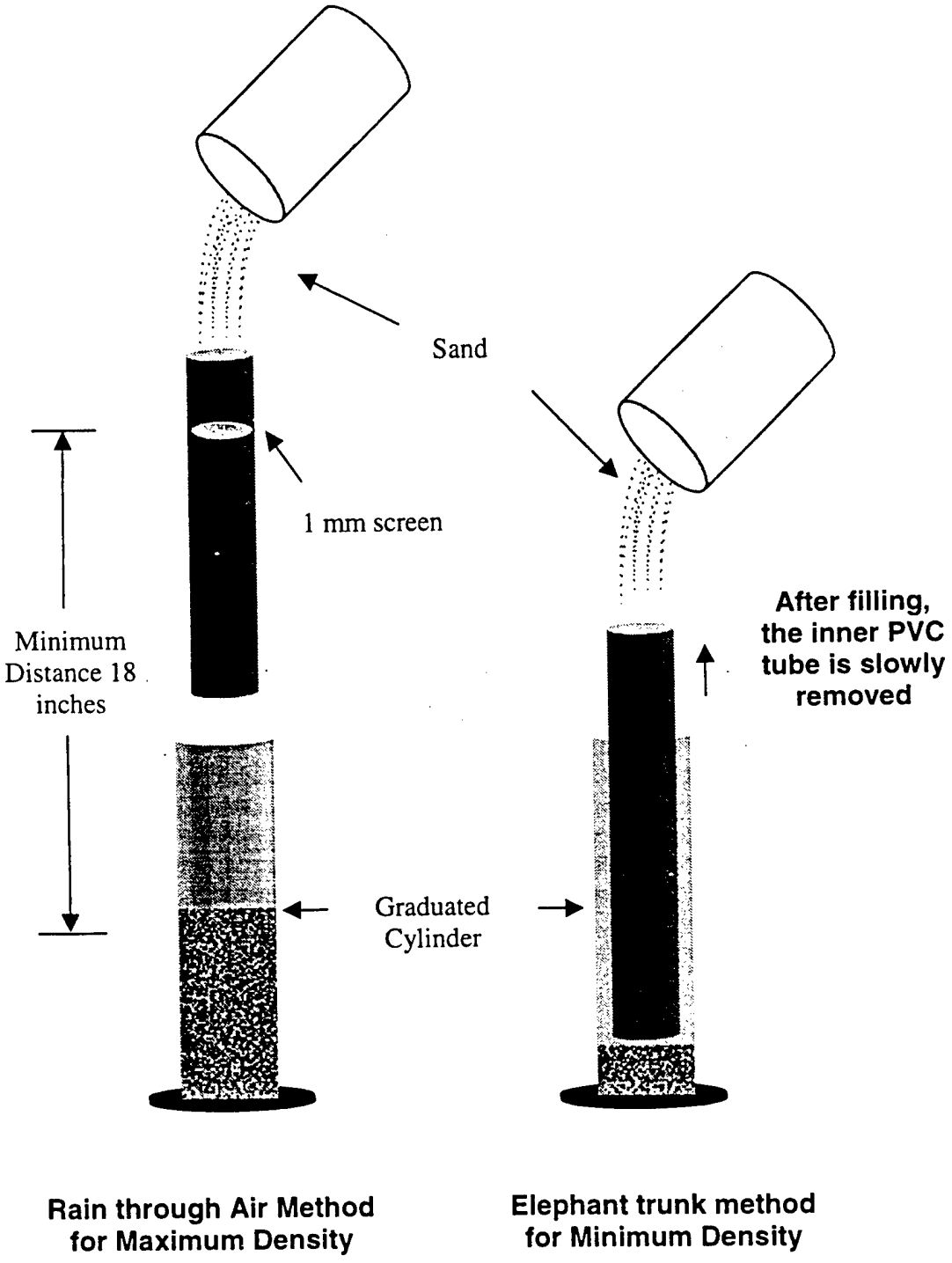

Figure 2-2 Techniques for minimum and maximum density determination

2.2.2.2.4 Error Sources

Both of these simple, inexpensive methods do however have their drawbacks. The Rain-Through-Air method may read too low of maximum densities if the sand is poured into the PVC tube too fast. A rate at which sand should be poured into the PVC tube is not explicitly stated anywhere. The Rain-Through-Air method also falls short of the standard vibrating table method in that the standard test will reach a maximum density after a certain amount of time on the table. The Rain-Through-Air method has no way to confirm that the density calculated is the maximum density. The Rain-Through-Air method also is thought to have difficulty measuring extremely angular sands. Angular sand types tend to get caught on the dispersion screen when poured through the PVC tube. Problems of this nature were not encountered during the density determinations on the angular sands used for this research. The Elephant Trunk method will also yield erroneous data if the PVC tube is pulled out too fast. The PVC tube must be pulled out very slow to impart the least amount of energy into the sand grains as they roll into position.

2.2.2.2.5 Results

Using the Rain-Through-Air method and the Elephant Trunk method previously described, minimum and maximum densities were determined for each grain size of sand. Three to five tests were conducted on each sand type and the extreme values were recorded. The extreme values determined are presented and used for relative density determination. The reason is for this type of testing, the extreme values are important rather than average values. These values will have the most variance on relative density and in turn shear strength and behavior. Table 2-3 gives the extreme values determined for each soil type.

ASTM D 4253 and ASTM D 4253 Test Method C were conducted on the bulk grade of Ottawa sand. The standard maximum density test yielded $\gamma_{d\,max} = 1.77$ g / cm^3. For the standard minimum density test a $\gamma_{d\,min} = 1.51$ g / cm^3 was found. These are consistent with the Rain-Through-Air method and the Elephant Trunk method as reported below.

Table 2-3 Maximum and Minimum Densities and Void Ratios

Soil Type	Particle Size	$\gamma_{d\,max}$ (g/cm3)	e_{min}	$\gamma_{d\,min}$ (g/cm3)	e_{max}
Ottawa	P20 – R30	1.79	0.48	1.52	0.74
Ottawa	P30 – R40	1.77	0.50	1.50	0.77
Ottawa	P40 – R60	1.74	0.52	1.49	0.78
Ottawa	P60 – R100	1.74	0.52	1.49	0.78
Ottawa	Bulk Sand	1.77	0.50	1.52	0.74
Granusil®	P20 – R30	1.58	0.68	1.31	1.03
Granusil®	P30 – R40	1.56	0.70	1.28	1.07
Granusil®	P40 – R60	1.53	0.73	1.26	1.11
Granusil®	P60 – R100	1.38	0.92	1.19	1.23

With these values of maximum and minimum density one can calculated the mass of sand to place in the shear box, of known volume, to obtained the desired relative density for the direct shear test. Sample preparation will be discussed in a later section.

2.2.2.3 Grain Shape

Relative density and shear strength in sands depends on several factors including particle shape. Particle shape is a parameter that can be estimated for correlation to depositional environment, relative friction angle and shear strength. Particle shape is divided into two major categories, roundness and sphericity. Roundness and sphericity were investigated for this research in order to understand its affect on shear strength and behavior against surfaces of various roughness.

Roundness is the ratio of the radii of the particle's irregularities to the average curvature. Sphericity is described as the ratio of the diameter of an equivalent area, to the diameter of a circumscribing circle. The visual procedure for determining these two parameters is the same. It is essentially done by looking at one grain at a time and comparing it to a chart with typical schematic representations of grains. The most effective means of doing this is to use a microscope to look at one grain at a time. Roundness is usually determined by visually comparing particles to the standard particles in a Krumbein chart (Krumbein, 1941). Sphericity is most commonly measured using a Rittenhouse chart, which was developed to visually estimate sphericity (Rittenhouse, 1943). The Rittenhouse chart is a two-dimensional method of measuring the three-dimensional parameter sphericity that has been shown to provide consistent results (Edil *et al* 1975).

Sand grain shape was determined by visual analysis for this research. The Krumbein chart was used for this research for grain roundness comparison and the Rittenhouse chart was used for sphericity.

2.2.2.3.1 Significance

Given the particle shape numbers for a soil, the following general conclusions can be made. With a decrease in roundness, there is a corresponding decrease in void ratio at a given state. With a decrease in uniformity, there is a decrease in both the minimum and maximum void ratio. With an increase in the roundness, there is an increase in the difference in the maximum and minimum void ratios. These relations are important because the shear strength and behavior of sand is greatly affected by relative density. A small change in the uniformity can cause a significant difference in dry density calculations (Holtz and Kovacs, 1981).

2.2.2.3.2 Error Sources

The errors in this method are mostly due to operator variation. Each test has a high degree of subjectivity, meaning each operator may chose different values from the charts. There is also a tendency for the observer to pick grains that would be exciting or challenging to quantify. These grains may not be representative. To help remove error, a glass plate was used and a random batch sample was spread around on the plate and systematically reviewed. To be conservative, the estimates should be assumed to be on the high side because the shear strength and density values are lower on the high side of roundness.

2.2.2.3.3 Results

The results of the particle evaluation are an average of over 75 particles by a visual inspection technique. Edil *et al* (1975) based the results of their grain shape analysis on 25 particles. Table 2-4 shows the average roundness and sphericity determined for both sand types.

Table 2-4 Roundness and Sphericity for Ottawa and Granusil® Sand

Soil Type	Particle Size	Roundness	Sphericity
Ottawa	P20 – R30	0.78	0.79
Ottawa	P30 – R40	0.76	0.77
Ottawa	P40 – R60	0.70	0.77
Ottawa	P60 – R100	0.66	0.75
Granusil®	P20 – R30	0.12	0.65
Granusil®	P30 – R40	0.13	0.63
Granusil®	P40 – R60	0.14	0.67
Granusil®	P60 – R100	0.14	0.69

2.2.2.4 Specific Gravity and Mineralogy

Ottawa sand is primarily pure quartz with rounded to sub-rounded particles. Granusil® is a highly angular and also consists mainly of quartz. Specific gravity tests were performed on the two sands used for the testing program. ASTM D 854 Standard Test Method for Specific Gravity of Soils was followed. Two tests were conducted on each of the two sands. For both sands the specific gravity was found to be 2.65. These values are consistent with 2.66 for Ottawa sand reported by Edil *et al* (1975) and 2.65 for Granusil® sand reported by Granusil® Mineral Filters, Emmett, Idaho.

2.2.2.5 Strength Parameters

The general aspects of shear testing are discussed in Section 2.2.4.1. In order determine the strength parameters of the sand independent of the image acquisition modifications done on the direct shear box, standard direct shear test were run in accordance with ASTM D 3080. Sand-on-sand direct shear tests were run on each of the four grades of both Ottawa and Granusil® sand. The bulk grade of Ottawa sand was also tested, as this was the material used for the degradation tests described in the following section. The grain size distribution curve for the bulk grade of Ottawa sand is shown below in Figure 2-3.

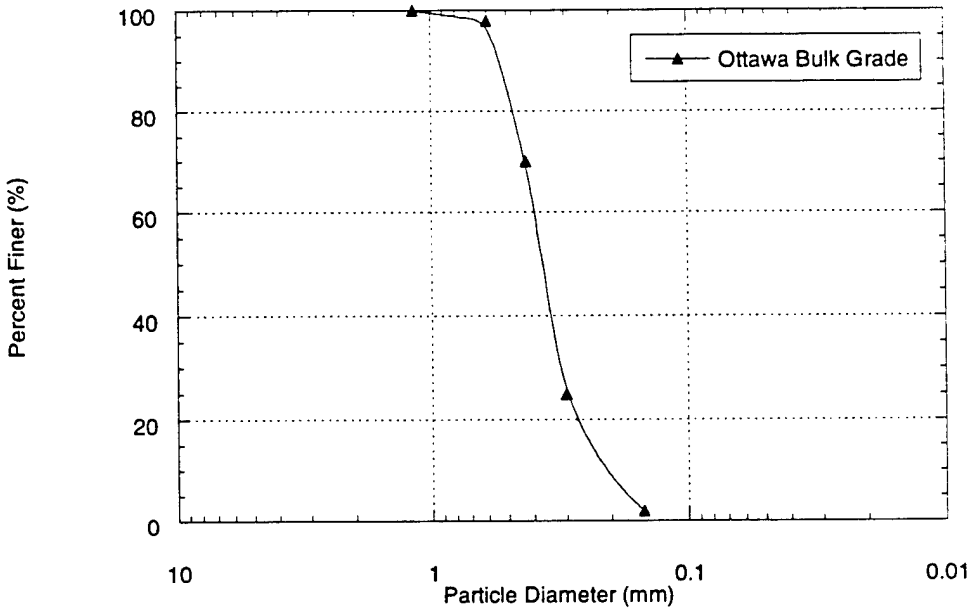

Figure 2-3 Grain Size Distribution Curve for Bulk Grade Ottawa Sand

All of the tests were run at 90% relative density and a strain rate of 0.3 mm / min. Normal stresses for the sand-on-sand tests were also 35 and 138 kPa. Table 2-5 is a compilation of the results of the sand-on-sand shear tests. The peak and residual friction angles for each soil type and grade are shown below.

Table 2-5 Peak and Residual Friction Angles for Ottawa and Granusil® Sand

Sand Type	Peak ϕ	Residual ϕ at 5-mm
Ottawa		
Bulk Grade	37.2°	32.0°
P20 – R30	35.5°	30.9°
P30 – R40	35.3°	31.6°
P40 – R60	37.3°	32.5°
P60 - R100	39.0°	31.9°
Granusil®		
P20 – R30	39.8°	37.9°
P30 – R40	38.1°	36.0°
P40 – R60	38.0°	36.6°
P60 - R100	34.7°	34.6°

2.2.3 Degradation Test

2.2.3.1 Introduction and Procedure

Following the selection of the initial four surfaces of various roughness, tests were run to determine whether the roughness of the structural surface material would remain constant from test to test. It is important that the material on the surface does not degrade from test to test in order to compare the strength and image data that was gathered.

A series of 10 constant stress direct shear tests were run using Ottawa sand at a high normal stress (138 kPa). The general aspects of shear testing are discussed in Section 2.2.4.1. The sand used for the degradation test was not sieved to any particular size for this test; rather the entire graded sample of sand was used. After each test, the sample of sand was discarded and a new sample of the sand was used for the next test. The sample of Ottawa sand was run at 90% relative density and the surface used for the tests was the 3M© 50-grit paper. Between tests the paper was visually inspected for degradation and then cleaned off with a high-pressure air hose. This method of cleaning the surface was used to insure not altering the surface with any abrasive techniques.

2.2.3.2 Results

Visual inspection of the surface, following each test, showed no signs of degradation. No grains of the surface appeared to be broken off and the mounting media of the grains on the surface appeared to be intact and unaltered.

Test results showed no trend in the following measurements; peak horizontal stress, residual stress at 5-mm displacement and horizontal displacement at peak horizontal stress. Figure 2-4 shows the stress-displacement curves for the degradation tests.

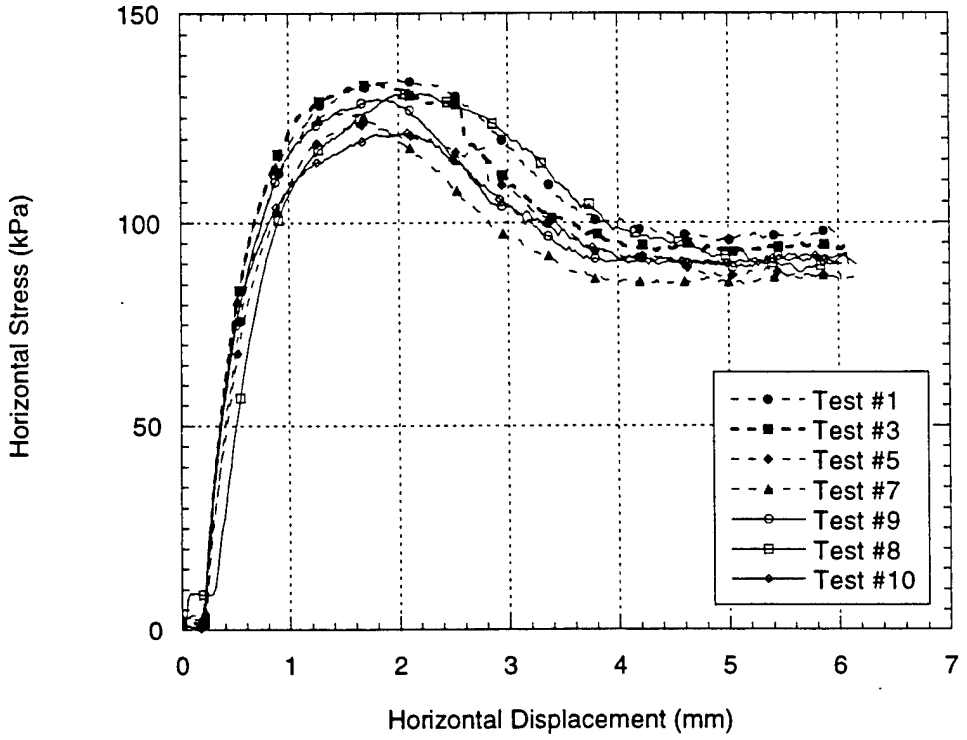

Figure 2-4 Stress-Displacement Plots of Degradation Test

2.2.4 Shear Testing

2.2.4.1 General Aspects

The direct shear test is the oldest and simplest form of a shear test (Das, 1994). This is a simple test used for determining the shear strength of a soil. The standard test procedures are explained in detail in ASTM D 3080. The main test equipment consists of a metal shear box in which the soil specimen is placed. The dimensions of the shear box used for this research are 63.5-mm x 63.5-mm x 25.4-mm. The box is split horizontally into halves. The tests conducted for this research were strain-controlled tests, done at a constant strain rate of 0.3 mm / min. The advantage of the strain-controlled test is that in the case of dense sand, peak shear resistance as well as residual shear resistance can be obtained and plotted.

The primary disadvantage of the direct shear test is that it produces a predetermined failure plane. Rather than allowing the soil mass to fail along the weakest plane, the plane is determined by the testing apparatus. Triaxial cells eliminate this disadvantage when testing for shear strength.

For this research, modifications were done on the shear machine as well as the shear box in order to test the sands against the structural surfaces. The primary modification to the shear box was the addition of the structural surface in the lower portion of the shear box. The sand placed in the upper portion of the shear box was then sheared against the tested surface. The addition of a window in the shear box was also added in order to capture images of the interface behavior. Figure 2-5 is a digital image of the shear testing setup.

2.2.4.2 Modified Direct Shear Box

Modifications were done on the direct shear box for the purpose of interface testing. On one side of the shear box a cutout was made for the installation of a viewing window. A glass window was fixed to the upper portion of the box and extends downward permitting a clear view of the structural surface interface in the lower portion of the box. Groves were cut in the lower box to allow 6-mm of displacement of the lower box with respect to the upper box. Within this grove the glass window slides. During shear testing, this grove in the lower box is filled with a porous foam sponge to prevent sand loss into the grove, while allowing the window to slide with respect to the lower box. The extending of the window over the surfaces allows the capturing of accurate strength data while acquiring images. This modification was done following the work by Ligler (1997), in which threaded rods were used to hold the upper box down during shear. The rods used in his research prevented the upper box from moving upward from rotation about the pulling point or from the dilation of the material. The viewing window on his box stopped at the intersection of the upper and lower halves. It was important that these halves remained in contact with each other in order to capture images of the interface. The strength recorded during his research was not representative of the interface material due to the increased friction between the upper and lower portion of the box. Figure 2-6 is a digital image of the modified direct shear box.

2.2.4.3 Specimen Preparation

Quality specimen preparation was important in order to obtain repeatable results from the direct shear tests. A pluviation apparatus used by Ligler (1997) was used for sand placement into the modified shear box. The apparatus was designed to aid in the placement of sand into the shear box so relative densities could be obtained in a repeatable, consistent manner. The apparatus works by raining the soil through a series of metal screens and letting the sand free fall to achieve the desired packing. 1-mm and 3-mm metal screens were placed in the device and the fall heights were varied until a consistent 90% relative density was obtained for each sand type and size. Figure 2-7 is a diagram of the device used for sample preparation.

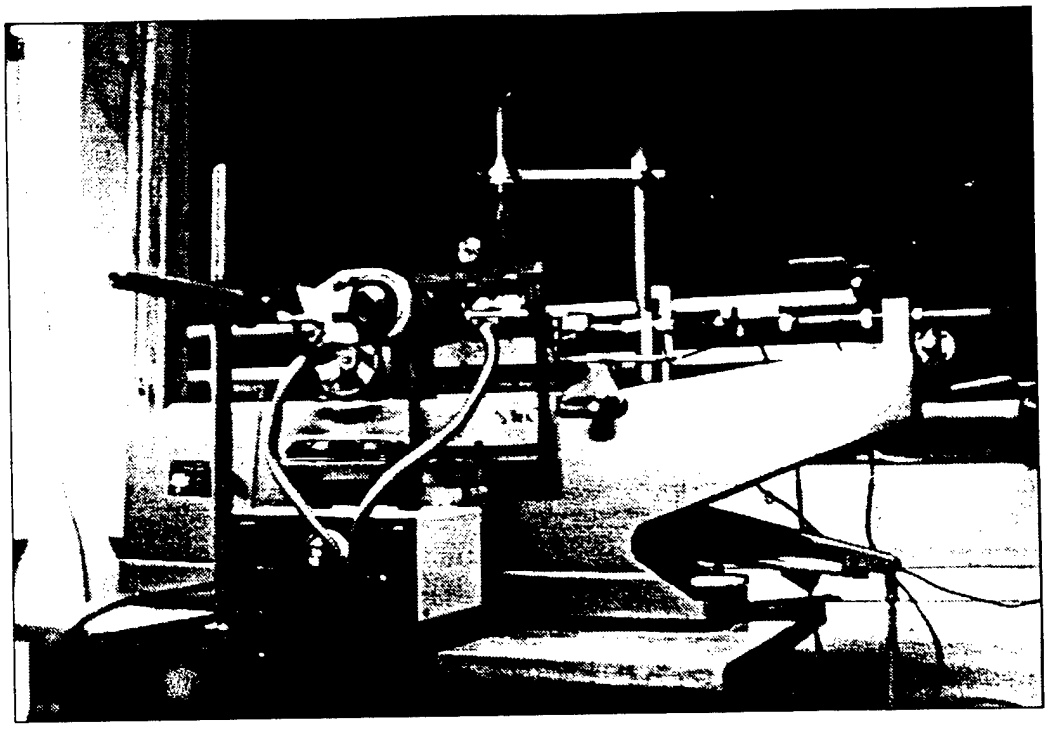

Figure 2-5 Digital Image of Interface Testing Setup

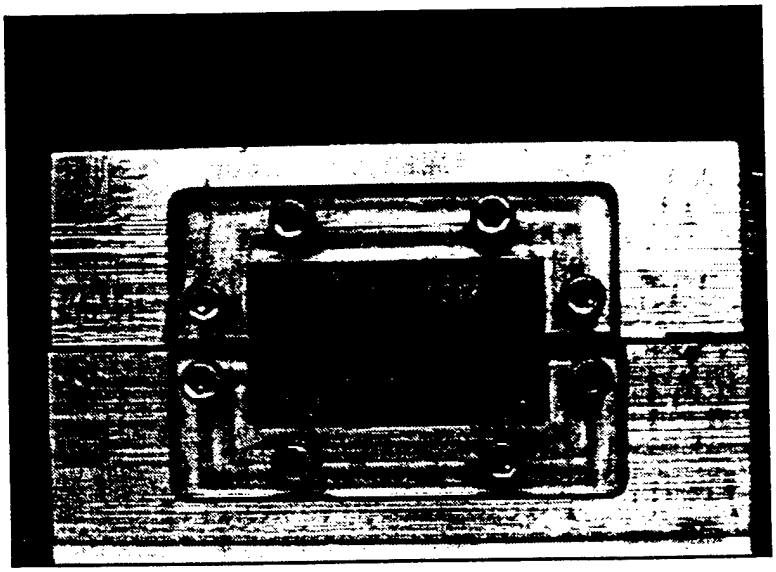

Figure 2-6 Digital Image of Modified Direct Shear Box

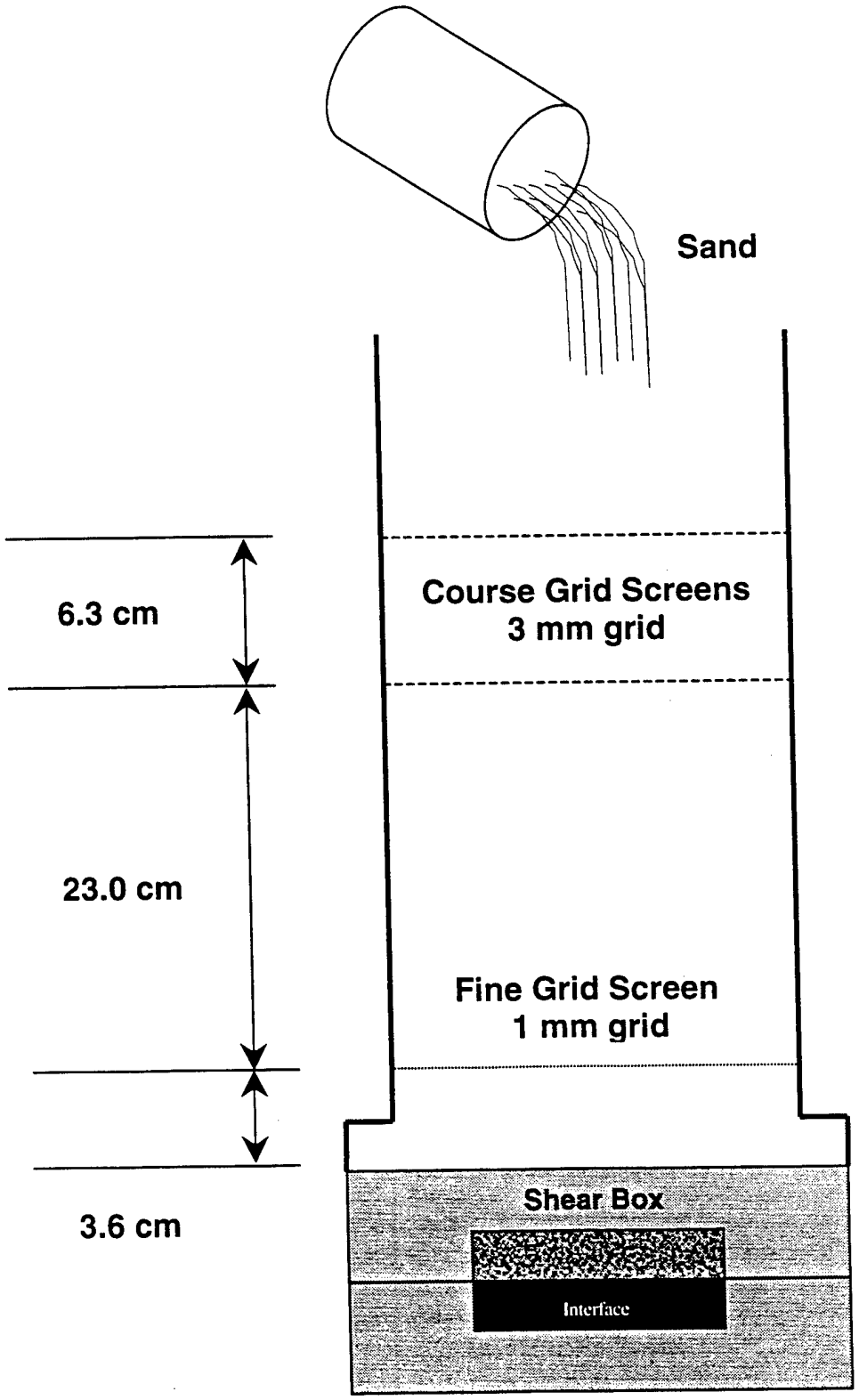

Figure 2-7 Diagram of Rain-Through Air Sample Preparation Device

2.2.4.4 Surface Characteristics

Ottawa and Granusil® sand were sheared against 6 different grades of industrial grade textured paper and one smooth steel surface. The structural surfaces were placed in the bottom half of the shear box and the sand was placed over them. The top of the surface was flush with the shear plane between the upper and lower box. The P120, P80 and P50 grit paper used for the testing were 3M© Regalite™ industrial grade mineral belt sanding paper. The P240, P180 and the P24 grit papers were also a 3M© industrial grade mineral belt. The mineral within the media of these papers was an aluminum silicate particle. Figure 2-8 shows a plan view of the four coarsest papers used during the interface testing.

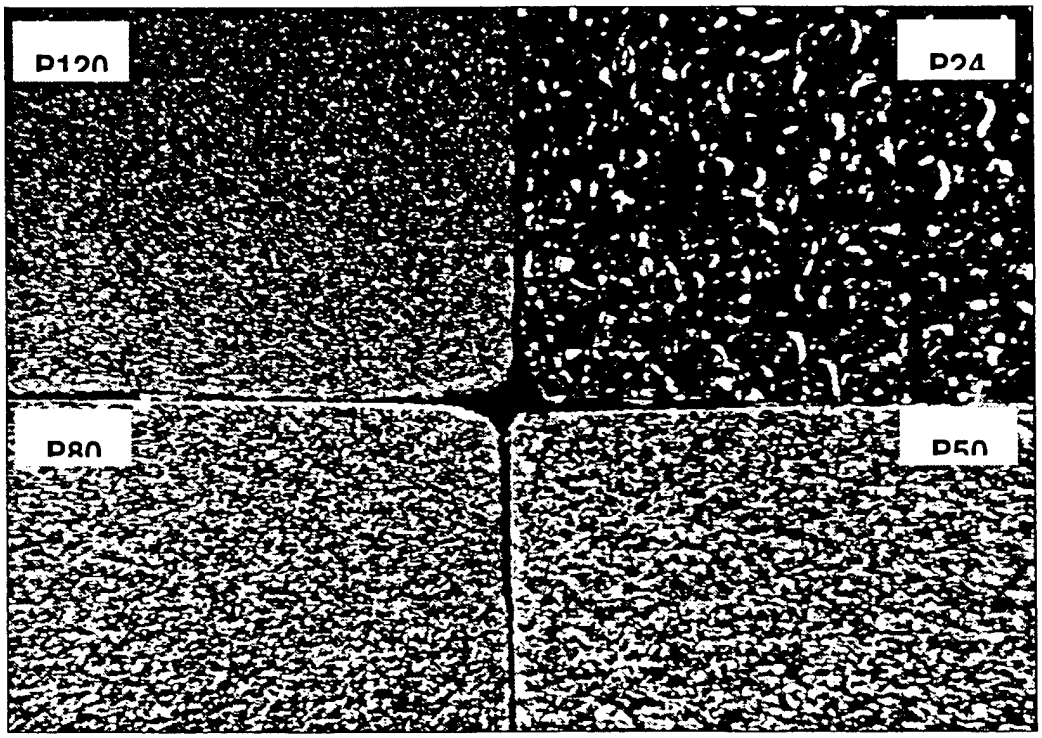

Figure 2-8 Digital Image of the four roughest surfaces

2.2.4.4.1 Surface preparation

The surfaces were prepared by cutting the paper to the desired dimensions and adhering them to a hard PVC surface by means of contact cement. The edges of the surface were ground to a smooth surface with a fine belt sander to ensure a representative interface along the edge to be captured by the imaging equipment.

2.2.4.4.2 Surface Geometry

Cross-sections of the surfaces were prepared by mounting the samples in a pressurized Bakelite mount. This allowed the samples to be viewed on edge with an optical microscope

while ensuring that a representative cross-section was maintained. After mounting the samples in the hard mounting media, the samples could be ground flat maintaining the cross-section. Images of the cross-sections were then taken and subsequently analyzed. The analysis consisted of using the image analysis software Optimus 6.1. When the image was calibrated to the magnification of the microscope used to take the image, the point morphometry feature of the software allowed for obtaining a scaled cross section of the surface.

To quantify the roughness of the smooth plate, a talisurf was used. A talisurf is a device used to obtain the profile of a surface by dragging a stylus over it. The mean amplitude for the steel plate was determined as ½ the R_y surface roughness parameter. The R_y parameter is defined as the maximum peak to trough spacing on the surface. Table 2-6 shows the mean amplitude of the surfaces determined from the point morphometry and the talisurf procedures.

Table 2-6 Surface Characteristics

Surface #	Description	Mean amplitude of surface (mm)
1	Smooth Steel Plate	0.0059
2	P240 paper	0.037
3	P180 paper	0.059
4	P120 paper	0.101
5	P80 paper	0.123
6	P50 paper	0.229
7	P24 paper	0.472

Figure 2-9 to Figure 2-14 show scaled digital images of the surface cross-section for surface #2 - #7. The material in the upper portion of the image is the Bakelite mounting material. Moving down from this media one can see the cross-section of the surface. The darker portion in the lower part of the image is the PVC sheet that the papers were adhered to.

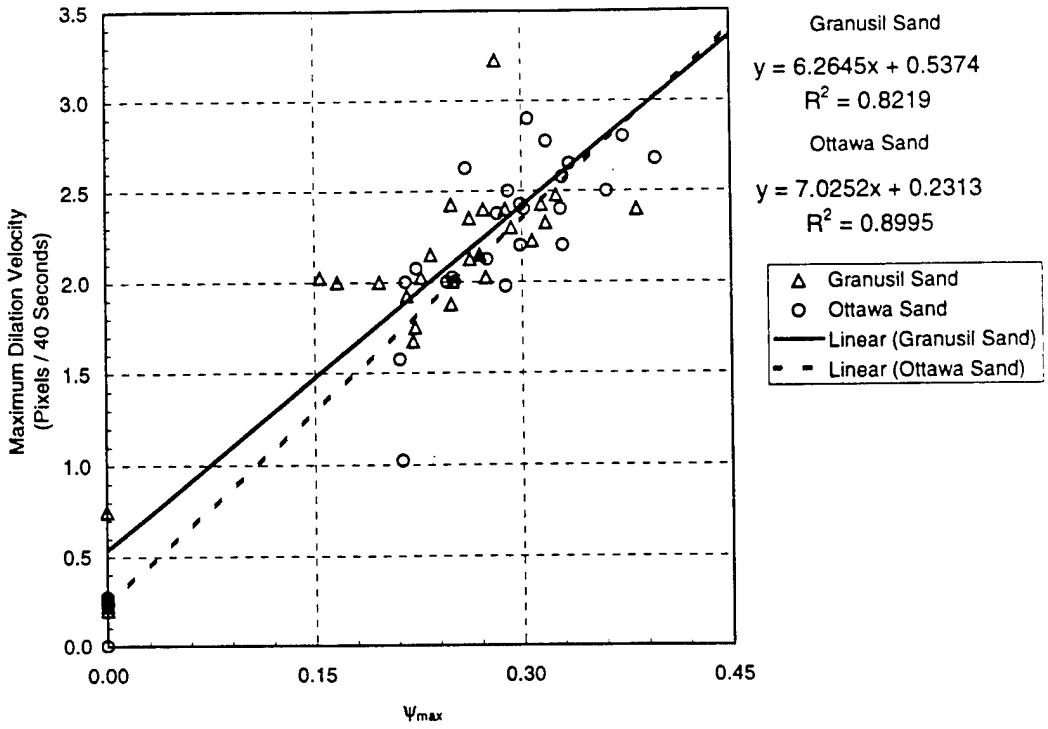

Figure 2-48 Maximum Dilation Velocity vs. Max Slope of Dilation Curve (ψ_{max})

2.3.5 Summary, Conclusions and Recommendations

The interface shear zone of a granular soil against a steel structural surface was successfully imaged and subsequently analyzed. The analysis of these images was accomplished using software that employed a block-based matching algorithm that yielded velocity vector data from image to image. Additionally, the strength data for this interface was also captured by conventional means and subsequently analyzed. Based on the analysis of this data, the following conclusions are drawn:

Image Data

1. For simulated shallow and deep soil elements (constant stress and constant volume tests) the only factor that is significant to the interface shear zone behavior is the roughness of the structural surface. This effect is most pronounced when the surface being used is very smooth. The addition of small ridges on this surface magnifies the measured response parameter.
2. A redesigned shear box and shear machine would aid in the acquisition of quality images. It is recommended that the present shear box window geometry be altered in order to fully view the moving structural surface.

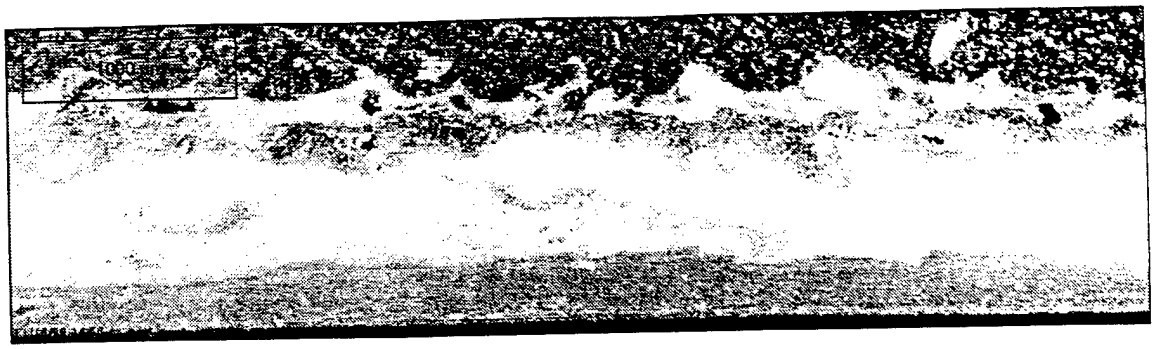

Figure 2-12 Cross-section of Surface P80

Figure 2-13 Cross-section of Surface P50

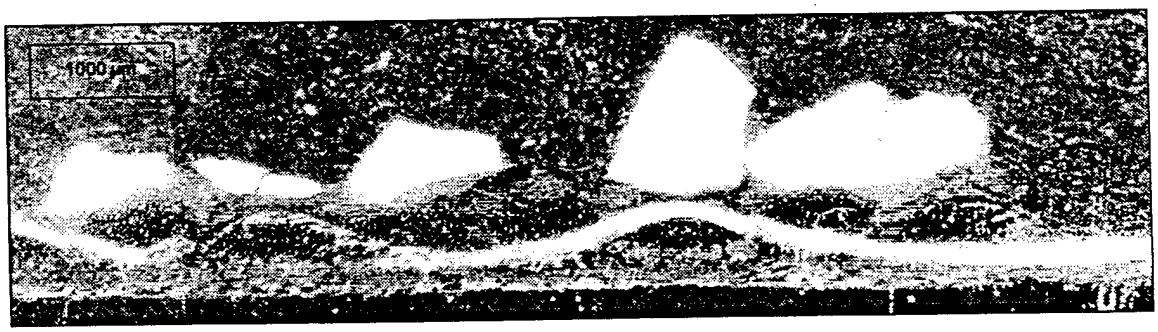

Figure 2-14 Cross-section of Surface P24

Figure 2-15 is a plot of the data obtained from the surface characterization using the point morphometry feature of Optimus 6.1. The vertical scale is different for the two plots to better display the period of the aspirates of the surfaces.

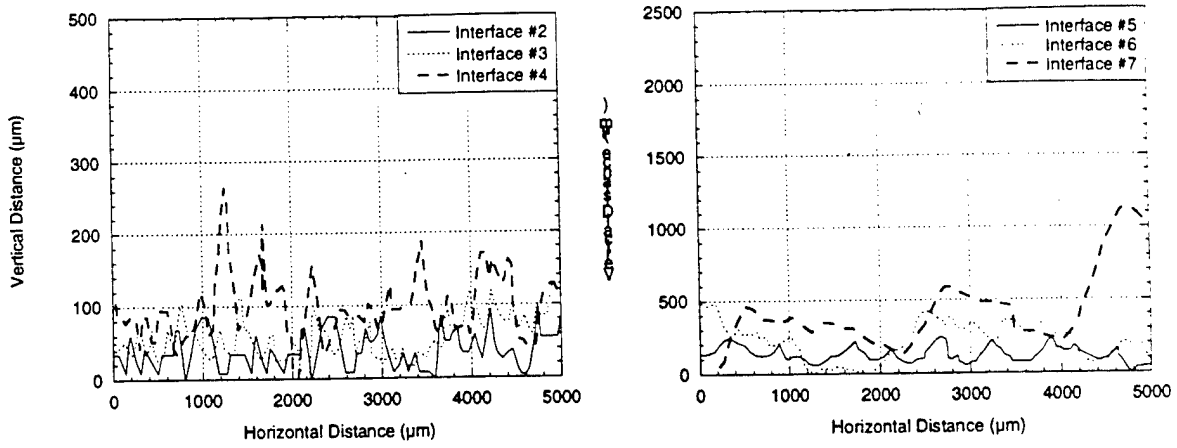

Figure 2-15 Plot of typical Cross-sections of surfaces

2.2.4.5 Data Acquisition and Instrumentation

National Instruments from Austin, Texas was the producer of much of the hardware and software used for data and image acquisition. Data acquisition was accomplished using the Lab-PC+ DAQ board and standard NI-DAQ driver software. The Image data was recorded using the monochrome image acquisition board, IMAQ PCI_1408 and IMAQ Vision LabVIEW application software.

The IMAQ hardware included transmitting the video signal from the camera into the IMAQ PCI-1408 board through a BNC video cable. The images are then transferred into the memory system of the computer and saved on the hard drive.

The DAQ hardware consisted of two LVDT's, load cells, and a signal conditioning and amplification system. LVDT's and load cells were amplified by a Validyne signal conditioning unit, Model PS 171. From this signals were fed into the NI LAB PC+ DAQ board. The load cells used were Revere Transducer model 363-D3-500-20P1 and the LVDTs were Schlumberger Industries model AG / 5.

2.2.4.6 Imaging Equipment

The images of the interface zone were captured using a standard 1/3 in. format charged couple device (CCD) digital video camera module. The camera used was a Sony© XC-73 monochrome C mount camera. A Navitar F/2.8 close focus macro zoom lens with a focal length of 18-mm to 108-mm was attached to the camera. The addition of a Prinz 52-mm polarizing filter reduced the reflected light off of the shear box window. A Cuda single port fiber optic 150W illuminator provided the lighting with flexible dual branch fiber optic light guides.

The dimension of the image captured was approximately 16 mm X 8 mm, with an image size of 640 X 320 pixels, making a pixel equal to 0.025 mm X 0.025 mm. A strain rate of 0.3 mm / min corresponds to a pixel shear rate of 12 pixels / min. Capturing images every 40

seconds allowed for the best resolution of the MPEG routine given a limited availability of CPU resources. This capture rate gave displacements of 7.9 pixels / 40 seconds of time. A MPEG software module was used to determine particle velocities. The details of the routine will be discussed in the following section.

2.2.5 Image Processing

Image processing refers to analysis or modification of pixel information to derive additional information for a specific application. Digital image processing is based on digital, rather than pictorial, information. The intensity levels of each unit picture element (pixel) in digital form are used for enhancement and analysis purposes to derive the desired information (Guler, 1997).

The image processing for this research included capturing grayscale images of the granular soil in contact with the shearing surface in the modified direct shear box. A LabVIEW application, *Live Camera* VI was created in order to position the camera prior to interface testing. The image size captured was 640 X 320 pixels capturing the physical dimensions of 16 mm X 8 mm. In setting up the position of the camera, the surface was placed at the lowest possible extent on the captured image. This allowed for as much of the soil mass as possible within the captured image. In the *Live Camera* VI a histogram was added to sample the original brightness of the captured image. This sampling quantified the number of grayscale values within a range of 0 to 255 pixel values. The aperture of the camera was adjusted until the mean value of the pixel grayscale values was approximately 128.

2.2.5.1 MPEG

The main problem in development of this application was to determine sand grain movements (velocities) during shear testing. This determination requires following sand particles in successively captured image frames (Guler, 1997). After researching several methods to accomplish this, a custom method based on the MPEG routine was found to provide the best performance. MPEG, adapted from Motion Picture Video Algorithms, uses a block-based matching algorithm to analyze subsequent image frames.

Block-based matching is the accepted motion estimation and compensation method by Motion Picture Expert Group (MPEG). In a block matching method, it is assumed that image frames are composed of moving blocks rather than particular objects within the frame. Block matching searches for a constant size of block taken from the previous reference frame within the next frame based on a matching criterion. This method only assesses translation of particles and does not account for particle rotation. There are three parameters that dictate the performance of the block based matching method: matching criteria, search strategy and determining the block size (Guler, 1997).

A macroblock is a small unit of image frames defined with respect to the actual object size within the image. It is required to define an even number of macroblocks because the images horizontal and vertical resolutions are divided by the macroblock's horizontal and vertical size. Side length can be any value depending on the magnitude of motion. The macroblock is assumed to be located right in the middle of the search window prior to starting a search.

The idea of block based matching is depicted in Figure 2-16. In this figure, Frame k is the reference frame and Frame k+1 is the search frame. The displacement of pixel n_1,n_2 is found by searching Frame k+1 for a macroblock of size N X N for the best matching block.

The search window determines the extent of the search. The size of this window is determined by expected motion. For this research, the search window was set at twice the distance the shear box would displace between subsequent images.

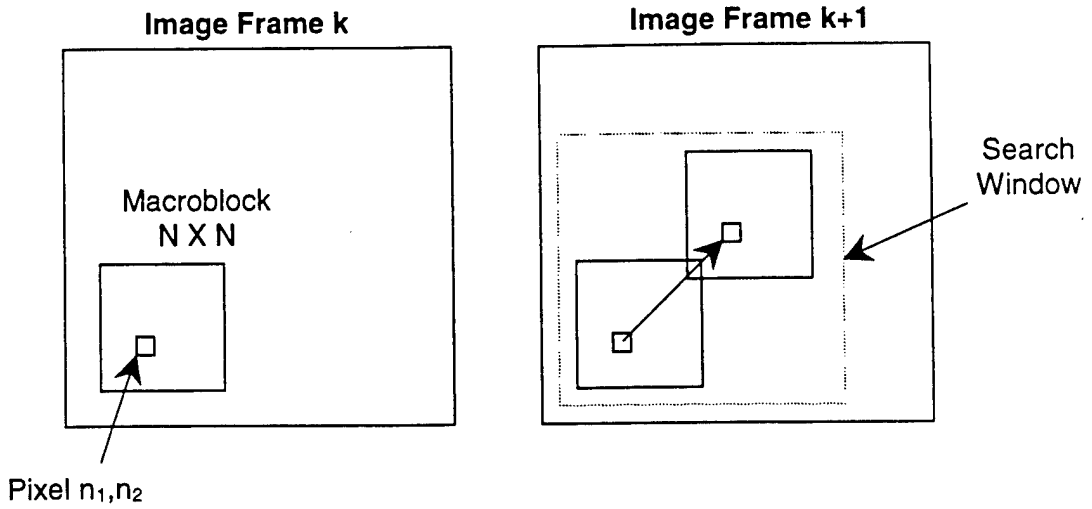

Figure 2-16 Schematic of Block Based Matching

There are different matching criteria designed for motion estimations by the block-based matching method. In this research, the minimum absolute difference criterion was used. The minimum absolute difference can be defined by the following equation.

$$MAD(d_1,d_2)=\sum\left| p(x_k,y_k)-p(x_{k+1}+d_1,y_{k+1}+d_2)\right|$$

$$(m_1,m_2)=\arg\min MAD(d_1,d_2)$$

In this equation m_1,m_2 are the displacements in the horizontal and vertical directions, corresponding to the minimum of the sum of absolute differences, MAD. For the current macroblock, $p(x_k,y_k)$ are the pixel values at x_k,y_k within the current macroblock in Frame k and, $p(x_{k+1}+d_1,y_{k+1}+d_2)$ are the pixel values at the $(x_{k+1}+d_1, y_{k+1}+d_2)$ to search for the MAD within Frame k+1.

2.2.6 Data Reduction

For this project the data was reduced primarily by custom LabVIEW code written to incorporate the custom MPEG routine and by the use of Microsoft Excel macros. In the following sections these data reduction tools are listed and explained.

2.2.6.1 Image and Shear Data Collection VI

Image and Shear Data Collection VI is a LabVIEW *VI* (Virtual Instrument) that was written to acquire and save all images and strength data during the shear testing. This *VI* captures images and strength data at specified time intervals and saves it on a predetermined location on the hard drive. Frame averaging is employed in the *VI* to reduce the noise on

the images prior to further image processing. Guler (1997) reported that frame averaging should be used to reduce pixel value fluctuation. When a camera is focused on a static scene, the pixel grayscale fluctuates with time. The use of frame averaging reduces this noise by averaging pixel grayscale values in successive images before saving the composite image on the hard drive.

2.2.6.2 Image Analysis VI

Image Analysis VI is another application written in LabVIEW code to analyze sequential images and find motion vectors between successive images. The MPEG routine, (Section 2.2.5.1), is employed in this analysis. Following collection and saving of images of the direct shear testing with *Image and Shear Data Collection VI, Image Analysis VI* performs vector analysis and resaves a file with the results in an operator specified location on the hard drive. This vector data is then further reduced by another LabVIEW application called *Mean Vector VI*.

2.2.6.3 Mean Vector VI

Mean Vector VI is another data reduction application written for LabVIEW. This application plots and averages the motion vectors calculated by *Image Analysis VI*. The result is an average of all velocity vectors horizontally across the image. *Mean Vector VI* saves the average of the displacements into 3 separate files for the X-component, Y-component and Magnitude of displacement respectively. Profiles of the shear zone are then plotted using Excel macros.

2.2.6.4 Slide Show VI

Slide Show VI is a LabVIEW application written to view the images taken during the shear test one after the other. This VI opens and displays successive bitmap (*.bmp) files recorded throughout the shear test. When displayed rapidly, a movie replay of the sand behavior though time is seen. This application has the ability to display at various rates and also to skip images at user-specified intervals. These movies help to visualize and better understand the shear zone behavior.

2.2.6.5 Excel Macros

Two Excel macros were written and used for plotting and saving both strength and image data. These macros loop through successive test folders and plot and re-save Excel files in the same folder.

2.3 Results and Analysis

This section explains the testing program, the statistical analysis and the results obtained from this research. Response parameters for both the strength and image data will also be discussed in this section.

2.3.1 Testing Program

Direct shear tests were performed on two sands against seven structural surfaces of various roughness at two constant normal stresses. The structural surfaces ranged from a smooth steel plate to various grades of 3M©'s industrial grade belt sanding papers fixed to PVC

surfaces. The direct shear tests were conducted as a constant stress test at two normal stresses, 35 and 138 kPa. The shear force was applied using a standard direct shear machine with a modified shear box designed for interface zone testing. The test was conducted as a strain-controlled test at a constant rate of strain of 0.3 mm / min. Throughout the test, a Sony© CCD digital video camera module captured images of the interface. Load cells (Revere Transducer model 363-D3-500-20P1) and LVDTs (Schlumberger Industries model AG/5) measured the loading responses and displacements respectively of the sand specimen.

The initial testing program was a series of 64 tests conducted on the surfaces made from 3M©'s industrial grade papers. The surfaces for this testing phase were the P24, P50, P80, and P120. Following interpretation of the data, three more surfaces were added to the testing program. These surfaces included a smooth steel plate, P240, and P180 belt sanding papers. These surfaces were added to better define the transition from a smooth to a rough surface in terms of the measured responses. The interface testing totaled 112 tests. The variables or test parameters are presented in Table 2-7. The mean particle size is presented along with the sand sizes and the mean amplitude of the surface is presented along with the surface type.

Table 2-7 Interface Testing Program Variables

Variables	Levels
2 Sand Types	Ottawa
	Granusil®
4 Sand Sizes	P20 – R30 (0.7250 mm)
	P30 – R40 (0.5125 mm)
	P40 – R60 (0.3375 mm)
	P60 – R100 (0.2000 mm)
7 Structural Surfaces	Smooth Steel Plate (0.0059 mm)
	P240 (0.037 mm)
	P180 (0.059 mm)
	P120 (0.101 mm)
	P80 (0.123 mm)
	P50 (0.229 mm)
	P24 (0.472 mm)
2 Normal Stresses	35 kPa
	138 kPa

In addition to the interface testing, sand-on-sand images were captured during shear testing in order to compare to the interface testing. For these tests a thin piece of film was used to cover the grove in the lower box that the piece of glass slides along during shear. This film was used to keep the sand out, while still allowing the glass to slide. These tests were only successful at low normal stresses. At a high normal stress (138 kPa) the film buckled and restricted the movement of the glass. During the test, double peaks in the stress-displacement curves would occur and glass would break.

2.3.2 Interface Responses

This section shows the parameters determined from the shear tests used in the statistical analysis and data interpretation. These parameters were determined to find out what test variables are significant on the effect of the measured responses. The parameters are separated into two parts, the mechanical parameters and the image parameters. The mechanical parameters are those parameters measured and recorded during the shear testing by the load cells and the LVDTs. The image parameters are those parameters obtained from the image analysis software conducted on the images captured during the shear testing.

2.3.2.1 Mechanical Parameters

For the constant stress direct shear tests, four mechanical parameters were determined from the load and displacement data. These mechanical parameters are common to the direct shear test. The four mechanical parameters are as follows:

1. Peak Strength
2. Residual Strength
3. Failure Displacement
4. Maximum Slope of Dilation Curve, ψ_{max}

The *peak strength* is defined as the peak value the load cell reaches during the test divided by the corrected area of the sample. The *residual strength* is the stress on the soil associated with large strains. This is often termed the ultimate strength. This parameter was determined at 5-mm of horizontal displacement. In looking at the stress stain curves for each test, all samples were at a residual stress state at this amount of displacement. The *failure displacement* is the amount the soil has sheared at peak strength.

Peak and residual interface friction angles (δ) were also determined from the measured strength data. This information can than be compared with the internal friction angles of the sand (ϕ) independent of interface testing.

The first three mechanical parameters are found from a stress-displacement plot of the test data. Figure 2-17 shows a typical stress-displacement plot of a dense sand. The mechanical parameters are marked on the figure.

Maximum slope of dilation curve, ψ_{max}, is the final mechanical parameter and is determined from a vertical vs. horizontal displacement plot. ψ_{max} is the maximum slope of this dilation curve. Figure 2-18 shows a typical dilation curve for a dense sand.

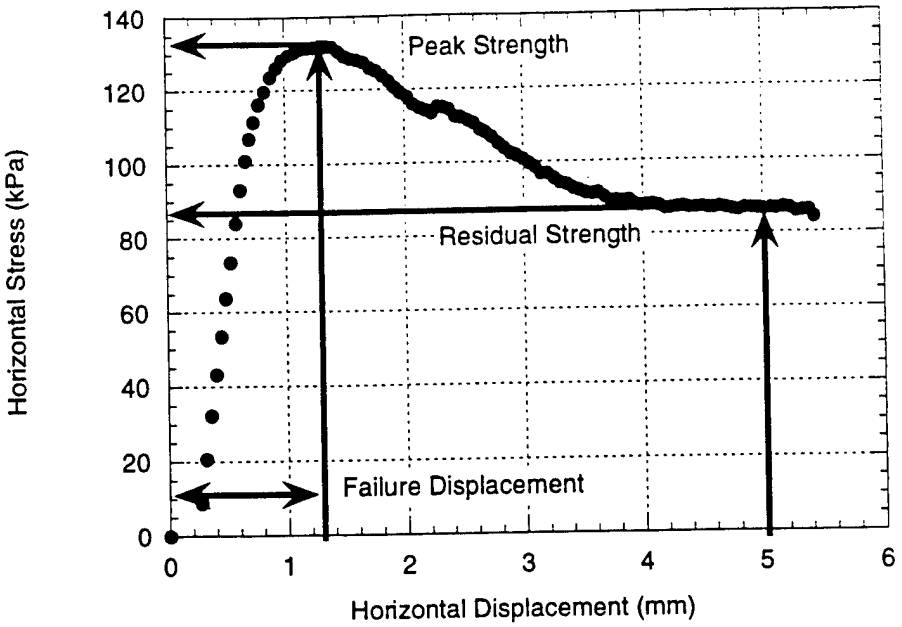

Figure 2-17 Mechanical Parameters obtained from a typical Stress-Displacement Plot (σ_n = 138 kPa)

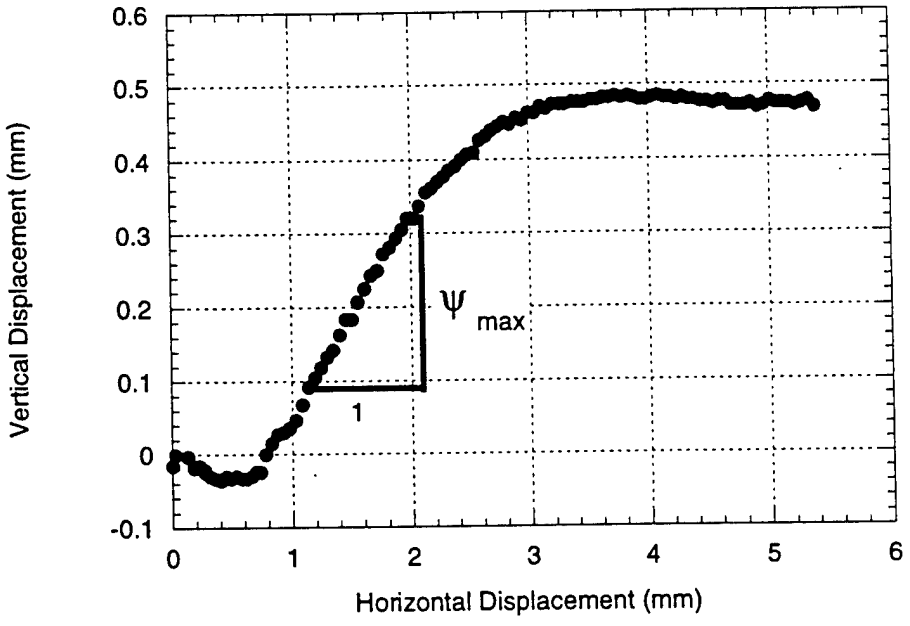

Figure 2-18 ψ_{max} obtained from a typical dilation curve for a dense sand (σ_n = 35 kPa)

Figure 2-19 is intended to aid in the visualization of the velocity profile plots included in this section. Figure 2-19a shows the location and size of the captured image along with the shearing direction. The upper half of the modified shear box is stationary and the lower portion moves relative to the upper half.

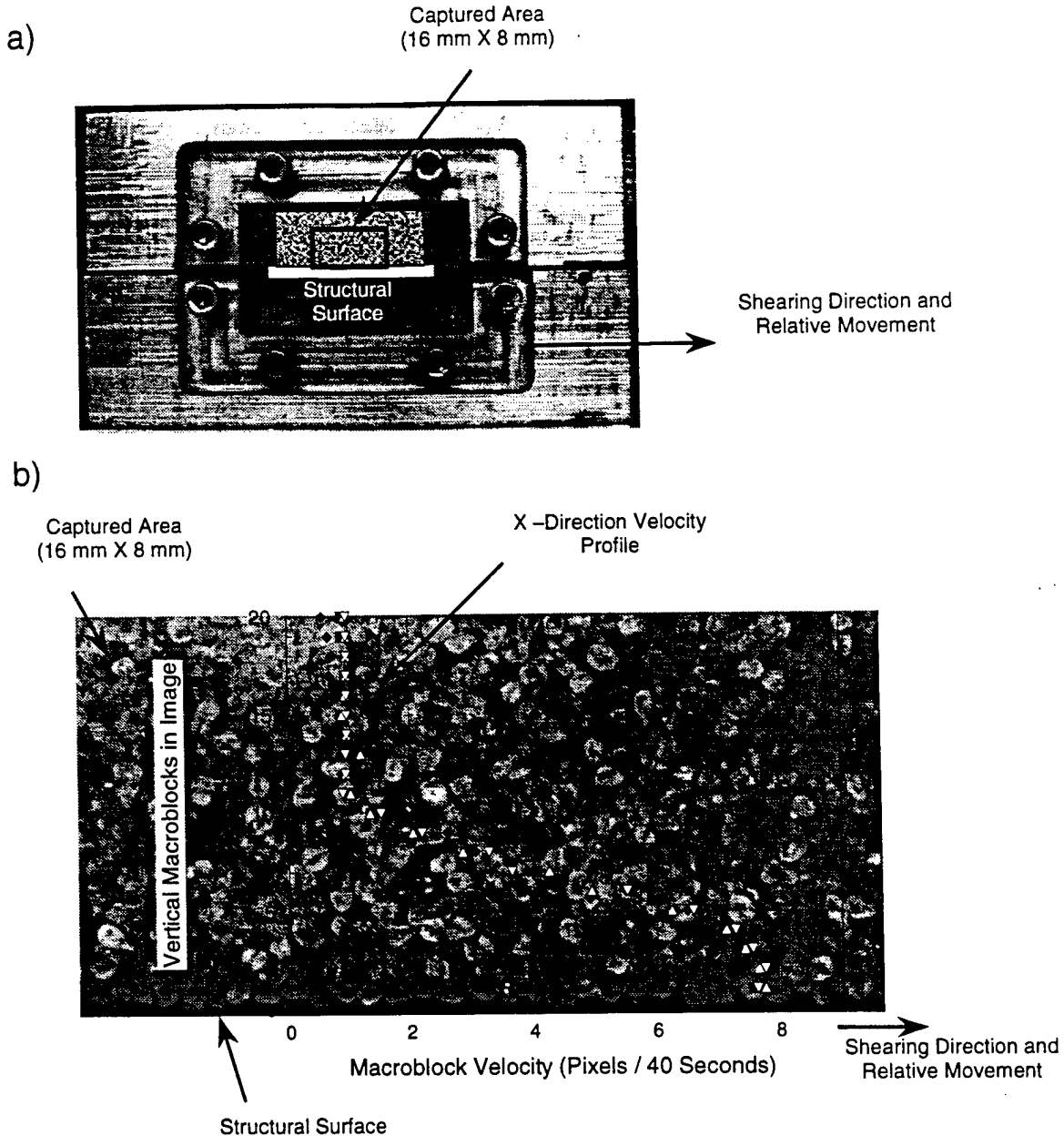

Figure 2-19 Diagram for Visualization of Velocity Profile Plots

Figure 2-19b is an actual captured image with an X – direction velocity profile overlaid. The X – direction is the direction of shearing and parallel to the shear plane. The Y – direction is in the upward direction perpendicular to the shear plane. The structural surface is located at the very bottom of the image. When *Slide Show VI* is used to replay a movie of the sand behavior, the structural surface moves to the right at a constant velocity. The shear zone will develop within the bounds of the overlaid plot. The plot that overlays the image in Figure 2-19b is an X – direction velocity profile at a time late in the shear testing once the shear zone has developed as much as the test setup will allow.

As the shear zone develops through time, the velocities in the profile transition from a vertical line to what is shown on Figure 2-20. At early stages of the test, the velocities throughout the soil mass are all the same. This represents rigid body motion. As time and shear displacement progress, the shear zone develops. Once the shear zone is as developed as the test setup will allow, the image parameters are determined. In Figure 2-20 one can see that the soil mass in the upper portion of the profile still has some velocity at late stages in the test. This velocity is what is termed the neutral zone velocity.

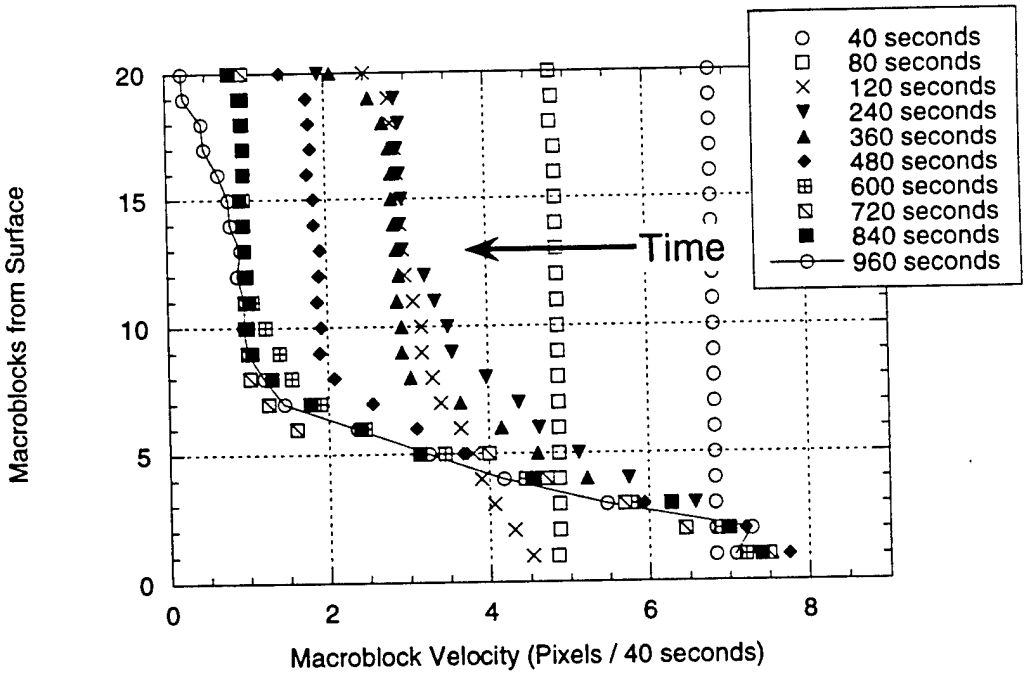

Figure 2-20 Development of the Shear Zone with time (X – direction velocity profile)

Six parameters are obtained from the image analysis performed on the images captured during the direct shear test. Five of the six parameters are obtained from an X – direction velocity profile. The sixth parameter is obtained from a Y – direction velocity profile. The six measured parameters obtained from the image analysis are as follows:

1. Velocity at the structural surface
2. Shear Zone Thickness

3. Fully Developed Shear Zone Thickness
4. Velocity of the Neutral Zone
5. Slope of the Velocity Profile
6. Maximum Dilation Velocity

Image parameters 1 – 5 listed above are determined from an X – direction velocity profile at a time late in the shear testing once the shear zone has developed as much as the test setup will allow. The first five of the previously defined parameters are shown graphically on Figure 2-21. The figure is a velocity profile of the last five images taken during the shear test. At this point the shear zone is as fully developed as possible with the amount of strain allowed (6-mm) by the modified direct shear box.

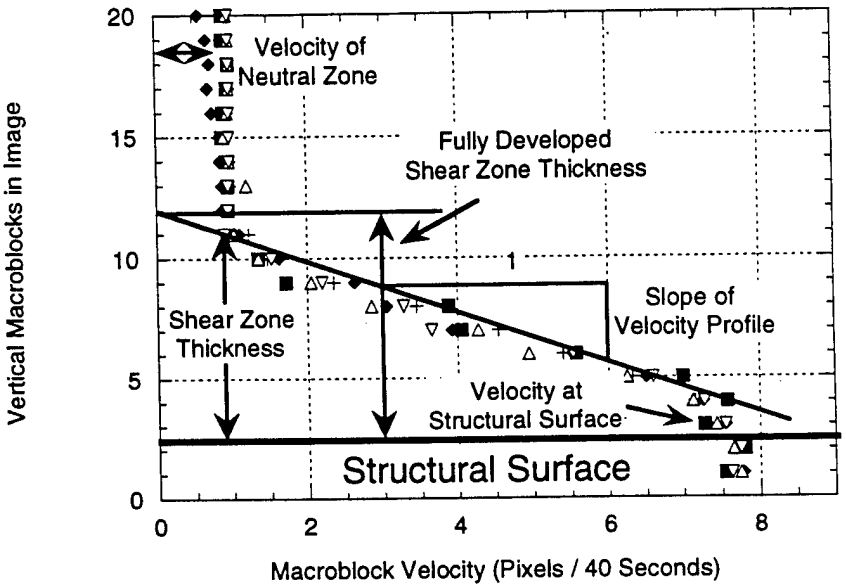

Figure 2-21 Image Parameters obtained from a typical X – direction velocity profile

The *velocity at the structural surface* is taken as the velocity of the sand particles in contact with the structural surface. This parameter explains the amount of slipping that occurs at the structural surface. If the particles are fully engaged by the surface this velocity will be equal to the velocity of the surface, 7.9 pixels of displacement per 40 seconds of time, corresponding to a 0.3 mm / min displacement rate. The *shear zone thickness* is defined as the distance from the structural surface to the inflection point of where the velocities reduce and transition into what is defined as the *neutral zone*. The *fully developed shear zone thickness* is used to determine what the shear zone thickness would be if the test could be carried out to larger amounts of displacement. If the shear zone were to fully develop, this parameter defines what is thought would be the thickness of the shear zone. This parameter is found by extending the *slope of the velocity* profile to a zero *neutral zone velocity*. The slope of the velocity profile is taken as the slope of the velocity plot through the shear zone. This generally extends from the particle velocity at the surface up to the point where velocities begin to reduce and transition into the *neutral zone*. The *neutral zone*

velocity is defined as the velocity of the soil mass that is not within the shear zone. Depending on testing parameters the shear zone does not always fully develop, and the upper soil mass still has a velocity during later stages on the test.

The *maximum dilation velocity* is the final image parameter that was obtained from the image analysis. This parameter is taken from a Y – direction velocity profile. The maximum dilation of a soil sample should occur at a point in time consistent with the displacement at the peak horizontal stress. The dilation velocity can be seen graphically on Figure 2-22.

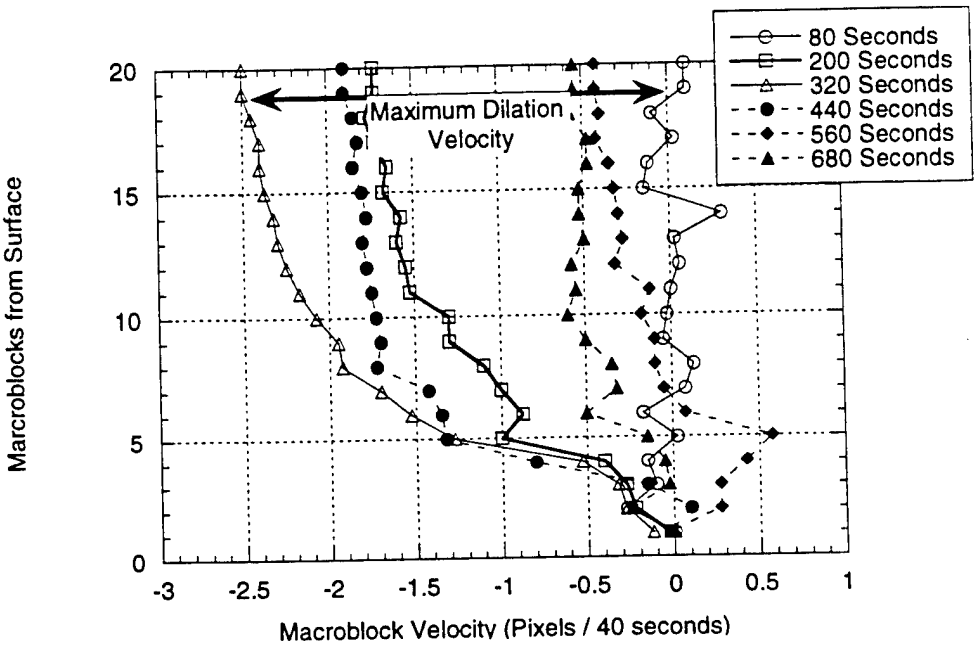

Figure 2-22 Image Parameter obtained from a typical Y – direction velocity profile

2.3.3 Results

This section will discuss the factors that influence the behavior of each parameter. Response surface methods are used to examine the relationship between one or more response variables and a set of quantitative experimental factors. Response surface methods are often employed to determine how the controllable factors optimize or effect the response. Response surface designs are usually chosen when curvature is expected in the response surface (Berthouex *et al,* 1994). The plots for both the mechanical and image parameters are included in this section. For interpretation of the data, lines are used to connect the data points. This does not imply that there is a linear relationship between data points, but is used for visualizing the trends. In the discussion of the results, Ottawa sand is referred to as the rounded sand where as Granusil® is referred to as the angular sand. Typically only one normal stress is shown here in the results section for each parameter. The normal stress that best displayed the discussed parameter is shown. All response plots are included in Sundberg(1998).

2.3.3.1 Mechanical Parameters

For the constant stress direct shear tests, four mechanical parameters were determined from the load and displacement data. These mechanical parameters are common to the direct shear test. Peak and residual interface friction angles (δ) were also determined from the measured strength data. This information can then be compared with the internal friction angles of the sand (ϕ), measured independent of interface testing.

2.3.3.1.1 Peak Strength

For both sand types at the high and low normal stresses, the largest increase in peak strength occurs from the transition from the smooth steel plate (0.0059-mm) to the 0.037 mm surface (P240 paper) as shown on Figure 2-23. After the initial increase in peak strength with an increase in surface roughness, the peak stress levels off when the failure is forced within the soil mass. From the 0.037-mm surface to the 0.123-mm surface, slipping occurs along the surface for the larger grain sizes. The transition to full interlocking with the surface can be observed within this region of surface roughness.

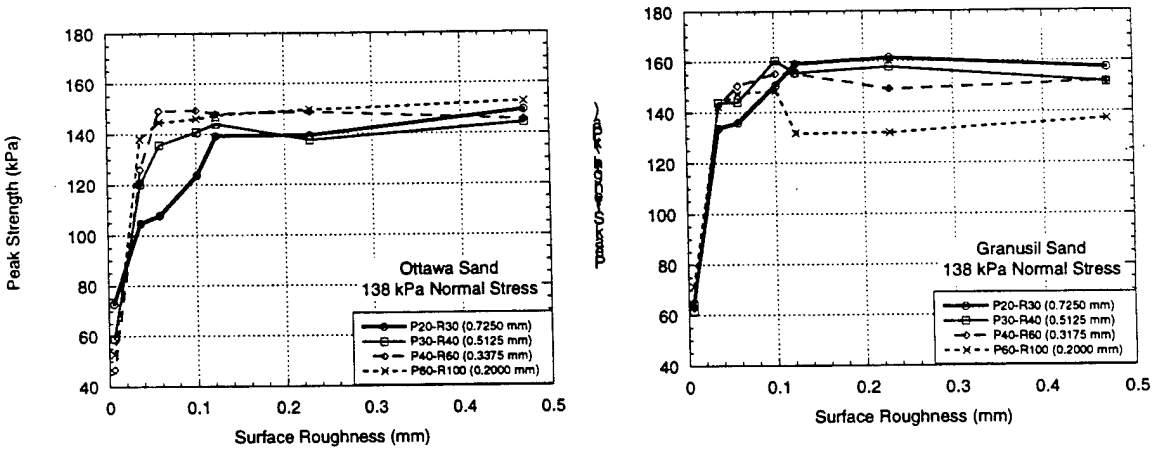

Figure 2-23 Peak Strength

For a given combination of surface roughness and sand size, the maximum horizontal stress has leveled off and become constant at a surface roughness where the mean amplitude of the surface is approximately the same size as the D_{50} / 2 of the sand. For example, along surface rougher than 0.1-mm surface roughness, the peak strength for the P60 – R100 sand size is constant. At this point it is believed that all of the sand particles along the surface are mobilized by the surface and the shear failure occurs within the soil mass. On surfaces rougher than the surface in which the peak strength occurs, the values of peak strength level off due to the failure occurring within the mass of soil. Therefore, there is a limiting surface roughness for a given size of sand grain beyond which increasing surface roughness has no effect.

The angular sand showed higher peak strength than the rounded sand for both normal stresses. When sheared along the roughest surface, when the failure occurs within the soil

mass, trends are seen with the different grain sizes. For the angular sand the grain shape analysis showed an increase in angularity with an increase in particle size (see Section 2.2.2.3). With an increase in angularity there is an increase in shear strength due to the interlocking of the particles (Edil *et al*, 1975). Along the roughest surface, this trend is observed. This behavior was also observed with the sand-on-sand friction angles (see Section 2.2.2.5). For the rounded sand there was a decrease in roundness with an increase in particle size (see Section 2.2.2.3). The smaller grain sizes show higher peak strength when all the particles are mobilized by the surface. Therefore, the maximum peak strength is associated with maximum particle angularity but not grain size.

2.3.3.1.2 Residual Strength

The parameter of residual strength shows very similar trends as the parameter of peak strength with increasing surface roughness. Figure 2-24 shows the parameter of residual strength with increasing surface roughness. The same trend for slipping along the surface is observed from the 0.037-mm to 0.123-mm surface. The largest increase in residual strength is also the transition from the smooth steel plate (0.0059-mm) to the 0.037-mm surface. The maximum residual strength has leveled off and become constant at a surface roughness where the mean amplitude of the surface is approximately the same size as the D_{50} / 2 of the sand. This trend is the same as discussed in the previous results about peak strength. The effects of the roundness variation with grain size, as discussed in the previous section, can also be seen along the roughest surface when all particles are mobilized and the failure occurs within the soil mass.

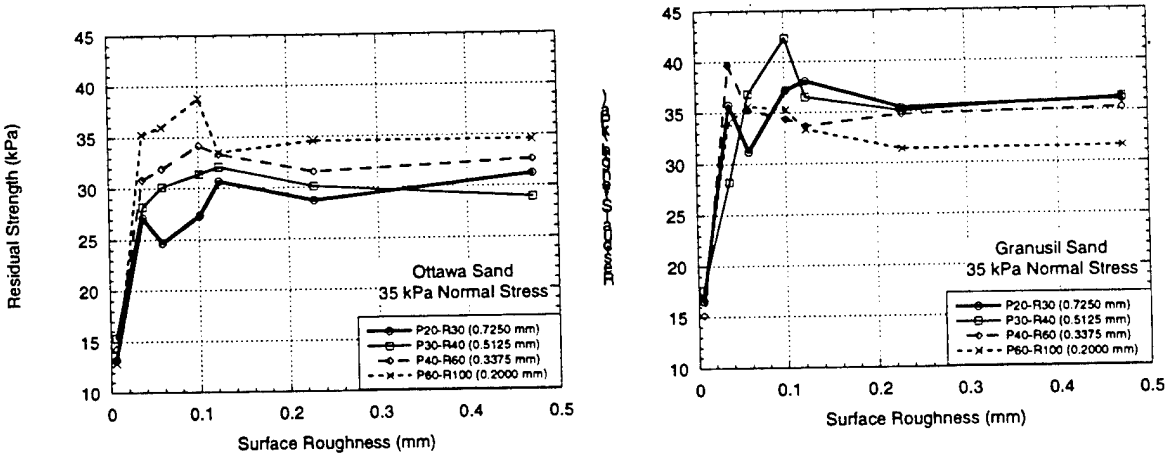

Figure 2-24 Residual Strength

2.3.3.1.3 Failure Displacement

The parameter of failure displacement is shown with increasing surface roughness in Figure 2-25. The angular sand tended to reach peak strength at a larger amount of displacement than the rounded sand. No trend was observed for an increase in sand size for either sand type. At low normal stresses (35 kPa), the peak stress occurs at a lower amount of

horizontal displacement compared to the higher normal stress (35 kPa). This trend was observed for both sand types but is more pronounced with the angular sand. All plots for this parameter are included in the appendix. With an increase in surface roughness, there was a small increase in the amount of horizontal displacement of the surface before the peak shear stress occurred.

2.3.3.1.4 Max Slope of the Dilation Curve - Ψ_{max}

The strength parameter of ψ_{max} is shown with increasing surface roughness in Figure 2-26. For both sand types, a high normal stress results in smaller values of ψ_{max} than the low normal stress. Along the smooth steel surface (0.0059-mm), no dilation was measured for either the angular or the rounded sand. During these tests against the smooth surface, there was complete slipping along the surface. As the surface roughness increases from 0.037-mm (surface P240) to 0.123-mm (surface P80) there is a gradual increase in ψ_{max}. Along surfaces rougher than 0.123-mm the value of ψ_{max} levels off and there is little variance. At this surface roughness the failure occurs within the mass of the soil.

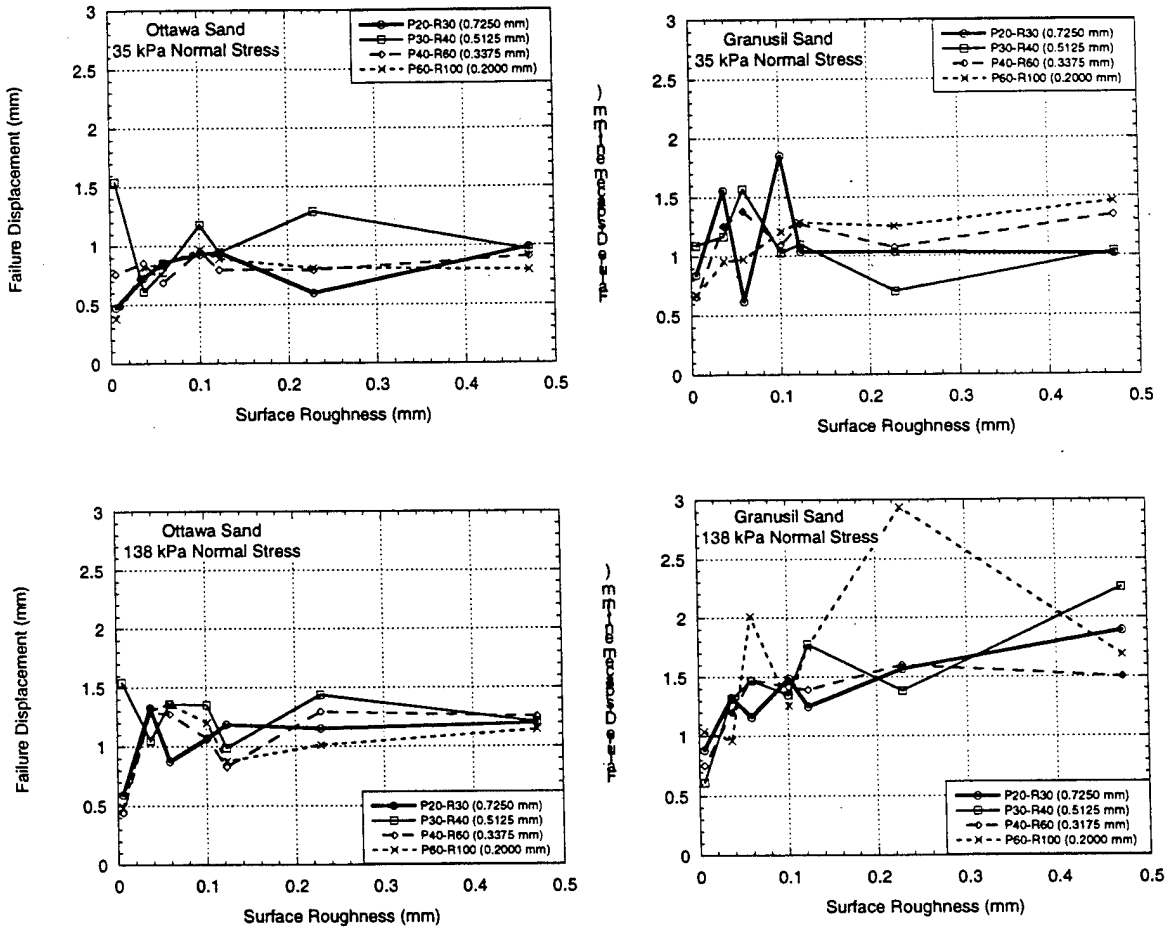

Figure 2-25 Failure Displacement

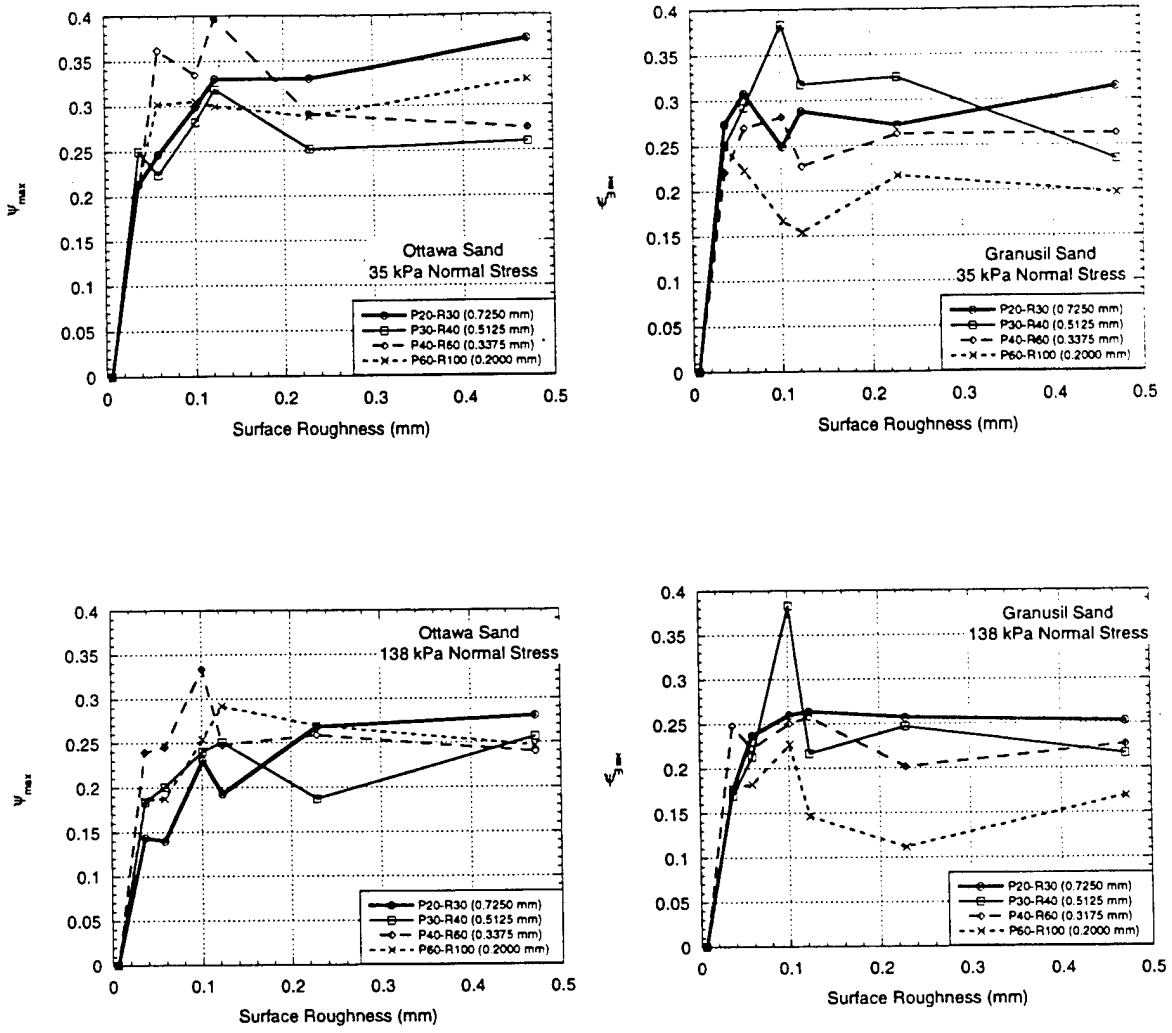

Figure 2-26 ψ_{max} – Slope of the Dilation Curve

2.3.3.1.5 Peak and Residual Interface Friction Angles

The strength data was also used to plot the results in terms of friction angles. Up to a surface roughness in which the particles are fully mobilized by the surface, an increase in both peak and residual friction angle is observed for both sand types. Once the shear failure is forced within the soil mass, these friction angles level off. This trend can be seen in Figure 2-27 and Figure 2-28 with peak and residual δ as a function of surface roughness. The bounds of the internal friction angle (ϕ) are shown on Figure 2-29.

One would expect that at a surface roughness that mobilizes all sand particles, forcing the shear failure to occur within the soil mass, that δ would converge to a value equal to ϕ. The results from this research showed consistently higher interface friction angles (δ) than the

internal sand friction angles (ϕ) when the shear failure was within the soil mass (see Figure 2-27 and Figure 2-28). This leads to a strength ratio > 1.0 where the strength ratio, $f_o = \delta / \phi$. Values of δ were found to be on the order of 14 – 18% higher than the respective ϕ value for a given sand size. These high values of δ are suspected to result from the test set-up and the direct shear device used. In the direct shear test, shear stresses in the specimen are not uniformly distributed. With the addition of a structural surface in the lower portion of the shear box, these boundary effects may have been magnified increasing the shear stress. A non-planar failure region within the upper portion of the shear box is also thought to contribute to these results. Within the captured image, the extent of the shear zone is at some distance away from the surface when the particles along the structural surface are mobilized by the shearing surface. However, the extent of this zone within the soil, outside of the captured image is not known. A non-planar failure region forced within the upper shear box may increase δ to a value higher than that of ϕ. Figure 2-30 illustrates this idea. There may be other explanations; however, additional research is necessary to clearly establish the cause of this observation.

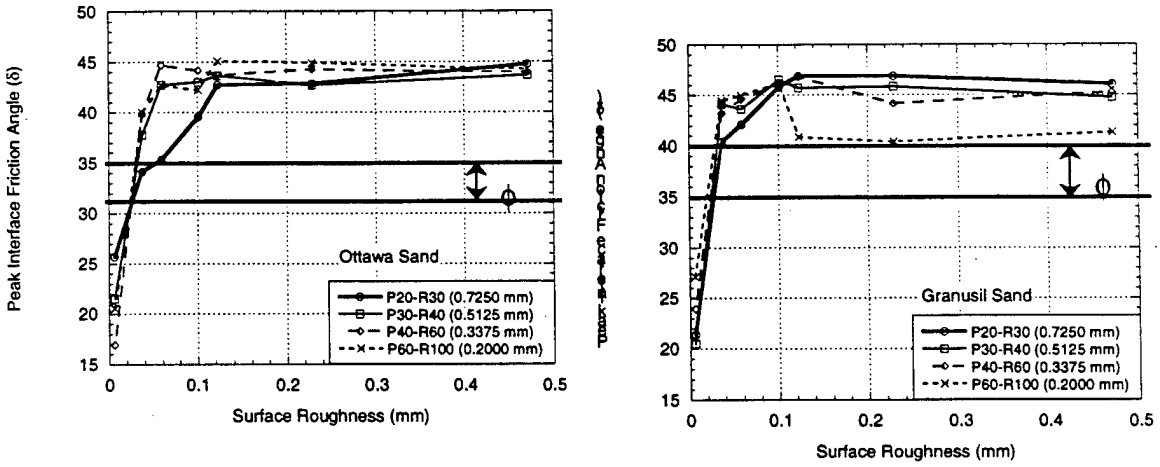

Figure 2-27 Peak Interface Friction Angles (δ)

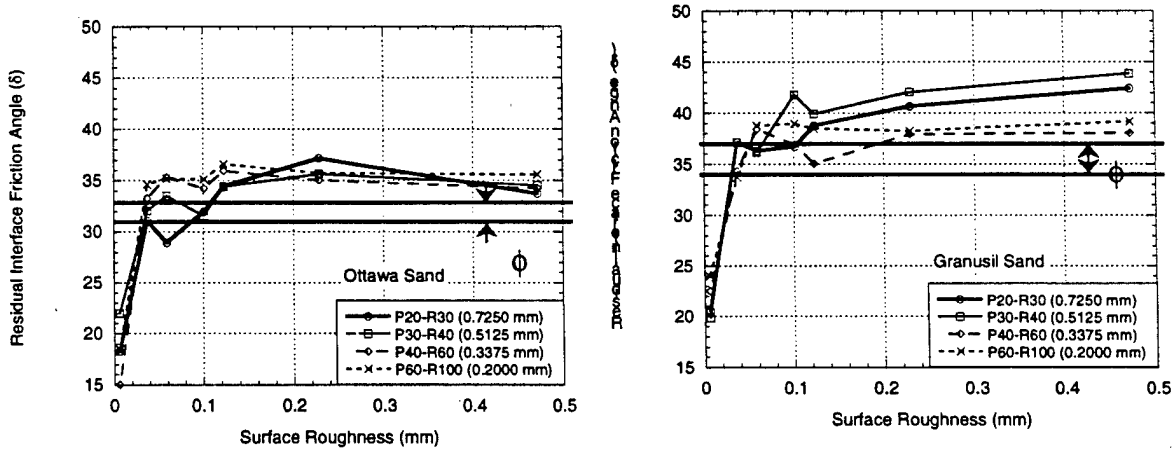

Figure 2-28 Residual Interface Friction Angles (δ)

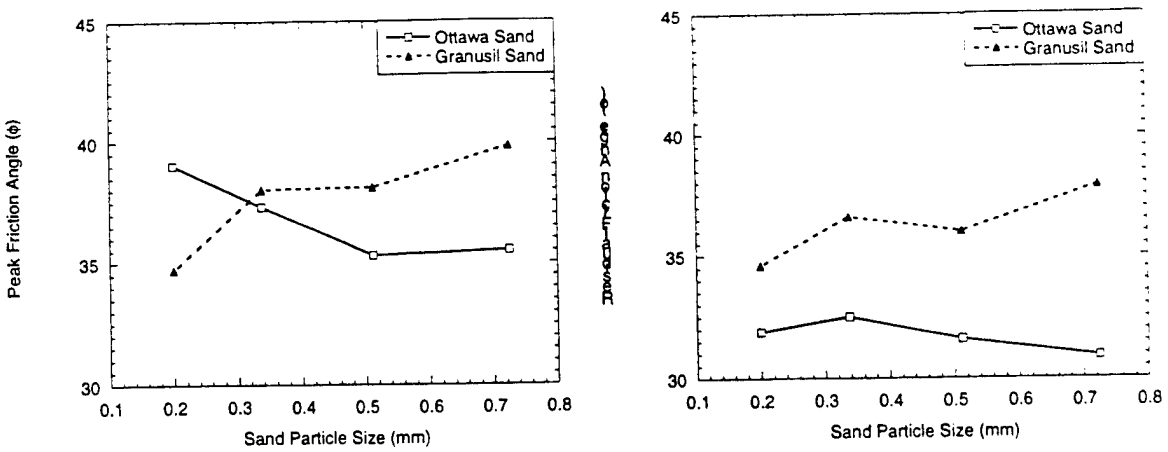

Figure 2-29 Internal Friction Angles of Sand (ϕ)

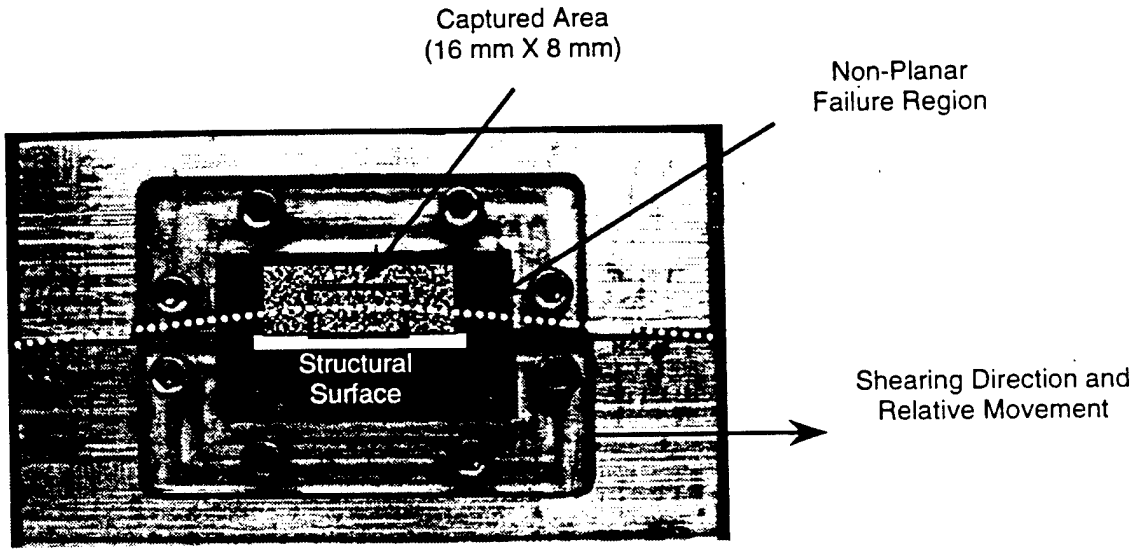

Figure 2-30 Illustration of Non-Planar Failure Region

2.3.3.2 Image Parameters

It was found that the normal stress had a minimal effect on many of the image parameters. Paired t-tests were conducted between the data sets for the high and low normal stresses. The results are given in Table 2-8 with "Yes" indicating that the mean difference fell within the range of zero under a 95% confidence interval. This means that with a 95% confidence level there is no difference between the parameter measured from the high and low normal stress. Also the null hypothesis, that the data sets are not the same, has to be rejected. "No" indicates that the parameter did not pass the paired t-tests indicating normal stress is

significant. It is believed that individual tests, shown by outlying data points well outside of the trend, may be the only significant reason for this. For interpretation of the image parameters, the normal stress that best shows the discussed parameter is presented. This is done to better illustrate the effects of grain size and surface roughness on the parameters. The image parameters were also plotted connecting the data points with a line. This does not suggest linearity in the data between points, but was done for better visualization of trends in the data. All response plots and the paired t-tests are included in the Appendix of this report.

Table 2-8 Results of Paired t-tests for the effect of Normal Stress on Image Parameters

Image Parameter	Granusil® Sand	Ottawa Sand
Velocity at the Structural Surface	YES	YES
Slope of the Velocity Profile	YES	NO
Shear Zone Thickness	YES	NO
Fully Developed Shear Zone Thickness	NO	NO
Velocity of Neutral Zone	YES	YES
Maximum Dilation Velocity	NO	NO

2.3.3.2.1 Velocity at the Structural Surface

Normal stress showed no effect on the velocity at the structural surface for both of the sand types. Figure 2-31 shows the parameter of velocity at the structural surface with increasing surface roughness. The velocity of the particles at the structural surface was 0 pixels / 40 seconds of time for both sand types along the smooth steel plate (0.0059-mm). In the transition to the 0.037-mm surface some of the particles are mobilized, however there is still some slipping along the surface. When the mean amplitude of the surface is equal to ½ the mean diameter of the soil particles, the soil particles are fully engaged by the surface and the velocity of the soil along the surface is equal to the surface itself. Because of this engaging with the surface the trends for the velocity at the interface are the same as for peak and residual strength. For both sand types, the finer sands have the highest velocity at the 0.037-mm surface. The finer particles are better engaged by this surface. The largest grain size (0.7250-mm) is first fully mobilized on a surface with mean particle amplitude of 0.229-mm. Rougher surfaces than this have no further effect on this parameter. After the 0.229-mm (Surface P50) surface roughness, the velocity of the particles along the surface is equal to the velocity of the surface itself. The plots show that the finer particle sizes are mobilized before the larger particles as surface roughness increases.

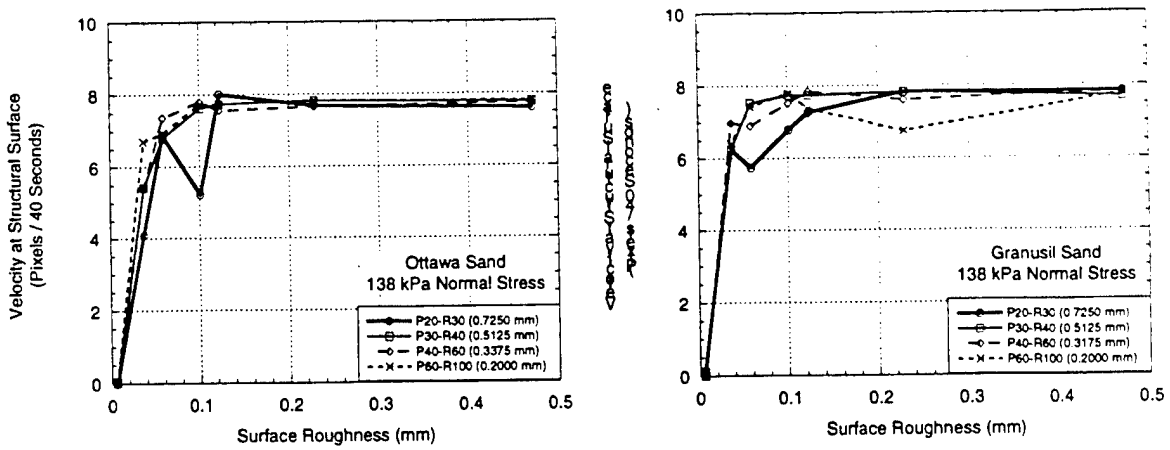

Figure 2-31 Velocity at Structural surface

2.3.3.2.2 Shear Zone Thickness

For this parameter the angular sand passed the paired t-tests for normal stress effect, where as the rounded sand did not. Individual points outside of the trend as seen in the figure below is most likely the significant reason for this. Figure 2-32 shows the parameter of shear zone thickness with increasing surface roughness.

The shear zone thickness and the fully developed shear zone thickness will be presented in two different forms. One will be in distance away from the structural surface in macroblocks and the other will be in particle diameters. The captured image size was 16 mm X 8mm, and the image size was 640 X 480 pixels. The size of a macroblock was 16 X 16 pixels corresponding to a physical dimension of 0.4 mm X 0.4 mm. With the mean grain size of the particles, shear zone thickness can be determined in particle diameters. A macroblock is a finite distance of 0.4-mm whereas thickness in particle diameters is relative to the grain size of the sand.

The shear zone thickness for both sand types increased with increasing roughness. The most significant rate of increase was again from the smooth steel plate (0.0059 mm) to a 0.037 mm. After a surface roughness of 0.037 mm the thickness of the shear zone continues to increase but at a slower rate. The magnitude of the shear zone thickness in macroblocks is very similar for both the rounded and angular sand types except for the rounded sand along a surface roughness of 0.123 mm and rougher. Along these surfaces the rounded sand shows a higher shear zone thickness than the angular sand. For the angular sand, there is an increase in shear zone thickness in macroblocks with an increase in particle size. For the rounded sand this response is not so prevalent. The rounded P20 – R30 sand tested on the three roughest surfaces has a thicker shear zone than the other sand sizes, while the finer rounded sands have a similar shear zone thickness.

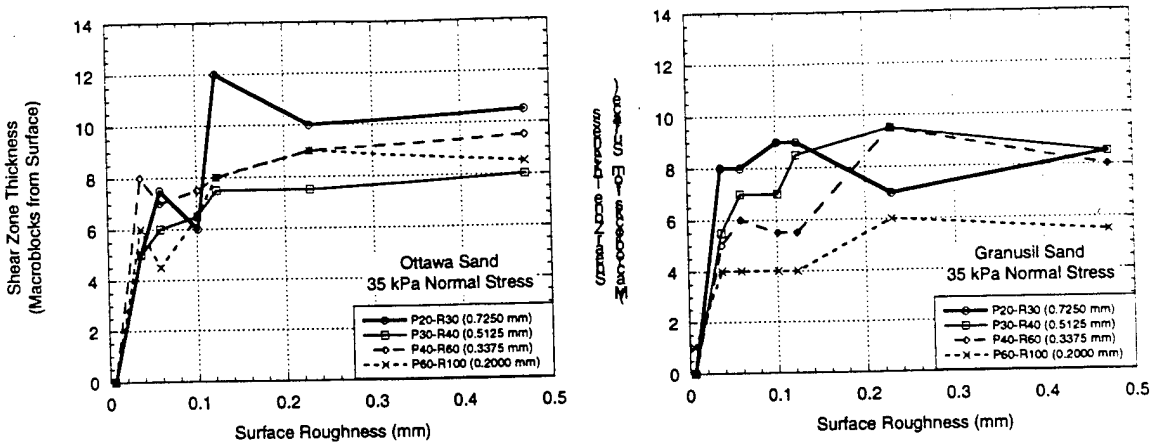

Figure 2-32 Shear Zone Thickness (Macroblocks from Surface)

When the parameter of shear zone thickness is presented in particle diameters from the surface, the trends are more pronounced as shown in Figure 2-33.

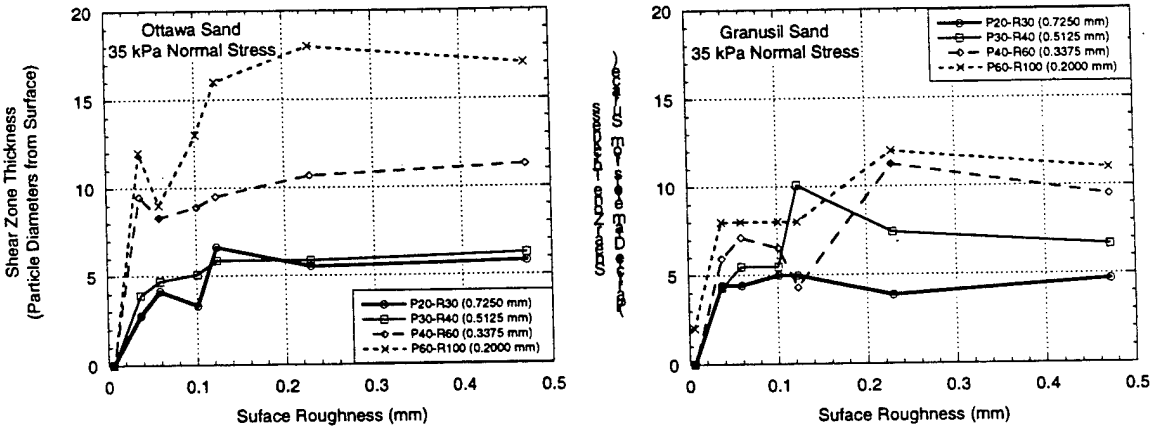

Figure 2-33 Shear Zone Thickness (Particle Diameters from Surface)

In general, the shearing of the surface affects more particles of the finer sands. For the rounded sand, sizes P20 – R30 and P30 – R40 show very little difference in shear zone thickness in particle diameters. The largest difference between the rounded and the angular sand types is the behavior of the P60 – R100 sand size. The rounded sand shows a higher shear zone thickness in particle diameters for the P60 – R100 size on all surfaces rougher than 0.037-mm.

2.3.3.2.3 Fully Developed Shear Zone Thickness

For this parameter neither the angular sand nor the rounded sand passed the paired t-tests for normal stress effect. The trends for this parameter are the same as for the measured shear zone thickness discussed in the previous section. The plots of this parameter are shown in Figure 2-34 and Figure 2-35.

The only difference in the behavior of this parameter compared to the measured shear zone thickness is that for the larger sand sizes, where the shear zone does not fully develop during the test, thicker shear zones are observed. When the slope of the velocity profile is extrapolated to a neutral zone velocity of zero, the fully developed shear zone thickness becomes greater than the measured shear zone thickness.

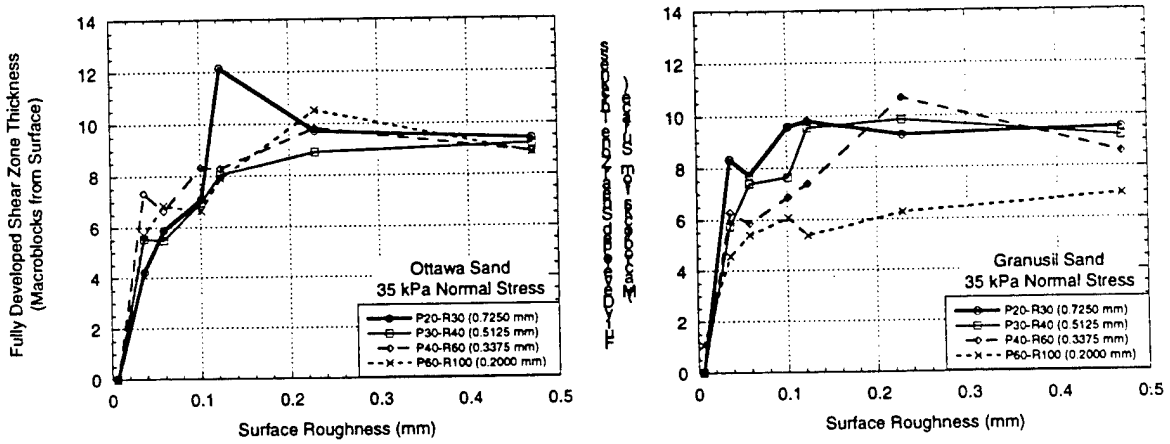

Figure 2-34 Fully Developed Shear Zone Thickness (Macroblocks from Surface)

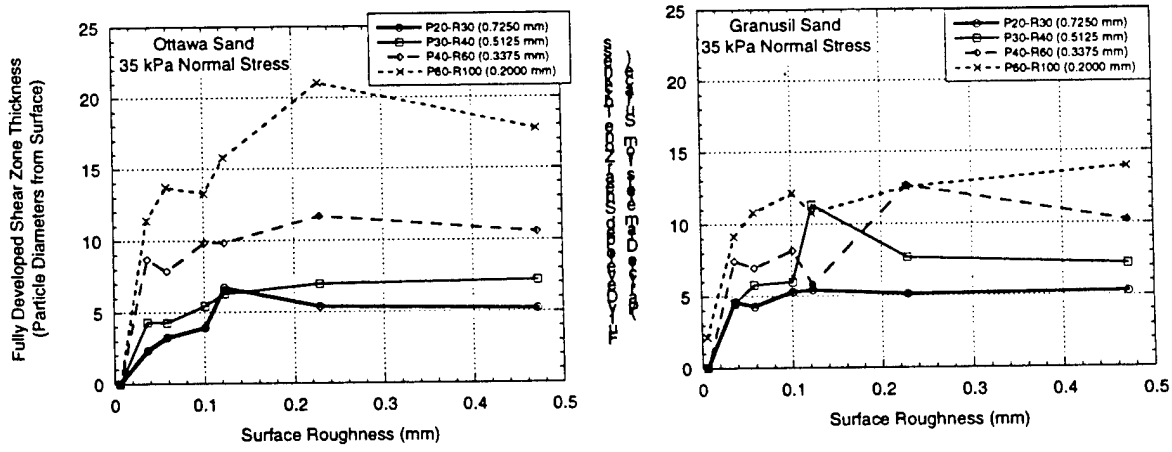

Figure 2-35 Fully Developed Shear Zone Thickness (Particle Diameters from Surface)

2.3.3.2.4 Velocity of Neutral Zone

For this parameter both the angular sand and the rounded sand passed the paired t-tests for normal stress effect. Figure 2-36 shows the parameter of velocity of neutral zone with increasing surface. For larger sand sizes, the shear zone does not fully develop and there is still some particle velocity of the neutral zone in the later stages of the test. The only sand size that the shear zone fully developed on all surfaces for both sand types, was the P60 – R100. In general the angular sand shows higher neutral zone velocities. This is consistent with the angular sand requiring more horizontal strain for it to reach the peak stress state. At late stages in the test the angular sand has a lesser-developed shear zone and as a result, higher neutral zone velocities.

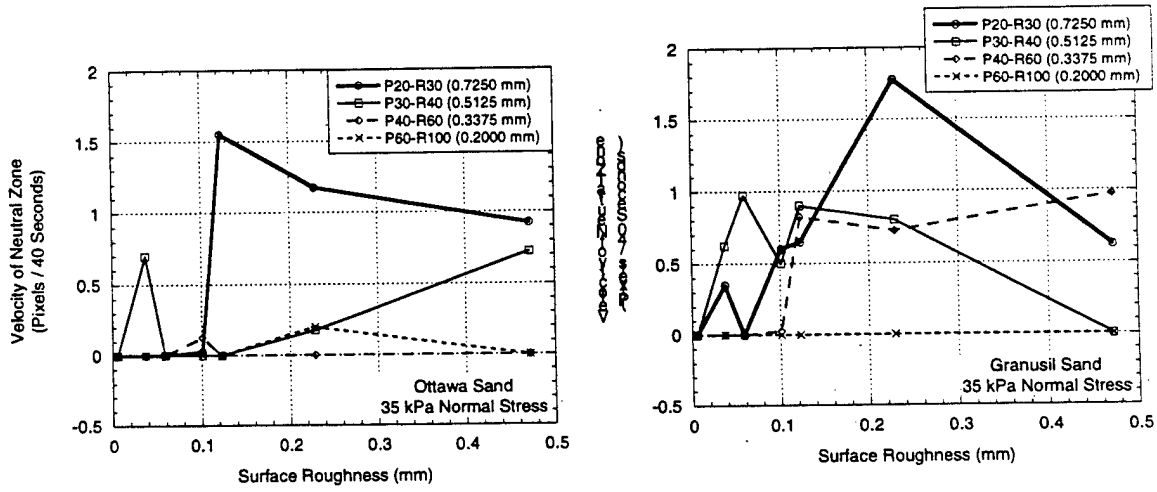

Figure 2-36 Velocity of Neutral Zone

2.3.3.2.5 Slope of the Velocity Profile

For this parameter the angular sand passed the paired t-tests for normal stress effect, where as the rounded sand did not. Figure 2-37 shows this parameter with increasing surface roughness. The only sand that was partially engaged by the smooth surface was the P60 – R100 angular sand. Because there was some engaging of the particles, a shear zone within the soil mass occurred and a slope of this velocity profile could be determined.

For both sand types the slope of the velocity profile increased with surface roughness up to around 0.059-mm. After this roughness the slope of the velocity profile decreased and leveled off with increasing surface roughness.

The slope of the velocity profile for sands with larger particle diameters is higher for both sand types. This is because with coarser sands the shear zone does not always fully develop, leaving a neutral zone velocity greater than 0 at larger strains. With the velocity of the surface being constant (7.9 pixels / 40 seconds) and a velocity of the neutral zone when this parameter is determined, an increased slope of the velocity profile through the shear zone will be observed.

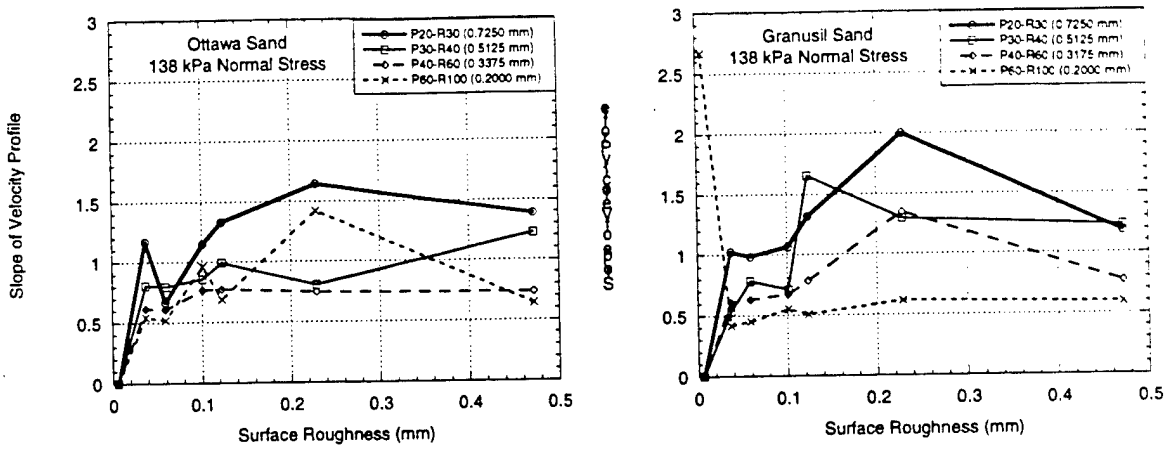

Figure 2-37 Slope of the Velocity Profile

2.3.3.2.6 Maximum Dilation Velocity

For this parameter neither the angular sand nor the rounded sand passed the paired t-tests for normal stress effect. The normal stress is a contributing factor to this parameter. As one would expect, with a higher normal stress, less dilation would occur in the soil mass (Holtz and Kovacs, 1981). This response was also found with the velocity of the dilation. Figure 2-38 shows the maximum dilation velocity with increasing surface roughness.

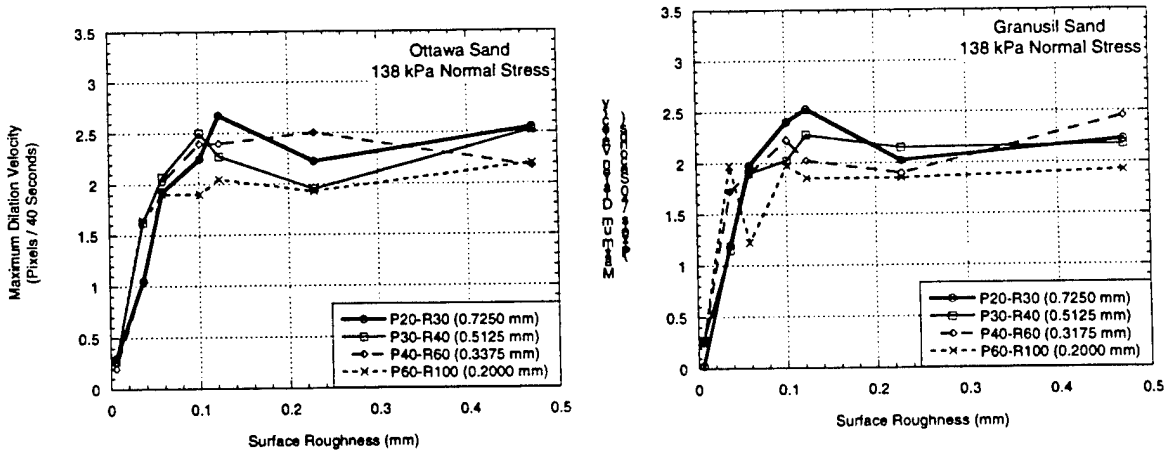

Figure 2-38 Maximum Dilation Velocity

Very small dilation velocities were found for both sand types along the smooth steel surface (0.0059-mm). From surface roughness 0.037-mm to 0.472-mm sand type showed a small effect. With an increase in surface roughness there is a gradual increase in the dilation velocity. An increase in sand size showed slightly higher dilation velocities.

2.3.3.3 Sand-on-Sand Direct Shear Tests

Image data was successfully obtained for the sand-on-sand tests at a low normal stress. For the high normal stress tests, double peaks occurred in the stress-displacement curve and the viewing glass would break from sand compressing the film and restricting the movement of the glass.

The results of the sand-on-sand tests will be compared to the low normal stress image parameters obtained from the interface testing. The image parameters determined from the sand-on-sand tests are as follows.

1) Shear Zone Thickness
    i) Macroblocks from surface
    ii) Particle Diameters from Surface
2) Slope of the Velocity Profile
3) Maximum Dilation Velocity
4) Velocity of the Neutral Zone

2.3.3.4 Shear Zone Thickness

The results of shear zone thickness will be presented in two forms. One will be in distance away from the structural surface in macroblocks, and the other will be in particle diameters away from the surface. These results are shown on Figure 2-39.

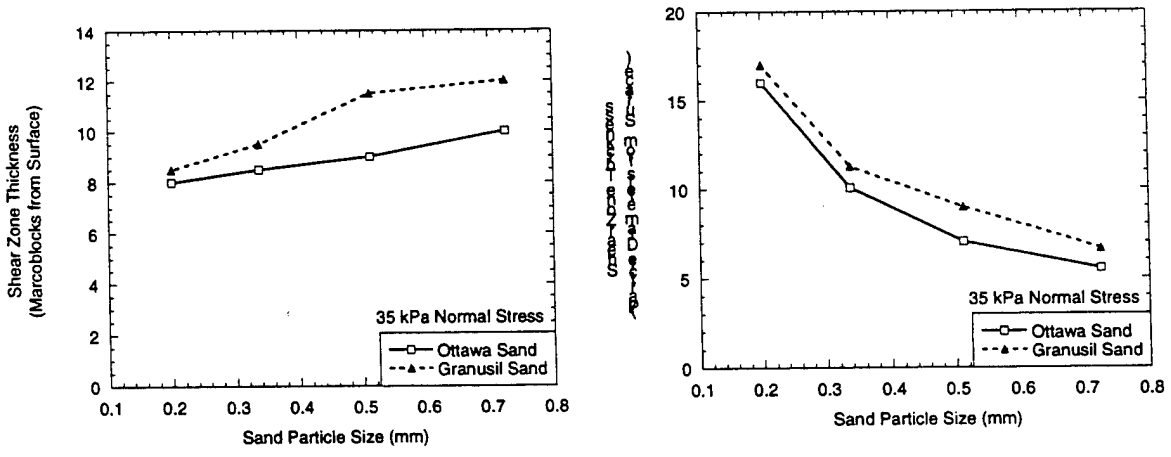

Figure 2-39 Shear Zone Thickness for Sand-on-Sand tests

For this parameter it was found that the angular sand produced thicker shear zones compared to the rounded sand. There is also an increase in the shear zone thickness in

macroblocks with an increase in particle size. For the rounded sand the magnitude of the shear zone thickness is very similar to the magnitude of the shear zone thickness determined from the interface testing along rougher surfaces than 0.101-mm. This is when the failure is within the soil mass and the parameter of shear zone thickness has leveled off. For the angular sand the magnitude of the shear zone thickness for the sand-on-sand tests is slightly thicker than those determined from the interface testing.

In particle diameters from the surface, there is a decrease in the thickness of the shear zone with an increase in particle size. This is because macroblocks is a finite distance whereas particle diameter varies with sand size. This agrees with the observations made for the interface testing. The range of shear zone thickness in particle diameters is within the range of shear zone thickness determined from the interface testing.

2.3.3.5 Slope of the Velocity Profile

The slope of the velocity profile through the shear zone of the sand-on-sand test was determined. The results are shown in Figure 2-40. For both sand types, the P40 – R60 (0.3175-mm) sand size had the steepest slope of the velocity profile for the sand-on-sand tests. The magnitudes of the slopes found from the sand-on-sand tests are consistent with those from the interface testing. In the sand-on-sand tests the shear zone fully developed and the same shearing rate of 0.3 mm / min was used for these tests.

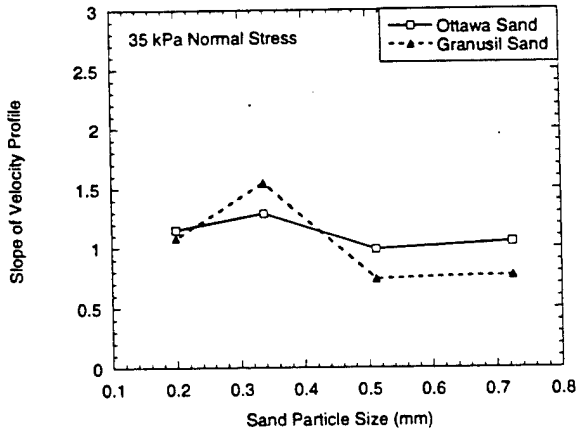

Figure 2-40 Slope of the Velocity Profile for Sand-on-Sand tests

2.3.3.6 Maximum Dilation Velocity

The maximum dilation velocity of the sand-on-sand tests at low normal stress for all tests showed vertical pixel velocities around 2 pixels / 40 seconds of time for all tests except for the P60 – R100 angular sand. These results are shown in Figure 2-41.

The magnitude of the dilation velocity for the sand-on-sand tests is slightly less than the interface tests. This can be explained by compression of the soil mass in the lower portion of the shear box during the sand-on-sand tests. In the interface tests all particle movement is within the upper portion of the box and no compression of the surface can occur. With

some compression of the soil in the lower portion of the shear box for the sand-on-sand tests, smaller dilation velocities are measured.

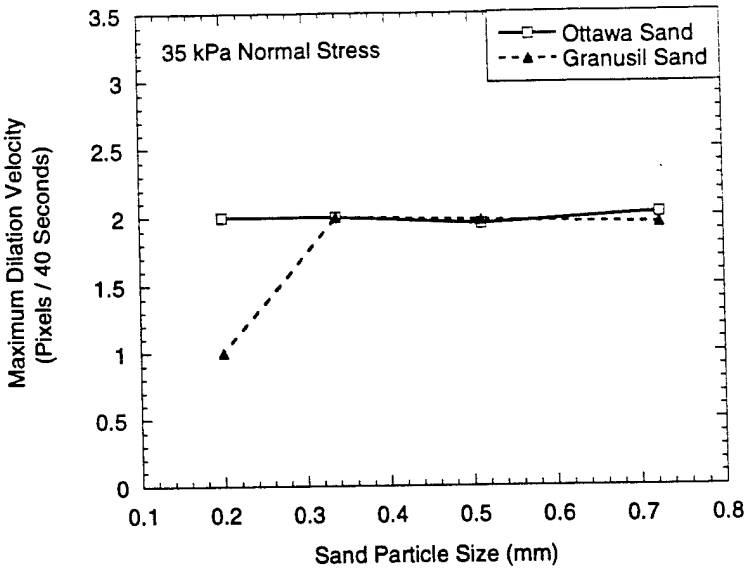

Figure 2-41 Maximum Dilation Velocity for Sand-on-Sand tests

2.3.3.7 Velocity of the Neutral Zone

For all sand-on-sand tests, the shear zone fully developed giving neutral zone velocities of 0 pixels / 40 seconds of time. This is shown graphically in Figure 2-42.

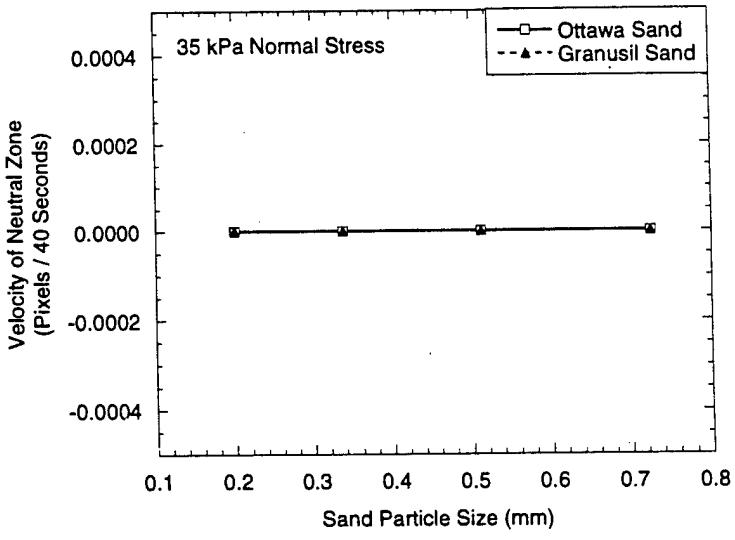

Figure 2-42 Velocity of Neutral Zone for Sand-on-Sand tests

2.3.4 Correlation of Mechanical and Image Parameters

Mechanical parameters obtained from this research were correlated to the image parameters by various regressions. Peak and residual friction angles were related to the velocity at the structural surface, shear zone thickness, and the fully developed shear zone thickness. The slope of the dilation curve was also related to the maximum dilation velocity. This section will present these relationships. No relation was found between the neutral zone velocity and any of the mechanical parameters. The relationships were determined for both normal stresses and for each sand type. In this section, only the low normal stress (35 kPa) and the peak friction angle plots will be presented. The reason for this is that the trends for the low and high normal stresses and for peak and residual friction angles are very similar. Differences occur in the regression equations but not the overall trends.

2.3.4.1 Velocity at Structural Surface

Figure 2-43 shows the relation between the velocity at the structural surface and the peak interface friction angle (δ). These two parameters can best be related by the linear relationship shown. As the interface friction angle (δ) increases, the sand particles are better engaged by the structural surface, increasing the velocity of the soil particles along the surface. The cluster of data at 7.9 pixels / 40 seconds is from when all particles are engaged by the surface and the velocity is equal to that of the structural surface (7.9 pixels / 40 seconds). Because there was such an increase in interface friction angle (δ) with an increase in surface roughness there is very little data between 25° and 35°. The behavior within this range is uncertain and should be noted. The R^2 values show acceptable fits for these data sets.

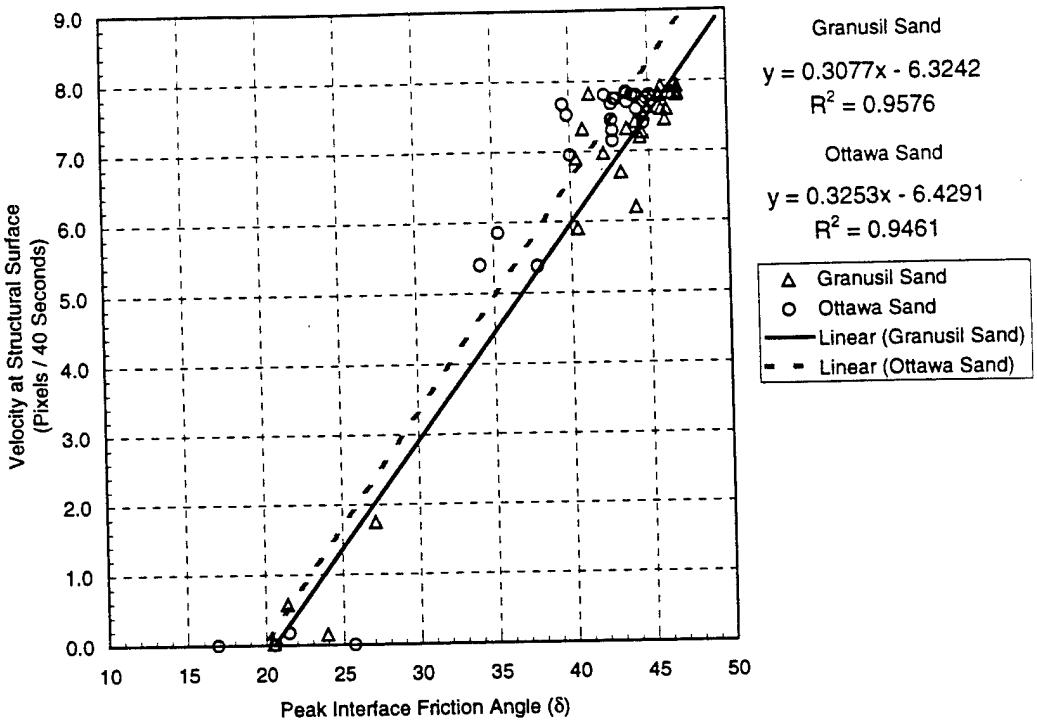

Figure 2-43 Velocity at Structural Surface vs. Peak Interface Friction Angle

2.3.4.2 Shear Zone Thickness

Shear zone thickness was related in both forms the data was presented in Section 2.3.3.2.2, in macroblocks from surface and in particle diameters from surface. Figure 2-44 shows the relation between the shear zone thickness in macroblocks from surface and the peak interface friction angle (δ). Figure 2-45 shows the relation between the shear zone thickness in particle diameters from surface and the peak interface friction angle (δ).

This parameter, in both forms presented, can best be related by the power function shown on each plot. As the interface friction angle (δ) increases, the sand particles are better engaged by the surface, increasing the shear zone thickness. Because there was such an increase in interface friction angle (δ) with an increase in surface roughness there is very little data between 25° and 35°. The behavior within this range is uncertain and should be noted. The R^2 values show acceptable fits for these data sets. The maximum thickness of the shear zone is 12 macroblocks equal to 4.8-mm. In terms of particle diameters, it is 18 particle diameters.

2.3.4.3 Fully Developed Shear Zone Thickness

The fully developed shear zone thickness was also related in both forms the data was presented in Section 4.3.2.3, in macroblocks from surface and in particle diameters from surface. Figure 2-46 shows the relation between the fully developed shear zone thickness in macroblocks from surface and the peak interface friction angle (δ). Figure 2-47 shows the

relation between the fully developed shear zone thickness in particle diameters from surface and the peak interface friction angle (δ). The trend in this data is very similar to the shear zone thickness correlation previously presented. This parameter in both forms presented can also be related by a power function. This correlation is shown on each plot respectively. As the interface friction angle (δ) increases, the sand particles are better engaged by the surface, increasing the shear zone thickness.

If the shear zones were able to fully develop, by running the tests out to larger amounts of displacement, this relation to the peak interface friction angle is expected. The R^2 values show acceptable fits for these data sets. The reason the fully developed shear zone thickness is larger than the measured shear zone thickness is that with larger particles the shear zone does not always fully develop. When the slope through the velocity profile is extrapolated to a neutral zone velocity of 0 pixels / 40 seconds, this leads to a fully developed shear zone thickness greater than the shear zone thickness.

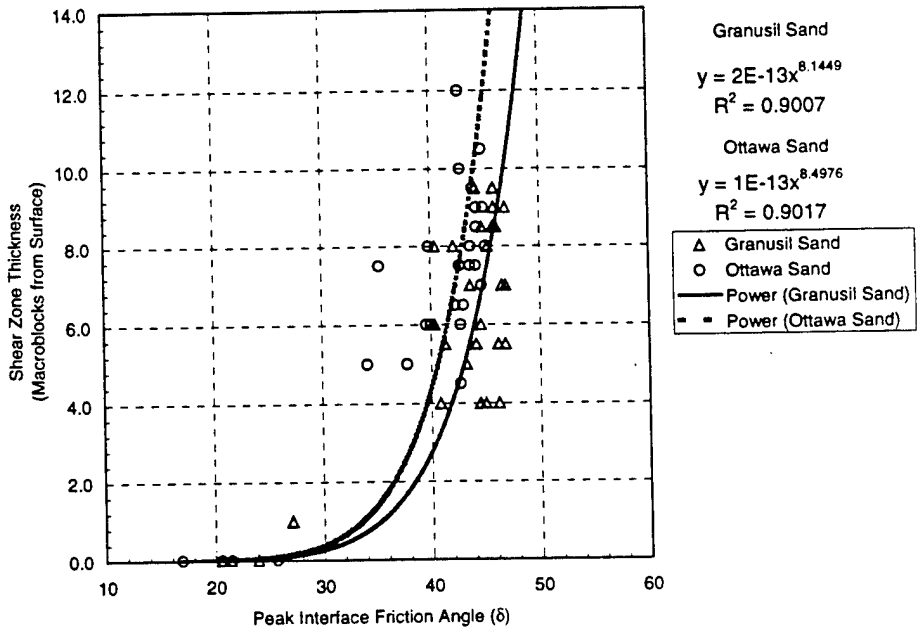

Figure 2-44 Shear Zone Thickness (Macroblocks from Surface) vs. Peak Interface Friction Angle

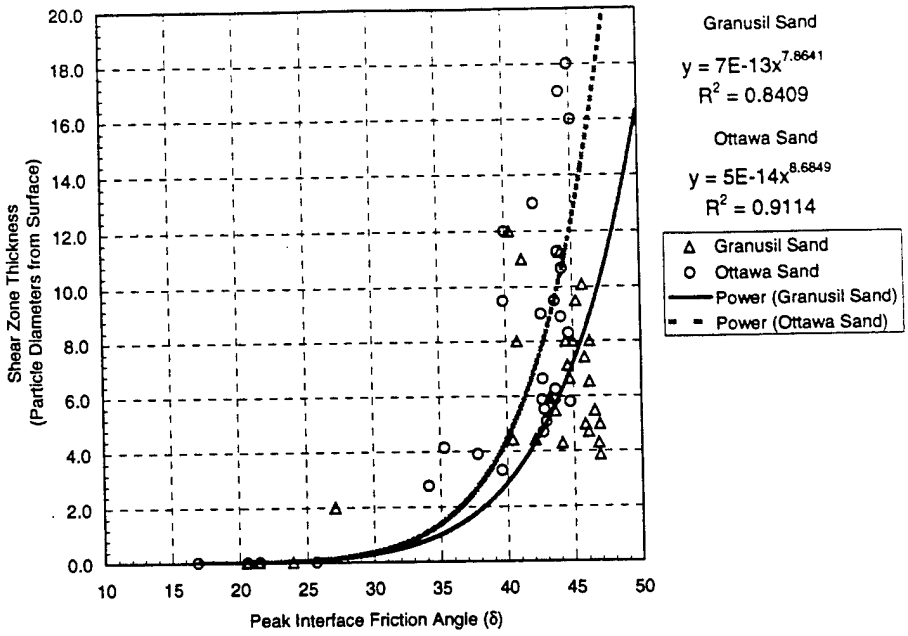

Figure 2-45 Shear Zone Thickness (Particle Diameters from Surface) vs. Peak Interface Friction Angle

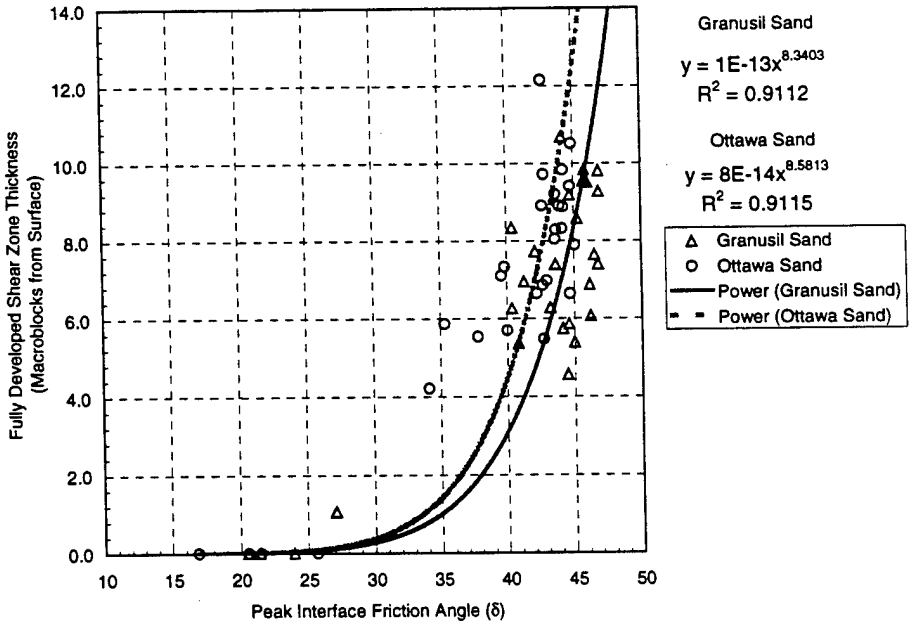

Figure 2-46 Fully Developed Shear Zone Thickness (Macroblocks from Surface) vs. Peak Interface Friction Angle

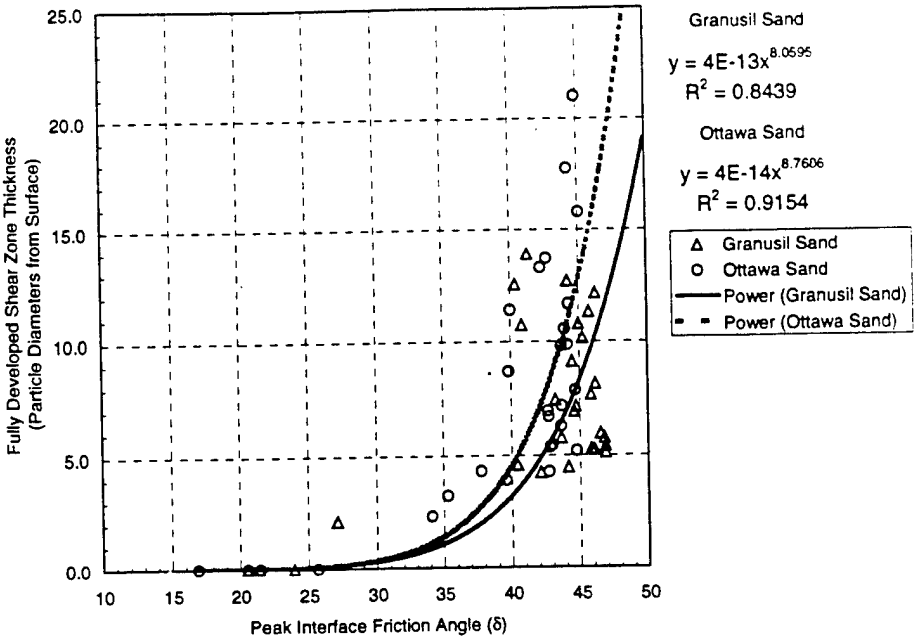

Figure 2-47 Fully Developed Shear Zone Thickness (Particle Diameters from Surface) vs. Peak Interface Friction Angle

2.3.4.4 Particle Dilation Correlation

The mechanical parameter, slope of the dilation curve (ψ_{max}) was related to the maximum dilation velocity. These two parameters can best be related by the linear relationship shown in Figure 2-48. Dilation curves with steeper slopes tend to have higher dilation velocities. Because there was such a significant change from the smooth steel surface (0.0059-mm) to the 0.037-mm (P240 paper) there is very little data between ψ_{max} of 0.00 and 0.15. The trend in this region is uncertain and should noted.

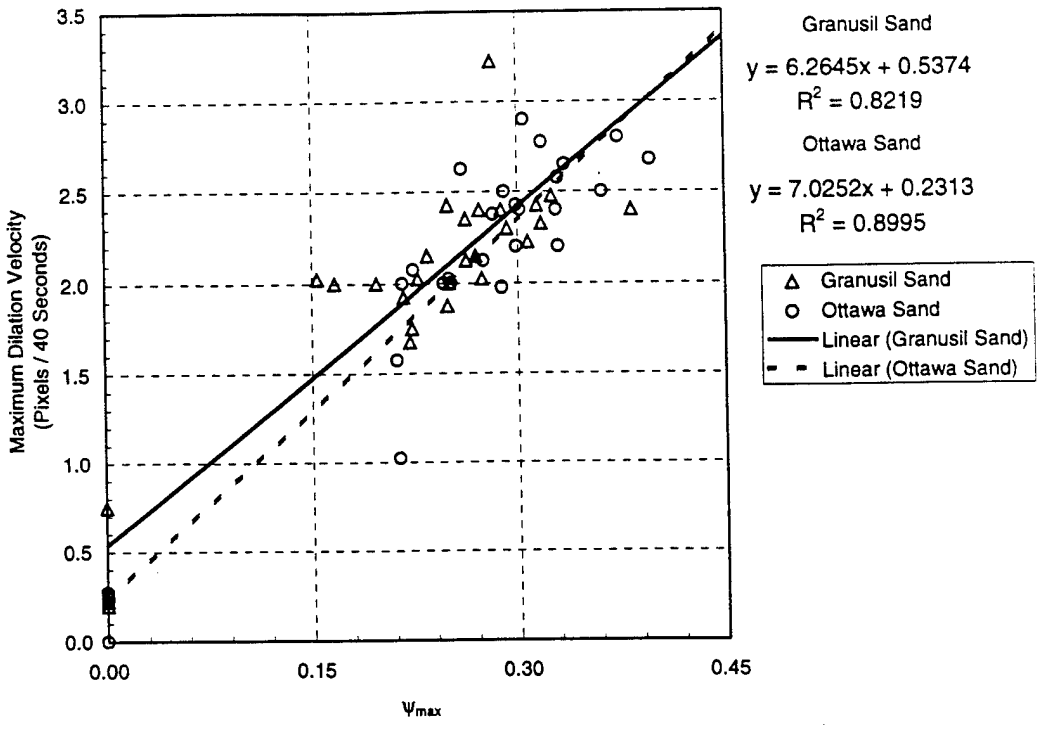

Figure 2-48 Maximum Dilation Velocity vs. Max Slope of Dilation Curve (ψ_{max})

2.3.5 Summary, Conclusions and Recommendations

The interface shear zone of a granular soil against a steel structural surface was successfully imaged and subsequently analyzed. The analysis of these images was accomplished using software that employed a block-based matching algorithm that yielded velocity vector data from image to image. Additionally, the strength data for this interface was also captured by conventional means and subsequently analyzed. Based on the analysis of this data, the following conclusions are drawn:

Image Data

1. For simulated shallow and deep soil elements (constant stress and constant volume tests) the only factor that is significant to the interface shear zone behavior is the roughness of the structural surface. This effect is most pronounced when the surface being used is very smooth. The addition of small ridges on this surface magnifies the measured response parameter.
2. A redesigned shear box and shear machine would aid in the acquisition of quality images. It is recommended that the present shear box window geometry be altered in order to fully view the moving structural surface.

Strength Data

1. For a simulated shallow soil element (constant stress test), the factors that are significant to the strength response behavior of the soil are the normal load, surface roughness, and a combination of both.
2. For a simulated deep soil element (constant volume test), the factor that is significant to the strength response behavior of the soil is the surface roughness.
3. As mentioned above, a redesigned shear box geometry would aid in the acquisition of strength data. The addition of the threaded rods, while beneficial to the image data was significantly detrimental to the quality of the strength data. It is recommended that the shear machine be further modified to allow the recording of accurate strength data without the addition of the threaded rods to prevent the upward movement of the shear box.

2.4 References

Albrecht, Brian, *Factors affecting the desiccation of compacted clay*, Final Report for Stat 424 Engineering Statistics (Madison WI, (University of Wisconsin,) 1997

ASTM D-422 Standard test method for particle size analysis of soils.

ASTM D-854 Standard test method for specific gravity of soils. *Test method A - Procedure for Oven-Dried Specimens.*

ASTM D-3080 Standard test method for direct shear test of soils under consolidated drained conditions.

ASTM D-4253 Standard test method for Maximum index density of soils using a vibratory table.

Bieganousky, W. A. and Marcuson, W. F., III, "Uniform Placement of Sand, " *Journal of the Geotechnical Division*, ASCE, Vol. 102, No. GT3, Mar., 1976, pp.229-233.

Bowles, Joseph E. Engineering Properties of Soils and their Measurement, 4th ed. (New York: McGraw-Hill, Inc., 1992).

Box, G.E.P., W.G. Hunter, and J.S. Hunter, Statistics for Experimenters, (New York: John Wiley & Sons, 1978).

Das, Braja M. Principles of Geotechnical Engineering (Boston: PWS Publishing Company, 1990)

Donohoe, G.W., M.F. Boccabella and J.J. Gill, "Segmentation and Object Tracking for the Microstructure Analysis of Soil," Proc. 26th Asilomar Conference on Signal, Systems and Computers, Pacific grove, CA, Nov. 4-6,1991.

Edil, Krizek, and Zelasko (1975) "Shear Behavior of sands as a function of Grain Characteristics. Istanbul Conference on SM & FE, vol. 1 pp 55-64.

Guler, Murat, *Image Processing Techniques in Geotechnical Engineering*, Master's degree thesis, University of Wisconsin, Civil Engineering Department, 1997.

Holtz, Robert D. And William D. Kovacs An Introduction to Geotechnical Engineering (Englewood Cliffs, New Jersey: Prentice Hall, 1981).

Hryciw, Roman D, and Masyhur Irsyam, "Behavior of Sand Particles Around Rigid Ribbed Inclusions During Shear," Soils and foundations, The Journal of the Japanese Society of Soil Mechanics and Foundation Engineering, Vol.33 No. 3 pp1-13 (1993).

Hryciw, Roman D., Scott A. Raschke and Masyhur Irsyam, *Interface Mechanics of Particulate Media with Ribbed Inclusions*, UMCEE Report No. 94-19, University of Michigan, Ann Arbor, Michigan, June 15, 1994.

Hryciw, Roman D., Scott A. Raschke, *Computer Vision for Large Deformations in Particulate Media: a Manual for "Particle Tracer"*, UMCEE Report No. 96-16, University of Michigan, Ann Arbor, Michigan, June 30, 1996.

Kimura, Ichiro, and Toshi Takamori, "Image Processing of Flow around a Circular Cylinder by using Correlation Technique." *Flow Visualization* IV Ed. Veret, C. pp. 221-226. Washington: Hemisphere, 1986.

Macari, E. J., Parker, J. K., and Costes, N. C., "Measurement of Volume Changes in Triaxial Tests Using Digital Imagine Techniques," Geotechnical Testing Journal, GTJODJ, Vol. 20, No. 1, March 1997, pp. 103-109.

Means, R. E. And J. V. Parcher Physical Properties of Soils (Columbus, OH: Charles E. Merrill books Inc. 1963)

Mitchell, James K. Fundamentals Soil Behavior, 2nd ed. (New York, John Wiley and Sons, 1993)

Raschke, Scott A., and Roman D Hryciw, "Micro-Deformations in Sand by Digital Image Processing and Analysis," *Presented at the Transportation Research board Annual Meeting, Session A2K01: Small Magnitude Measurements in Geotechnical Applications.* (Preprint of publication in TRB Research Record), (1996).

Walker, B. P., and Whitaker, T., "An Apparatus for forming Uniform Beds of Sand for Model Foundation Tests," *Geotechnique*, Vol. 17, 1967, pp.161-167.

Zelasko, Krizek, and Edil (1975) "Shear Behavior of sands as a function of Grain Characteristics. Istanbul Conference on SM & FE, vol. 1, pp 55-64.

3. Section Three, Numerical Simulations of Interface Experiments

3.1 ABSTRACT

An enhanced discrete element method for the numerical modeling of particulate media is presented. This method models a particle of general shape by combining several smaller particles of simpler shape, such as a circle, into clusters that act as a single larger particle. The clusters more accurately model the geometry-dependent behavior of the particles, such as particle interlock and resistance to rolling. The method is implemented within the framework of an existing DEM program without the introduction of new contact or force algorithms. An extensive set of numerical "experiments" is performed which demonstrate the method's effectiveness. The granular media-structure interface shear test simulations are performed using both clustered and non-clustered particles. The results indicate that the clustered particles undergo less rolling and provide for increased shear resistance of the medium.

3.2 INTRODUCTION

Deformation of soil-structure systems usually involves the creation of an interfacial shear or slip zone that is very close to the structure. This interface is often only a few particle diameters wide and has large localized strains[1]. For particulate media such as sand, the influence of individual particle rotations, relative grain displacement, and grain crushing on interface behavior such as shear resistance and dilatancy are poorly understood. Presently, the basis for most analysis and design of systems involving structure-particulate media interfaces is rooted in empirical relationships. In this paper we describe some enhanced numerical methods for modeling particulate media, and conduct an extensive series of numerical "experiments" to help elucidate important phenomena in soil-structure interface behavior.

Soil is inherently discontinuous and can be effectively modeled by the discrete element method (DEM). This method was originally developed by Cundall[2,3] for modeling two-dimensional jointed rock masses by idealizing a rock mass to consist of plane polygon-shaped rigid particles that interact along deformable frictional boundaries. In two dimensions, each particle brings three degrees of freedom to the model. The method was subsequently enhanced by Cundall and Strack[4,5,6] for applications to soils by idealizing a soil

---

[1] Z. Chen and H.L. Schreyer, 'Simulation of soil-concrete interfaces with nonlocal constitutive models', *J. engrg. mech. div.*, ASCE, **113**, 1665-1677 (1987).

[2] P.A. Cundall, 'A computer model for simulation of progressive, large-scale movements in blocky rock systems', *Proc. Symp. Int. Soc. Rock Mech., Nancy*, II, Art. 8, (1971).

[3] P.A. Cundall, 'A computer model for rock-mass behavior using interactive graphics for the input and output of geometric data', *Report AD/A-001.602* U.S. National Technical Information Service, (1974).

[4] P.A. Cundall and O.D.L. Strack, 'The distinct element method as a tool for research in granular media', PART I, *NSF Report Grant ENG76-20711*, (1978).

mass to consist of an assemblage of circular shaped rigid disks for two-dimensional idealizations, or spheres for three-dimensional idealizations. The rigid disks or spheres are usually very large in number, and interact through deformable frictional contacts with neighboring particles.

Such an approach opens up pathways to new knowledge of particulate media because it is possible to observe and quantify phenomena and minute detail on a microscopic level. In contrast, laboratory studies are useful for providing macroscopic information on real materials, but resists attempts to glean microstructural information because of the difficulty in viewing and/or measuring phenomena that are interior to the specimen.

While modeling particulate media with discs or spheres is computationally simple, it has been found that the particles tend to roll or rotate excessively[7]. In order to reduce particle rotations to more realistic levels, some researchers have employed the ad hoc, and perhaps ill-founded practice of artificially constraining the rotations of particles periodically throughout the course of a simulation[8]. Comparison of numerical simulations with typical response of laboratory specimens shows that DEM simulations using simple discs or spheres usually underestimates the shear resistance of the medium when the medium is subjected to uniform compressive loading.

Many individuals have enhanced DEM to include particles with more complex shapes that more closely replicate those in natural media. Walton[9] and Issa and Nelson[10] employed arbitrary polygon-shaped elements that are reminiscent of those used in fractured rock mechanics and established that such an approach yields better qualitative agreement with experiments. However, such an approach has some computational disadvantages (e.g., the contact detection scheme may be time-consuming because of the large number of surfaces that require monitoring). In fact, Ting, et al[11] report at least one order of magnitude increase in execution time for simulations using polygon-shape particles compared to circular, or disc-shaped particles. Additional disadvantages arise from treatment of the vertices that are

---

[5] P.A. Cundall and O.D.L. Strack, 'A discrete numerical model for granular assemblies', *Geotechnique,* **29**,47-65 (1979)

[6] P.A. Cundall and O.D.L. Strack, 'The distinct element method as a tool for research in granular media', PART II, *NSF Report Grant ENG76-20711*, (1979).

[7] J.M. Ting, L.R. Meachum, and J.D. Rowell, 'Effect of particle shape on the strength and deformation mechanisms of ellipse-shaped granular assemblages', *Eng. comput.*, **12**, 99-108 (1995).

[8] R. Dobry and T. Ng, 'Discrete modelling of stress-strain behaviour of granular media at small and large strains', *Eng. comput.* **9**, 129-143 (1992).

[9] O.R. Walton, 'Particle-dynamics calculations of shear flow', in J.T. Jenkins and M. Satake (eds) *Mechanics of Granular Material: New Models and Constitutive Relations*, Elsevier, Amsterdam, 327-338 (1982)

[10] J.A. Issa and R.B. Nelson, 'Numerical analysis of micromechanical behaviour of granular materials', *Eng. comput.*, **9**, 211-223 (1992).

[11] J.M. Ting, B.T. Corkum, C.R. Kauffman, and C. Greco, 'Discrete numerical model for soil mechanics', *J. geotech. engrg. div.*, ASCE, **115**, 379-398 (1989).

present in polygon-shaped particles. Ambiguities occur in specifying whether a contact should be treated as edge-edge, edge-corner, or corner-corner, and switching from one contact type to another is difficult. There also is no unique outward normal direction at a vertex. Furthermore, extension from 2-D to 3-D is much more complex in comparison to extensions using simple particle shapes[12,7]. In order to address these problems, Ting et al[12] developed elliptically-shaped particles and established that such an idealization better replicates the resistance of particles to rotation that is observed in natural media. Also, an elliptical particle has a unique outward normal direction, and has a surface that is represented by a single function. Disadvantages with elliptical particles is that the contact detection algorithm, while substantially faster than that for polygon shaped particles, is still not as efficient as those for simple circular disks and spheres. Also, extensions that might allow for modeling of additional details of particle roughness are not clear.

In this paper, we develop an idea for modeling rough particles based on *clustering*. A cluster is an assemblage of particles having simple shape. While this idea is probably not new, in this paper we thoroughly explore its utility and usefulness in modeling natural particulate media, and attempt to glean important information on the micromechanical aspects of particulate media deformation. Work related to clustering has been done by Trent and Margolin, wherein they bond particles together to model fracture in cemented granular solids. Also, rigid clusters have been used by Walton and Braun[13] and Qiu and Kruse[14] to model particle flow in rotating drums and in conveyor transfer chutes, respectively. In Section 3.3, we provide a brief overview of DEM modeling. In Section 3.3.1, we describe clustering in detail and in Section 3.3.2, a periodic boundary treatment is described. The numerical simulations are described in Section 3.4 and the results of these simulations are thoroughly discussed in Section 3.5.

3.3 DISCRETE ELEMENT MODELING

We have conducted our DEM modeling using a highly modified version of the program TRUBAL[5,6]. In this implementation of DEM, particles are modeled as rigid circular discs in 2-D, or rigid spheres in 3-D. As shown in Figure 3-1, each inter-particle contact is modeled with a normal-direction spring and dashpot, and a spring-dashpot-slider assembly in the tangential direction. The nonlinear force-displacement relations are shown in Figure 3-2 in which it is seen that the normal direction behavior is linear-elastic with a no-tension limit, and the shear direction behavior is linear-elastic with a Coulomb friction limit. In 2-D, each particle has three degrees of freedom, two translational and one rotational. For many problems, the rate of loading is sufficiently high that inertial forces are important. However, even for quasi-static loadings, such as those considered in this paper, inertial forces are included in the discretization so that explicit time integration can be used to find a sequence

---

[12] J.M. Ting, M. Khwaja, L.R. Meachum, and J.D. Rowell, 'An ellipse-based discrete element model for granular materials', *Int. j. numer. analytic. meth. geomech.*, **17**, 603-623 (1993).

[13] O.R. Walton and R.L. Braun, 'Simulation of rotary-drum and repose tests for frictional spheres and rigid sphere clusters', *Joint DOE/NSF Workshop on Flow of Particulates and Fluids*, Sept. 29 - Oct. 1, 1993, Ithaca, NY.

[14] X. Qiu and D. Kruse, 'Analysis of flow of ore materials in a conveyor transger chute using discrete element method',

of equilibrium solutions. If inertial forces are omitted, which is certainly warranted for the slow loading rates considered in this work, an implicit solution scheme would need to be used. But, implicit methods are difficult to implement and achieve convergence for problems that are as strongly nonlinear as those considered here.

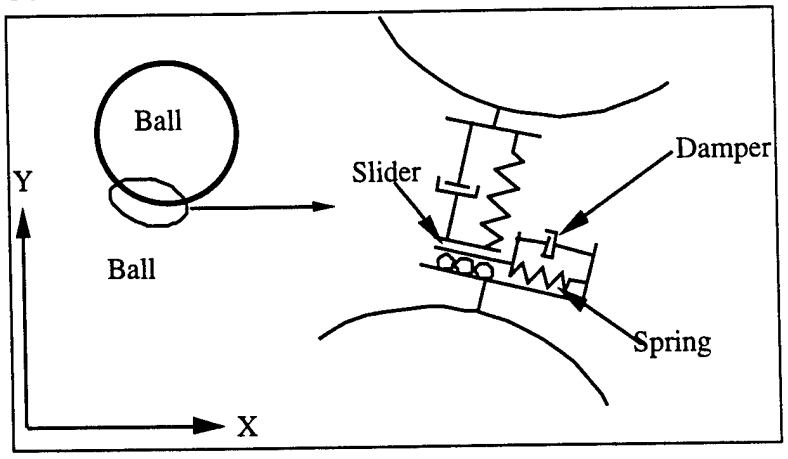

Figure 3-1 Particle contact model as idealized in DEM.

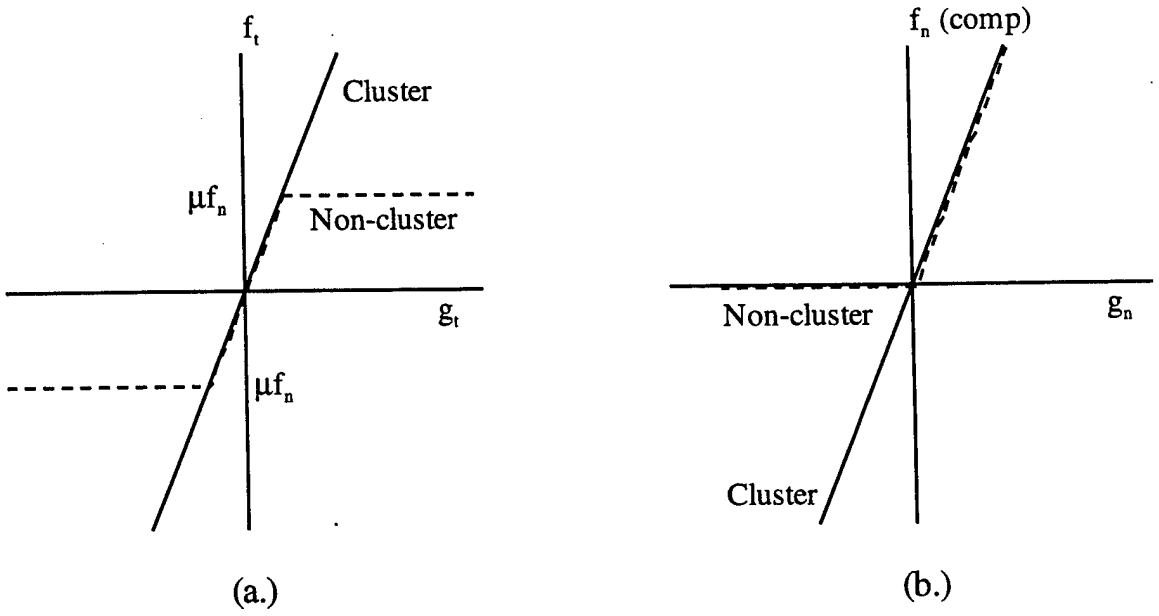

Figure 3-2 Interparticle load-displacement relationships. a.) The shear force load-displacement relationship. For the non-cluster particles, when the tangential forces reach μf_n the particles slip perfectly plastically. No slip is allowed between the particles which make up the cluster. b.) The inter-particle normal load-displacement relationship. No tension is allowed at contacts where non-clustered particles are involved.

The equations of motion are integrated in time using the explicit central difference method. This method is easy to implement for nonlinear problems such as this and is fairly robust and shows good accuracy, but is only conditionally stable. With no damping, the linearized

time step stability limit is $\Delta t < 2/\omega_{max}$ where ω_{max} is the instantaneous highest natural frequency of vibration for the system; see Cook, Malkus and Plesha[15]. In most implementations of explicit time integration, including TRUBAL, a global stiffness matrix is not formed and hence, computation or estimation of ω_{max} is not possible. Furthermore, bounding of ω_{max} using a Fried inequality is also not possible; see Plesha[16]. Thus, an ad hoc scheme for time step selection is used in TRUBAL wherein $\Delta t = \alpha\sqrt{m_{min}/k_{max}}$ in which k_{max} is the largest interparticle spring stiffness, m_{min} is the mass of the smallest particle, and α is user-selected parameter. Computational experience suggests that taking α to be of the order 0.1 is typically satisfactory to provide a stable computation. However, stability is not guaranteed by this criterion for all problems and it is quite possible to have a momentary instability that is subsequently arrested. Since no additional measures of solution stability, such as an energy balance, are implemented, users should be cautious of solution quality.

3.3.1 CLUSTERS

To model rough particles more naturally and effectively, we have developed the concept of a *cluster*. As shown in Figure 3-3a, naturally occurring particles are rarely circular and a disc or sphere does not closely model reality. Figure 3-3b shows a circular particle superimposed on a natural particle. As a discrete model, the circle also does not capture the effects of the particle shape or the surface asperities of the particle. As previously discussed, modeling of natural particles using circular particles results in excessive particle roll and in inaccurate moment computation due to applied normal forces[12].

By combining a number of simple circular-shape particles in a semi-rigid configuration, a better model of a natural particle is constructed. As seen in Figure 3-3c, a number of particles can be joined together in a configuration that closely resembles an actual particle. Any number of particles may be linked together to form a "cluster." The only requirement is that the particles forming the "cluster" rotate and translate essentially as a rigid body. Figure 3-3d shows examples ranging from three particle "clusters" to different configurations of six particle "clusters."

To force the individual particles of a cluster to behave as a rigid body, the interparticle contacts within the cluster are constrained to be linear-elastic as shown in Figure 3-2. Hence, interparticle contacts within a cluster are allowed to support unlimited tension and shear force. One of the advantages to clustering is that the internal workings of TRUBAL remain unchanged in regards to contact detection (which is very efficient for circular-shape particles), time integration, and internal force computations (excepting very minor modifications to render cluster interparticle contacts to remain linear-elastic). The program recognizes all of the particles that make up a cluster as a separate entity.

---

[15] R.D. Cook, D.S. Malkus, and M.E. Plesha, *Concepts and Applications of Finite Element Analysis,* John Wiley and Sons, New York, (1989).

[16] M.E. Plesha, 'Eigenvalue estimation for dynamic contact problems', *J. engrg. mech. div.,* ASCE, **113**, 457-462 (1987).

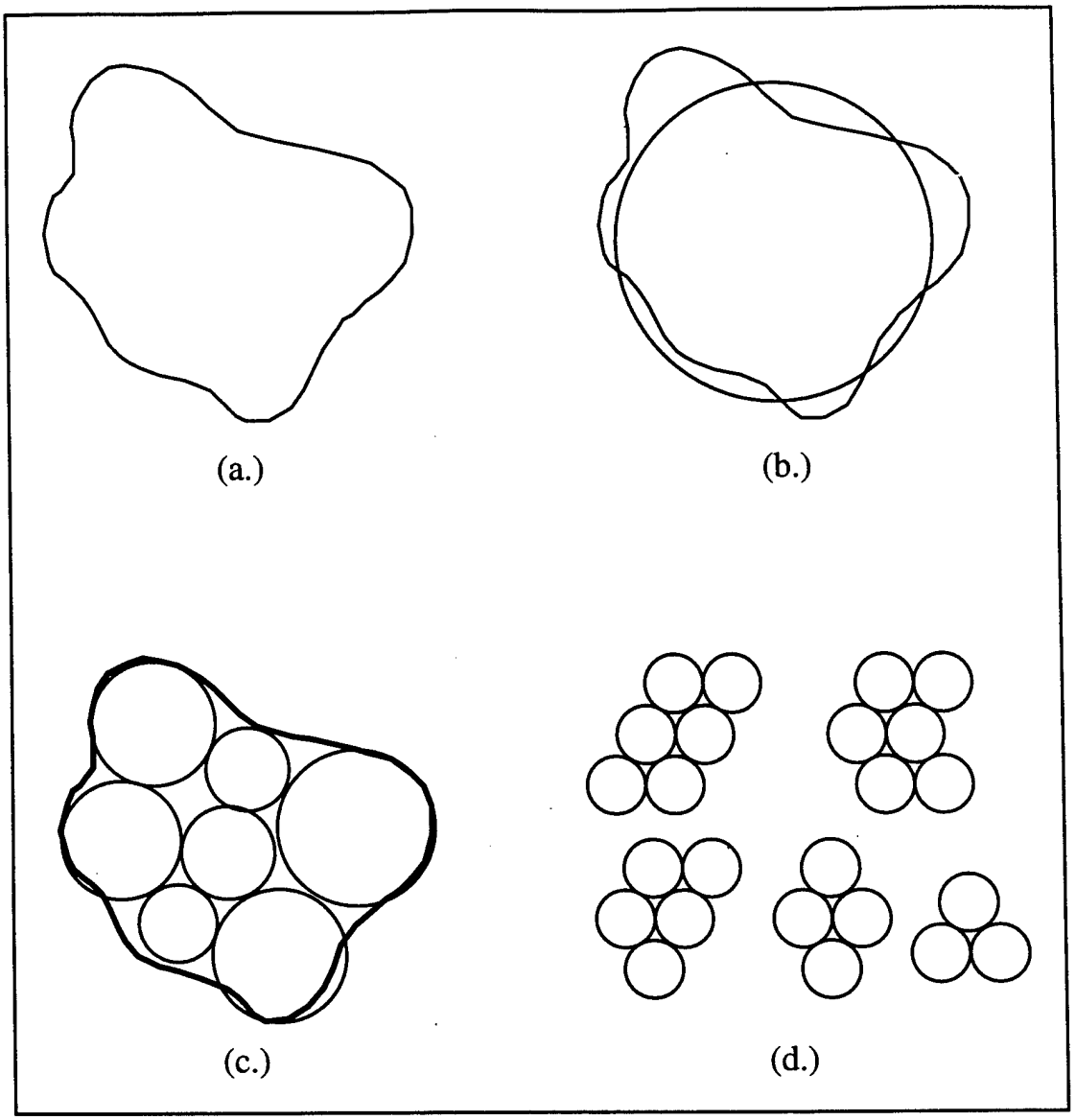

Figure 3-3 a.) Outline of sand particle. b.) DEM disc element superimposed over sand particle. As can be seen in this figure, the disc element does not model the geometry of an actual particle very closely. As a result, using discs results in excessive roll and inaccurate moment computations. c.) Any number of DEM particles are joined together in a rigid configuration, called a "cluster," which closely resembles the actual particle. The particles forming the "cluster" rotate and translate as a rigid body. d.) "Clusters" can be formed in any arbitrary combination and with any number of DEM particles. This figure shows several possible combinations. As a first step, the work done to this point uses "clusters" composed of three DEM particles.

Clustering offers many features. One of them is to handle particles of potentially very complex shape, though in this paper we restrict our attention only to three-particle clusters as shown in Figure 3-4. Phenomena such as damage and grain crushing, which could not be explored by prior DEM approaches, can be easily investigated. In a subsequent paper, we investigate some objective criteria for grain crushing and the implications of this on shear zone formation and behavior. Also, the simplicity and speed of the contact detection algorithms for simple-shape particles are retained. Extension to 3-D is very straightforward. The major disadvantage to clustering is a substantial increase in the number of degrees of freedom for a discretization. The circular or elliptical particles in DEM has three degrees of freedom (DOF). With clustering, each cluster has a total number of DOF equal to $3n_c$ where n_c is the number of particles within a cluster. Thus, an equivalent cluster model for a medium would have about n_c times the number of DOF as a model that uses just circular or elliptical particles. Considering that explicit time integration is used, this implies a roughly proportional increase in simulation time of about a factor of n_c using serial computing. However, in the case of circular particles, the results of a cluster simulation should be substantially more accurate, while in the case of elliptical particles, it is expected that the simulation time would be partially compensated by the more efficient contact detection algorithm used by clustering. Also, there would perhaps be an improvement in accuracy since it is possible to more accurately model the shape and roughness present in natural particles.

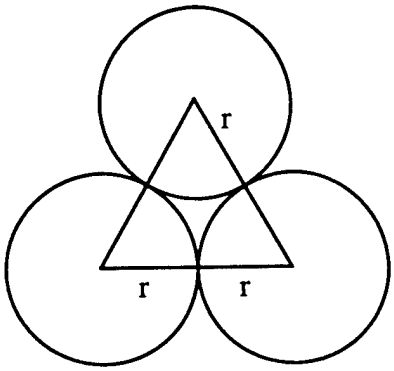

Figure 3-4 A simple three-particle "Cluster".

3.3.2 PERIODIC BOUNDARIES

Because of limited computing capacity, the total number of particles that can be realistically used in a DEM simulation is small in comparison to the actual number of particles existing in any laboratory sample or actual engineering situation. In order to increase computing efficiency as well as remove any deleterious boundary effects, *periodic boundaries* are

used. Campbell and Brennen[17] developed periodic boundaries for use in numerical simulation of granular shear flows. The periodic boundaries allow a particle to pass out of one side of the problem domain and automatically reappear on the opposite boundary such that truly periodic conditions are enforced. When the particle reappears at the opposite boundary, it has the same y-coordinate (see Figure 3-5) and velocity with which it left. Therefore, the control volume is infinitely replicated on both sides. This allows the side boundary condition to be infinite and thereby removes the unwanted influence of a nearby wall. In the DEM simulations where the number of particles is restricted due to computing capacity, removal of boundary effects of a wall greatly increases the accuracy of the solution.

For example in Figure 3-5a, as particle *i* passes out the right hand side boundary, another particle with exactly the same motion is introduced at the left boundary. That is, when particle *i* first touches the right boundary (or left), a new particle is introduced at the left boundary (or right) with the same horizontal position, y_i, and with vertical position decremented by the period L. As particle *i* straddles the right hand boundary, its position is x_i, y_i with total rotation θ_i. The new particle *i'* that was introduced at the left boundary has position x_i - L, y_i and rotation θ_i. During this period of time, the particles have exactly the same kinematics ($u_{xi'} = u_{xi}$, $u_{yi'} = u_{yi}$, and $\theta_{i'} = \theta_i$). Also during this period, particle *i* and *i'* are scanned for new contacts that might develop. Figure 3-5b shows the free body diagram for particle *i* in which contact forces f^1,t^1 through f^3,t^3 are produced from contacts of particle *i* with other particles near the right hand boundary while contact forces f^4,t^4 are produced from contact with a neighboring particle near the left hand boundary.

3.4 NUMERICAL SIMULATION

Simulations (i.e., numerical experiments) were performed to demonstrate the effectiveness of clustered particles compared to simple circular particles and to investigate microstructural interface phenomena. The parameters that are varied in these simulations are the use of clustered particles versus non-clustered particles, the roughness of the shearing structure surface, and the magnitude of the applied normal force. The simulations model a two-dimensional shear test where particles are first compacted into a domain, a constant normal stress is then applied to the mass of particles, and finally the bottom surface of the domain, which represents the rough surface of a structure, is displaced at a constant shear strain.

The non-clustered discretizations consist of 1000 simple circular particles and the clustered discretizations consist of 1000 three-particle clusters, (Figure 3-4). The particles in the non-clustered sets are discs with a radius of D=4.31 length units. The clusters are comprised of three discs with the center of each disc at the vertex of an equilateral triangle having sides of two times the radius of the discs. The discs in each cluster have a radius of 2.0 length units. This results in the radius of the circle circumscribing a cluster to be D=4.31 length units, i.e., equal to the radius of a non-clustered particle. In all cases, the particles in the non-clustered sets have the same material properties as the particles in the clustered sets. The mass density of each particle is 1.0 mass units per length unit cubed. The normal and shear stiffnesses at the contact between two particles, or a particle and a structure surface are $7.5x(10)^8$ force units per length unit. The coefficient of friction at the contact between

[17] C.S. Campbell and C.E. Brennen, 'Computer simulation of granular shear flows', *J. fluid mech.*, **151**, 167-188 (1985).

two particles or a particle and a surface is 0.4, similar to quartz particle-quartz particle surface friction[18]

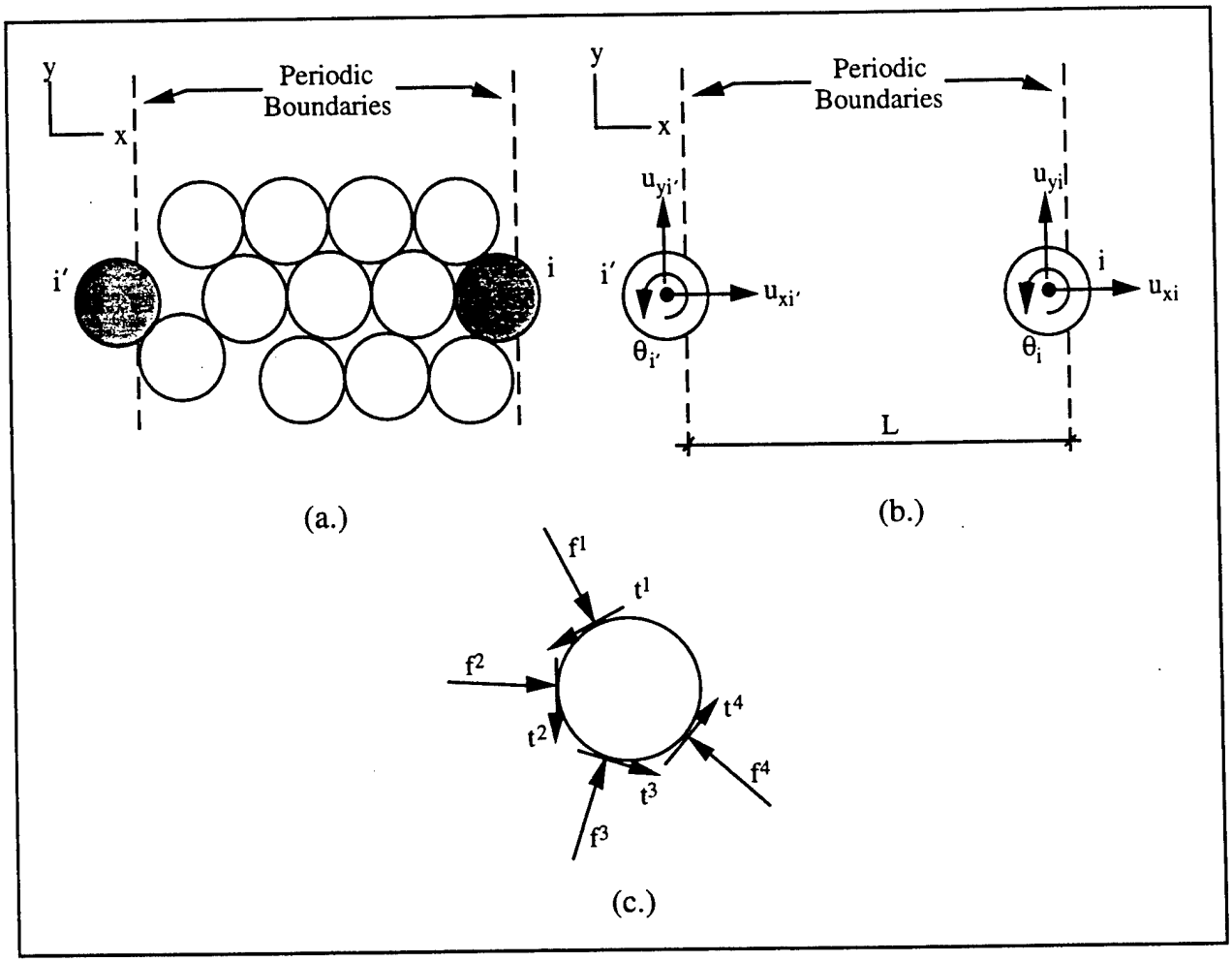

Figure 3-5 a.) Assemblage of circular particles with vertical periodic boundaries, b.) introduction of particle i' at left-hand periodic boundary as particle i leaves right-hand periodic boundary, c.) contact forces on particle i which straddles a periodic boundary.

The numbers for stiffness and mass are arbitrarily picked, but it is not expected that they change the dynamic characteristics of the problem for the following reason. The characteristic time scale for the medium is related to $\sqrt{m/k}$ where m and k are the mass and stiffness, respectively. Since we are integrating the equations of motion at very close to the stability limit for explicit time integration, and are shearing the surface wall uniformly at a

[18] P.W. Rowe, 'The stress-dilatancy relation for static equilibrium of an assembly of particles in contact', *Proceedings of the Royal Society*, **A269**, 500-527 (1962).

slow rate (relative to $\sqrt{m/k}$) over the entire duration of the simulation, the time scale for the loading relative to the time scale for structure response remains constant regardless of the particular values of *k* and *m*. This conjecture is supported by numerical experiments.

The non-clustered and clustered data sets were both generated in a domain that is initially 450 length units wide by 400 units high. The domain has a structure surface, or wall, on the bottom of the domain, periodic boundaries on the two vertical sides of the domain, and a horizontal surface at the top of the domain. The particles were then compacted by applying a normal force to the top surface, which acts as a rigid surface to constrain the particles within the domain. The domain can be viewed as simulating a two-dimensional vertical section in a ring shear test as opposed to a direct shear or a simple shear test because there are no vertical side boundaries but periodic boundaries. This compaction procedure generated clustered sets with an aspect ratio (Length:Height) of about 4:1 and non-clustered sets with an aspect ratio of about 3:1. The corresponding two-dimensional porosities were on the average 17 and 16 percent for the clustered and nonclustered sets, respectively. The porosity of the clustered sets is calculated with the intracluster void being counted as solid. Examples of non-clustered and clustered sets can be seen in Figure 3-6 and Figure 3-7, respectively. Three different normal forces are considered: $5.0x(10)^7$ force units, $10.0x(10)^7$ force units, and $20.0\ x(10)^7$ force units. Each data set was initially compacted under the lowest normal force, $5.0x(10)^7$ force units. On this initial particle structure, or fabric, the normal force was increased in a stepwise fashion, first to $10.0x(10)^7$ force units, then to $20.0\ x(10)^7$ force units. Applying the normal force increases in this fashion maintained the same basic particle assembly structure, thereby giving uniformity from simulation to simulation.

Several different cases were run for the clustered particles where all boundary conditions such as the geometry of the shearing surface and the applied normal stress were held constant while the packing arrangement of the particles was altered. The location of newly generated particles is based upon the random generation of locations within the specified domain. These locations are randomly generated from a program input seed value. By altering the seed, new configurations of particles were created. The results of these simulations showed that the general behavior from run to run was the same in regards to shear stress and dilation as well as the average shear displacement and rotation of the particles. The shapes of the curves were all qualitatively similar with minor quantitative differences.

There are four different roughnesses of the shearing surface (i.e., structure surface) that are considered. These roughnesses are modeled using a sawtooth shape with different amplitude and period. The first of the four shearing surfaces is a smooth wall with a coefficient of friction of 0.4, between the particles and the wall. The remaining cases use a sawtooth surface with a slope of 45° with respect to the horizontal, and with periods (being defined as the distance from the top of one sawtooth to the top of the next sawtooth) of $\lambda=4D$, $2D$, and $0.5\ D$ where *D* is as defined above. In the case of $\lambda=4D$ (the roughest surface considered here), the period of the sawtooth surface is four times the diameter of a cluster. The two finer surfaces have similar interpretations.

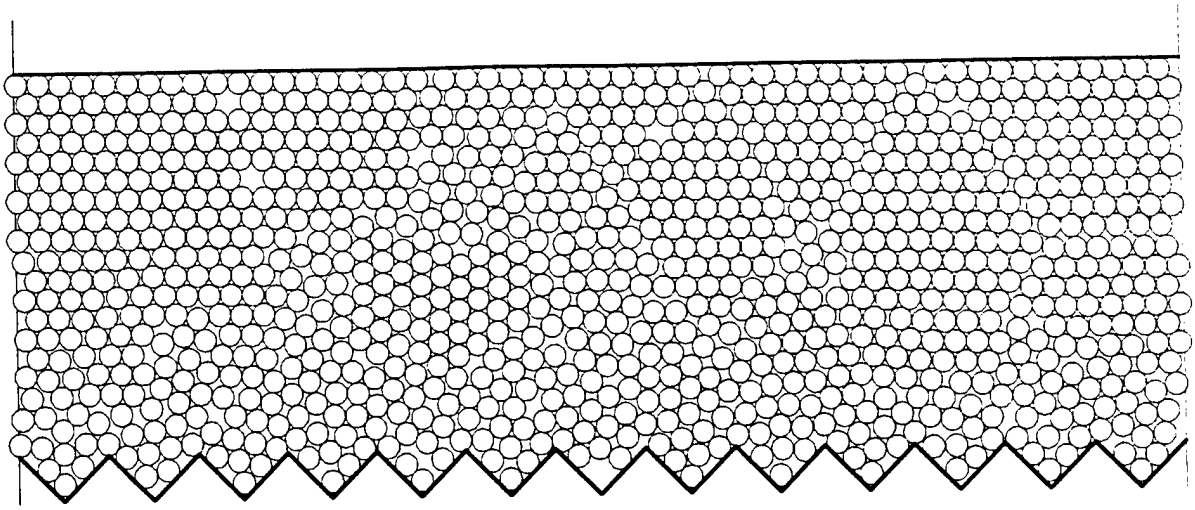

Figure 3-6 Compacted set of 1000 non-clustered particle. The sawtooth wall is the shearing surface. The sawtooth shown has a period of four times the diameter of the non-clustered particles, $\lambda = 4D$. Other simulation sets had shearing surfaces of $\lambda = 2D$, 0.5D, and no sawteeth (but where the particles in contact with the shearing wall were fixed to the wall). The sets also had applied normal stresses, $\sigma_n = 5x(10)^7$, $10x(10)^7$, and $20x(10)^7$ units of stress. The side boundaries of all sets are periodic. Periodic boundaries allow particles that exit one side to reappear on the opposite side with the same position and velocity.

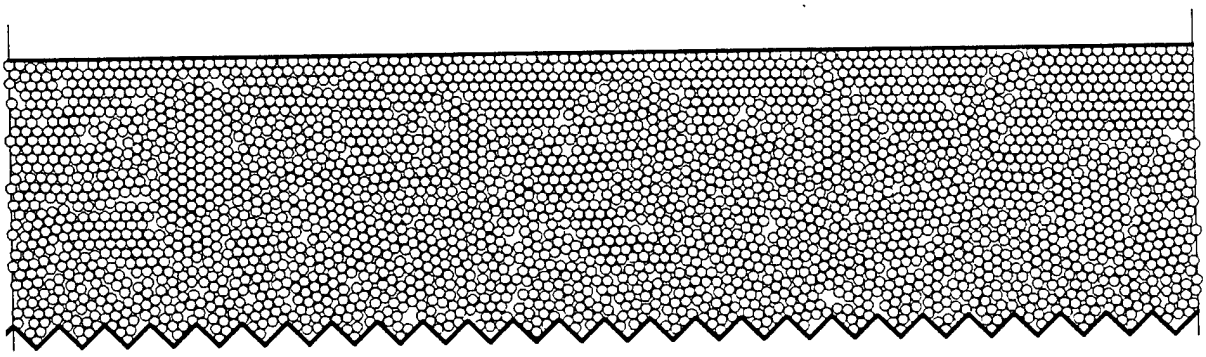

Figure 3-7 Compacted set of 1000 "clustered" particles (3000 DEM particles total). The shearing surface has a period of two times the "cluster" diameter. The "cluster" diameter is equal to the diameter of the non-clustered particles.

Once the sets have been compacted, the particles in contact with the top surface are glued to that surface. Hence, they have no rotation and no horizontal displacement, but do have the same vertical displacement as the top surface. This was done in order to insure that the shear zone, if one forms, would be within the medium or near the shearing surface, rather than at this boundary. A total of 24 numerical simulations were performed from which comparisons and verifications of the procedure are taken. In addition, a numerical simulation was performed with a three-fold increase in the width of the domain and a subsequent increase in the total number of clustered particles. This additional run was performed to verify that the width of the domain was sufficiently large for accurate use of the

periodic boundaries and that the results do not appreciably change with an increase in the domain size. This additional run also demonstrated that as the number of particles in contact with a rough structure surface increases, the smoothness of the shear stress vs. shear displacement curves increases. A numerical simulation with a three-fold increase in the height of the domain was also performed. The results of this run showed no significant qualitative variation from the results of the standard domain. These additional runs verified that if the domain is of sufficient size, a varying aspect ratio should have little effect on the results of the numerical modeling.

3.5 DISCUSSION OF RESULTS

Four basic measurements have been extracted from the numerical simulations:

1) the shear force required to displace the sawtooth shaped shearing surface,
2) the dilation of the mass of particles which is measured by recording the normal displacement of the top wall,
3) the particle displacements due to the displacement of the shearing surface, and
4) the rotation of the particles.

The particle displacement is measured as the change in the vertical and horizontal position of a particle with respect to its original position at the time when the shearing surface began displacing. The particle rotation is measured as the amount of rotation the particle undergoes from the time shearing surface displaces. The mass is divided into ten horizontal layers and the average displacement and rotation of the particles within each layer are computed. The applied force is proportional to an applied stress since the gross areas are the same in all simulations and will henceforth be referred to as a stress. Figure 3-8 is a montage of graphs showing the shear stress versus the tangential displacement of the shearing surface and the normal displacement of the top wall versus the tangential displacement of the shearing surface. Each graph in the montage contains three data sets that vary by the size of the applied normal stress. The three data sets use an applied normal stress of $5x(10)^7$ force units, $10\ x(10)^7$ force units, and $20\ x(10)^7$ force units, respectively. In each column of Figure 3-8, the graphs are grouped together as either clustered particles or non-clustered particles. The rows of the montage are grouped based upon the roughness of the shearing surface, with the top row having the greatest degree of roughness and the degree of roughness decreasing downward row by row. Figure 3-9 is a montage of the graphs showing the average displacement and average rotation in a layer versus the location of the layer. It is organized in the same manner as Figure 3-8 with the columns of graphs grouped according to whether the particles are clustered or not and the rows grouped according to the roughness of the shearing surface.

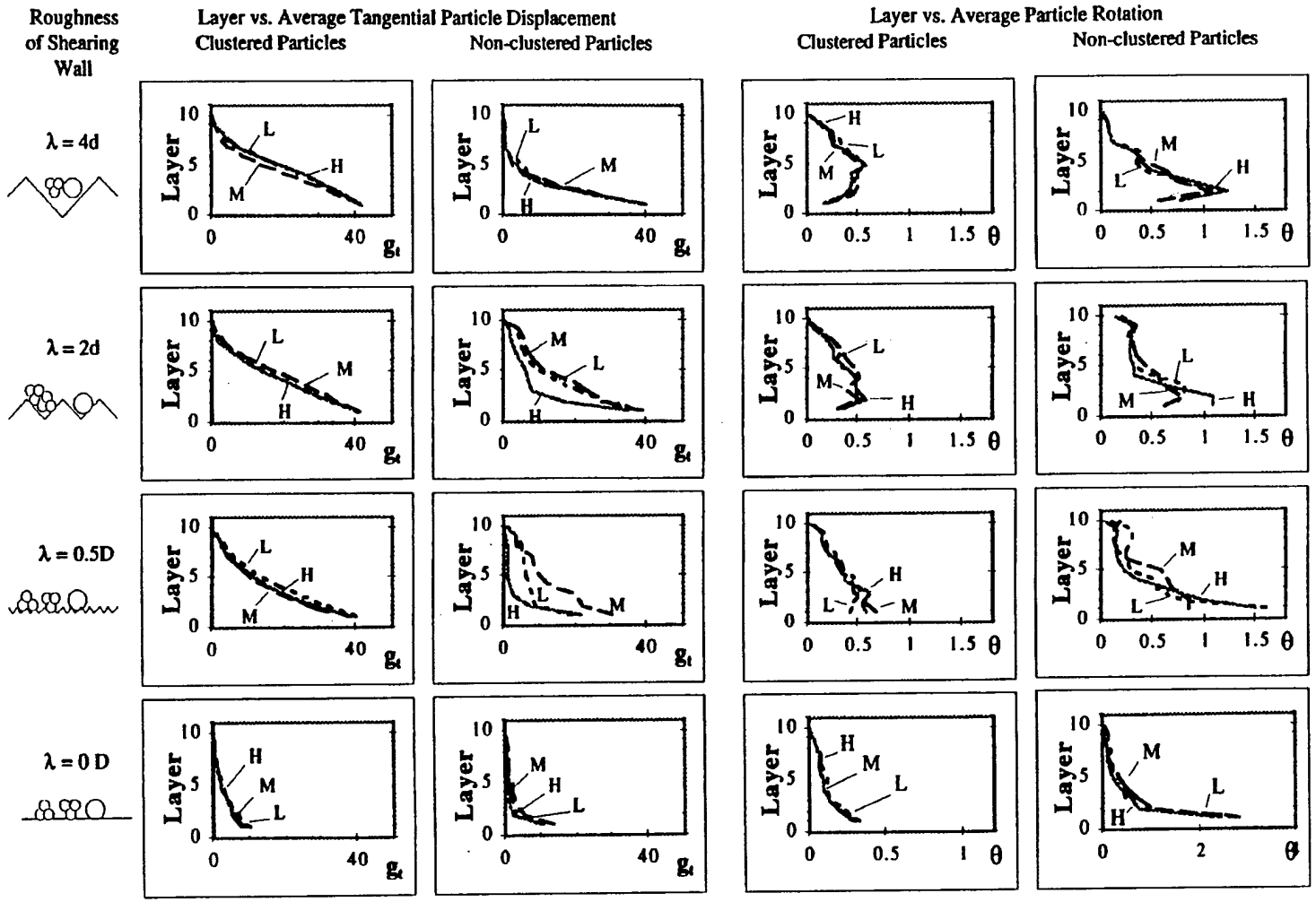

Fig. 3-9. Graphs of Average Displacement by Layer versus Tangential Displacement of Shearing Wall and Average Rotation by Layer versus Tangential Displacement of Shearing Wall for all cases. Each data set is divided into 10 equal horizontal layers with layer number one adjacent to the shearing wall and layer number ten farthest from the shearing wall. The average displacement (or rotation) in a layer is the average displacement (or rotation) of all particles in that layer. The value of shear displacement (g_t) is in length units and the value of average rotation (θ) is in radius

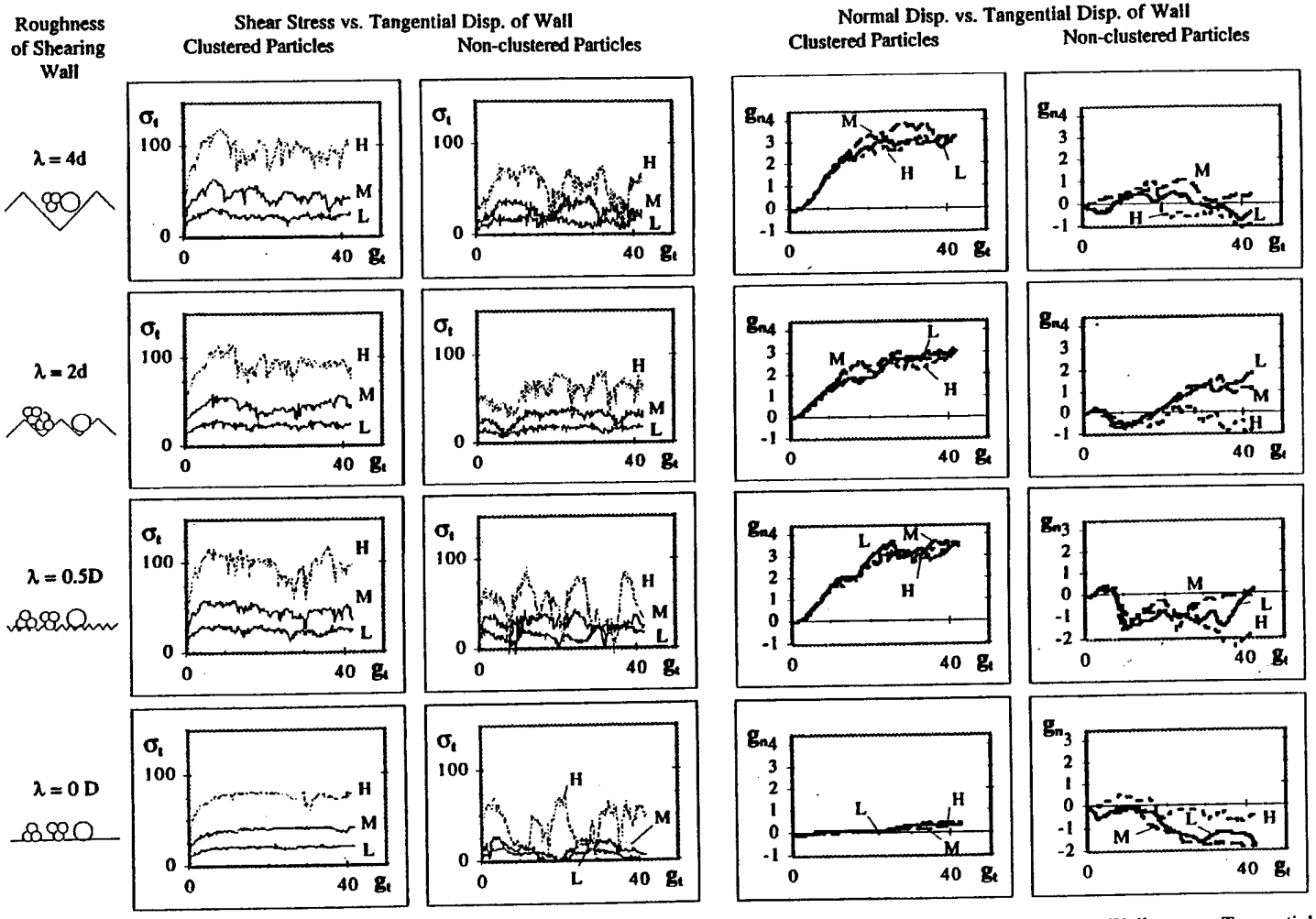

Fig 3 -8. Graphs of Shear Stress at Shearing Wall versus Tangential Displacement of Shearing Wall and Dilation of Top Wall versus Tangential Displacement of Shearing Wall for all cases. Each graph shows the results of three different normal loadings. The cases are differentiated by H, M, and L. H represents the case with $\sigma_n = 20 \times (10^7)$, M is the case with $\sigma_n = 10 \times (10^7)$, and L is the case with $\sigma_n = 5 \times (10^7)$. In the Shear Stress versus Tangential Displacement graphs, the value of shear stress (σ_t) is in 10^5 stress units. The values of shear displacement (g_t) and normal displacement (g_n) in all graphs are in length units

In all cases, the displacement that the shearing surface underwent was the same. The amount displaced was equal to about ten times the diameter of a clustered particle. The amount of shearing was decided based upon a reasonable number of time steps and achievement of steady state stress-strain behavior.

The shear stresses shown in the shear stress versus shear displacement plots of Figure 3-8 are computed by the summation of all horizontal force components that are in contact with the shearing surface. The relatively large fluctuations in the shear stresses seen as the shearing takes place could possibly be due to two related causes. The first is related to the number of particles used in the simulation. The contribution of each particle to the shear stress is summed for the total sawtooth wall. As particles make new contacts with the wall, and as particles lose contact with the wall, fluctuations in the stress are created. If too few particles are present, the contribution of each particle is a high percentage of the total, thus resulting in an abrupt fluctuation. A smoothing effect was seen in the trial run wherein the width of the domain and the number of particles were both increased by a factor of three. The second possibility is due to the stress networks in the medium building and collapsing as the wall shears. Walton[9] found fluctuations of ±25% for large particles, with the fluctuations being directly proportional to the size of the particle. The cluster particles seem to have a smaller fluctuation than the non-clustered particles, though not by a significant amount. This would conform to Walton's observation, since the mass and area of the individual particles in the clusters are smaller than those of the non-clustered particles.

Figure 3-8 shows that the shear stress versus horizontal displacement response of the cluster particle sets generated by displacing the sawtooth wall appear to have the same shape as would be expected for a medium packed sand of rounded sand grains (peak shear stress is the same or slightly higher than the steady-state (residual) shear stress)[19]. The noncluster sets have plots that are also similar in shape to the cluster sets but the shear stresses are somewhat lower than those of the cluster sets. The ratio of the maximum shear stress to normal stress can be viewed as the tangent of overall interface friction angle. The values obtained in the DEM analyses gave interface friction angles for the clustered sets comparable to those that would be expected between a well rounded, medium packed sand and a rough surface (~ 36°)[20]; however, the values for the nonclustered sets were lower (see Figure 3-10). A problem associated with DEM models that use non-clustered discs to model particles is that the maximum shear stress to normal stress ratios of the modeled particle assembly is lower than what it should be, due to the excessive rotation of the particles[12]. The comparison of clustered and nonclustered sets herein support this explanation.

An important observation about the relation of shear stress to surface roughness can be seen from Figure 3-8. The peak shear stress of the clustered particle sets, λ=4D, λ=2D, and λ=0.5D, are essentially the same. Whereas, the peak shear stress of the clustered particle set, λ=0, is substantially less. If the roughness of the shearing surface is such that the particles can become engaged with the surface, the shear strength of the particle mass is determined by the shear strength of the interface region and the mechanism of particles

---

[19] B.M. Das, *Advanced Soil Mechanics,* Hemisphere Publishing Corp., New York, (1983).

[20] Y.B. Acar, H.T. Durgunogly, and M.T. Tumay, 'Interface properties of sand', *J. geotech engrg. div.,* ASCE, **108**, 379-398 (1982).

sliding over each other and pushing each other out of the way. If the shearing surface is so smooth that the particles can not engage at all, the shear strength is reduced to a simple frictional sliding problem between the particle mass and the smooth surface.

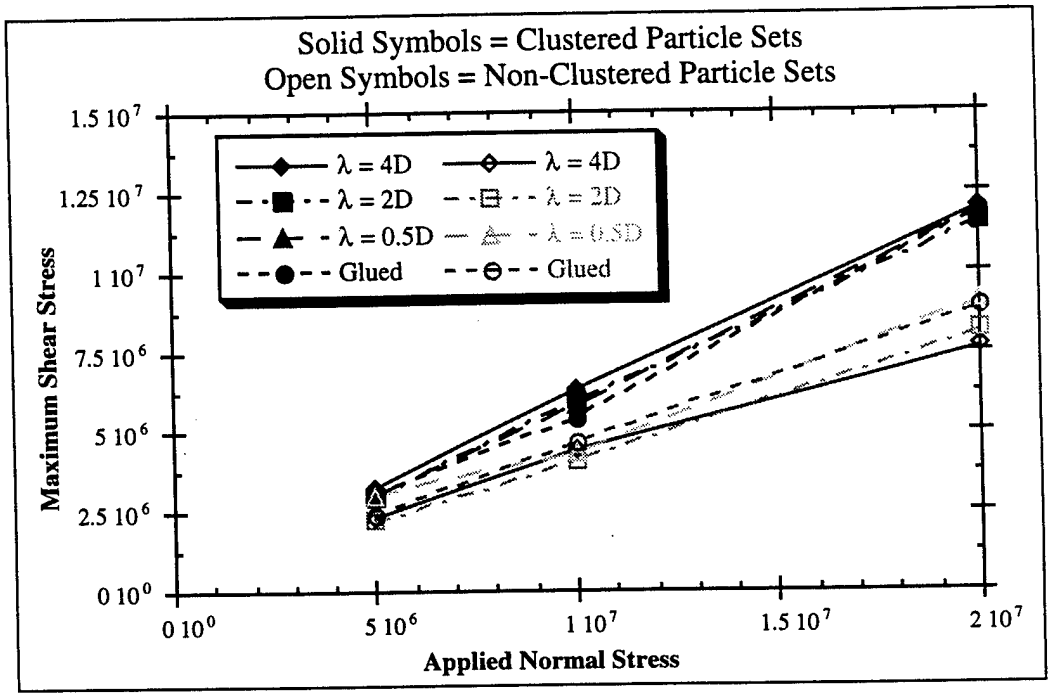

Figure 3-10 Graph of Maximum Shear Stress vs. the Applied Normal Stress. For each data set, the maximum value of shear stress that was reached during shearing is plotted versus the applied normal stress.

The dilation plots in Figure 3-8 indicate that the clustered particle sets have the same characteristics as a medium to densely packed sand. This is consistent with the corresponding shear stress plots. The dilation plots for the non-clustered particle sets are not as uniform or consistent. In all of the non-clustered particle sets, when the shearing begins, it acts as if it is a dense pack, initially compacting with subsequent dilation. Then, after a short period of dilation, it begins to compact again with varying amounts of compression and dilation. This effect could be caused by the high rotations present in the interface zone. Since the non-clustered sets have no interparticle locking, they will have a tendency to pack as densely as possible, with interparticle friction allowing for some dislocations. However, as the particles rotate, the rotations allow for the particles to overcome the interparticle friction and compact even more densely, after an initial period of dilation. As mentioned, dilation decreases after reaching a peak value in some of the non-cluster particle sets. Such a behavior is not observed in the any of the clustered sets. For realistic DEM simulations of granular materials, this observation points out the importance of inclusion of interlocking features. Even though clusters are an improvement in realistic modeling of granular soils, improvements are needed relative to differentiating the effects of normal stress on dilation. The authors are endeavoring to resolve this by adding new features to the DEM code (e.g. grain crushing).

The depth versus average displacement plots in Figure 3-9 did not show a very definite interface zone for the clustered particle sets. While not linear, the curves indicate a fairly uniform change of displacement as the distance from the shearing surface increases. For the noncluster particle sets, there was a very definite zone of localized displacement. The difference between the cluster and the noncluster cases may be due to the high rotations in the noncluster medium. The formation of shear bands seems to relate closely to the particles freedom to rotate. The particles may be acting similar to roller bearings, allowing the larger mass of the specimen to displace much less than the shearing surface. It appears that the cluster particles are excessively interlocked such that minimal rotations occur. Thus, a well-defined shear band, as seen in the non-clustered particles, is not evident. To lend support to this explanation, a series of simulations were performed in which the rotations of non-clustered particles were severely restricted. A definite trend was observed that decreasing freedom to rotate causes more uniform distribution of displacements throughout the mass resulting in the lack of a distinct zone of relative displacement. The lack of a distinct zone of relative displacement in the cluster particle sets, may indicate that at the interface, the particle rotation is more important than the relative particle displacement.

The plots of the depth versus average particle rotation and the plots of depth versus average particle horizontal displacement seen in the montage of Figure 3-9 shows how the clustered particles reacted differently than the non-clustered particles. For all cases, a zone of higher particle rotation is evident. However, the average noncluster particle rotation is nearly two times greater than the cluster rotation. This would seem to indicate that the clusters do in fact reduce the average particle rotation in DEM simulations. This is also confirmed by Figure 3-11, which shows the maximum average rotation plotted as a function of the applied normal stress. In all cases, the non-clustered particles had a higher average rotation than the clustered particles. Another item of note is that the rotations, in the simulations where the shearing surface is rough, λ=4D and λ=2D, are smaller in the layer adjacent to the surface than in the layer second from the surface. This is in contrast to the simulations with the smoothest shearing surfaces, λ=0.5D and λ=0D, in which the highest rotations in the layer are directly adjacent to the shearing surface. This can be explained by the particles in contact with the rougher surfaces being able to be fully engaged with the wall and thereby have their rotations subsequently reduced. In the case of the smoother shearing surface, the particles are larger than the sawtooth, therefore individual particles adjacent to the smooth surface are subject to less constraint than in the former case. This same phenomenon was seen by Tejchman and Wu[21] in the results of their finite element implementation of a Cosserat medium. They found that when they were modeling a sand-steel interface using Cosserat elements, the plots of the Cosserat rotation versus the height of the specimen for dense sand showed a very localized region of rotation. In addition, their two cases of the dense sand contacting a) a very rough plate and b) a moderately rough plate, were qualitatively identical to the plots of the non-clustered particles with a "rough" and "smooth" shearing surface.

A related observation from Figure 3-9 shows the influence that the degree of roughness of the shearing surface has on the location of the layer with the maximum average particle rotation. As the shearing surface becomes increasingly rougher, the layer of maximum average particle rotation moves farther from the shearing surface.

---

[21] J. Tejchman and W. Wu, 'Experimental and numerical study of sand-steel interfaces', *Int. j. numer. analytic. meth. geomech.*, **19**, 513-536 (1995).

Figure 3-10 is a plot of the maximum shearing stress obtained during a shearing event versus the applied normal stress. This figure shows that the peak shear stress of the clustered particles is markedly higher than that of the non-clustered particles. A probable explanation for this is that due to the increased natural resistance to rolling of the clustered particles, as a result of their triangle profile, they are interlocking and forcing more particles to frictionally slide thereby increasing the resistance to shearing. This is supported by Figure 3-11, which is a graph of the maximum average particle rotation (as obtained from Figure 3-9) versus the applied normal force. This figure shows that the maximum average rotation in all of the non-clustered runs is markedly higher than that for the clustered runs. Therefore, it can be seen that an increase in shearing stress is accompanied by a decrease in the rotations of the particles.

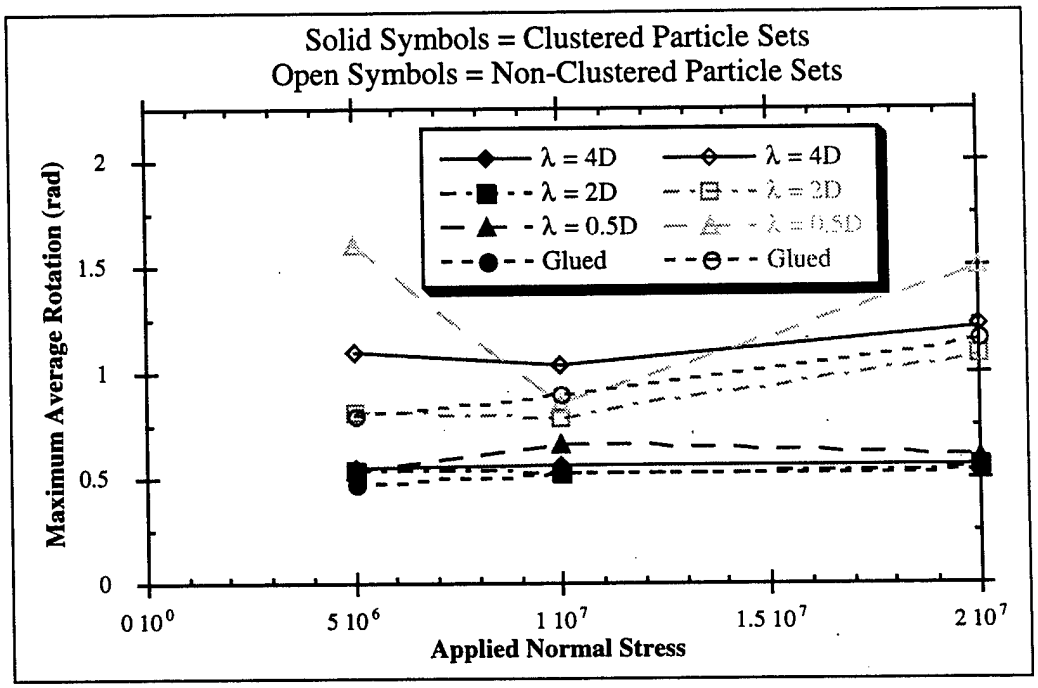

Figure 3-11 Graph of Maximum Average Rotation vs. Applied Normal Stress. For each data set, the maximum average particle rotation of any layer of the set is plotted versus the applied normal stress of the set.

3.6 CONCLUSIONS

An enhancement to the discrete element method for modeling particulate media has been presented. It has been shown that particles of general shape are effectively modeled by combining several smaller circular particles into a cluster that acts as a single larger particle. The creation of clusters can be done within the framework of existing DEM programs and without the need for new contact detection or force algorithms.

Numerical "experiments" simulating ring shear tests were performed comparing the cluster particles to non-clustered particles. The "experiments" were conducted with varying normal loads, roughness of the shearing surface, and particle types (clusters versus non-clustered).

Periodic boundaries were used in order to increase the computing efficiency and to remove any deleterious boundary effects. The simulations clearly demonstrated that the particle rotations were significantly reduced when cluster particles were used as compared to the non-clustered particles. As a result, the shear strength of the cluster particle assembly is increased when compared to the non-clustered particle assembly.

Overall behavior of the mass is qualitatively similar to those observed in experiments involving sands with round and angular particles. DEM revealed an intimate and detailed view of response at the particle level. In particular, the DEM simulations can be computer animated allowing enhanced visualization of all aspects of the particulate medium behavior.

Another feature of clustering is the opportunity to incorporate particle damage such as grain crushing, wear of roughness, etc. for more realistic simulation of particle medium.

4. Section Four, Constitutive Interface Modeling

4.1 Introduction

Determining an accurate means of characterizing the interaction between a structure and soil has been a goal of researchers for quite some time. Improvements in safety as well as economics are the result of more descriptive and reliable models. There is evidence that localized slip zones develop in soils along contact surfaces between soil and structures. These slip zones are characterized as being very narrow and typically have large relative deformations (Chen and Schreyer, 1987). It is the behavior of the slip zone that governs load transfer between a soil and a structure. In order to effectively use numerical models on particulate media - structure systems that involve large localized strains, accurate constitutive laws for the interface behavior are needed.

This paper reports the development of a new constitutive law that is based on micromechanical features such as particle diameter and number of particles that are active in the interface slip zone. The results of the new relationship are then compared to the results of physical tests and a numerical simulation that was performed by others.

4.2 Constitutive Model

The constitutive model is based on a two-dimensional contact problem. This approach was originally developed by Plesha (1987) for modeling the dilatancy and surface degradation behavior of geologic discontinuities. This model incorporates both macroscopic as well as microscopic features of the contact surface. It is adapted here for modeling the interface behavior of a particulate media - structure interaction problem.

4.2.1 Basis of Constitutive Equation

A general relationship can be developed based upon the macroscopic features of an interface and is applicable to a wide range of contact friction problems. The model is based upon two bodies in contact. For particulate media - structure interfaces, this contact region is defined as having two principal characteristics. The first is that the interface is thin, generally only several particle diameters wide. The second feature is that the particles in the zone undergo large relative displacements with respect to the particle mass. Outside of the interface region, displacements are more homogeneously distributed. The basis of the contact-friction problem is the displacement relationship between two bodies, body A and body B. As can be seen in Figure 4-1A, the interface region separates the particulate media (region B) from the surface of the structure (region A). Depending on characteristics such as particle size and shape, boundary stress, and structural surface roughness, the number of particles in the interface zone will vary. The interface region can be idealized as seen in Figure 4-1B. The displacement of the interface region can be determined by the change in position of body B with respect to body A in both the normal as well as the tangential direction, as defined by the unit vectors in the idealized interface.

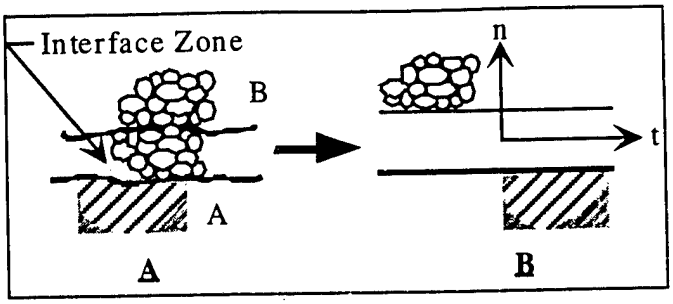

Figure 4-1. Idealization of Interface

The displacements at the interface can be characterized as elastic, or recoverable, deformation and plastic, or non-recoverable, deformation. Mathematically it is expressed

$$dg_i = dg_i^e + dg_i^p \qquad (1)$$

where the subscript i denotes tangential or normal displacement and the super scripts e and p indicate elastic or plastic deformation. The elastic deformations are accompanied by a change in stress, and the plastic deformations are due to permanent sliding and dilation within the interface zone. Using this formulation for the displacements, in conjunction with the ideas of non-associative plasticity, an incremental constitutive relationship can be found (see Jensen, 1998). It has the form of

$$d\sigma = \mathbf{E}^{ep} d\mathbf{g} \qquad (2)$$

where

$$\mathbf{E}^{ep} = \mathbf{E} \qquad \text{if } F<0 \text{ or } dF<0 \qquad (3)$$

$$\mathbf{E}^{ep} = \mathbf{E}\left[\mathbf{I} - \frac{\dfrac{\partial G}{\partial \sigma}\left(\dfrac{\partial F^T}{\partial \sigma}\mathbf{E} + \dfrac{\partial F}{\partial \alpha}\dfrac{\partial \alpha^T}{\partial \mathbf{g}}\right)}{\dfrac{\partial F^T}{\partial \sigma}\mathbf{E}\dfrac{\partial G}{\partial \sigma}}\right] \qquad \text{if } F = dF = 0$$

and where $F(\sigma,\alpha)$ is the slip function, $G(\sigma,\alpha)$ is the slip potential, σ is stress, g is relative displacement, E is the interface stiffness, and α is the orientation of interface particles (see description in the following section). This equation is applicable to a variety of contact problems, provided appropriate definitions of G and F are developed. Plesha (1987) discusses these for rock joints. In this work, appropriate expressions for soil-structure interfaces are developed. The next section discusses the physical (microstructural) model used and the slip function and slip potential which were derived.

4.2.2 Physical (Microstructural) Model

Constitutive laws differ by how well the slip function and slip potential are able to reflect the actual mechanical processes in the interface region. The success of deriving a constitutive law hinges on developing accurate and meaningful slip functions and slip potentials.

Numerical methods such as the discrete element method (DEM) and experimental methods such as video imaging of the interface, enables us to focus energy on the most influential characteristics. Through viewing video imaging (Ligler, 1997) and animations made from DEM simulations reported by Jensen *et al*. (1998), it was seen that particles form "chains" or stacks of particles that rotate as the shearing takes place. Particles forming chains, especially force chains, is a phenomena which has been observed by others (Cundall,1978; Williams and Rege, 1996) in DEM simulations. Oda (1997) has also noted the formation of these chains. The rotation of these particles stacks serve as the foundation of our slip function.

To begin, it is assumed that all of the particles in the interface are of uniform size, shape, and material properties. It is assumed that the particles are in the densest packing arrangement, which for two dimensions is a face-centered packing arrangement. A diagonal chain of particles is isolated, forming a 30° angle with the vertical, as shown in Figure 2. At the densest packing, each particle has six contacts. As soon as shearing occurs, two of the contacts are broken, leaving each particle in the interface with four contacts. Through observation of DEM and experimental methods, it has been noted that the largest forces have a large vertical component.

A free body diagram of a stack of particles is shown in Figure 2. As can be seen, the particles in the interface region have a self-equilibrating force f_{2n}. The interparticle tangential force, f_{2t} is related to f_{2n} by an interparticle coefficient of friction, μ_p. Based on our observations of many DEM simulations, we assume that the particles in the chain will rotate rigidly from the angle α until it reaches the vertical position. Observations from video imaging also supports the rotating chain model. In order for the chain to rotate, the contacts between the particles in the chain must not slip and the contacts associated with f_{2t} and f_{2n} will slip.

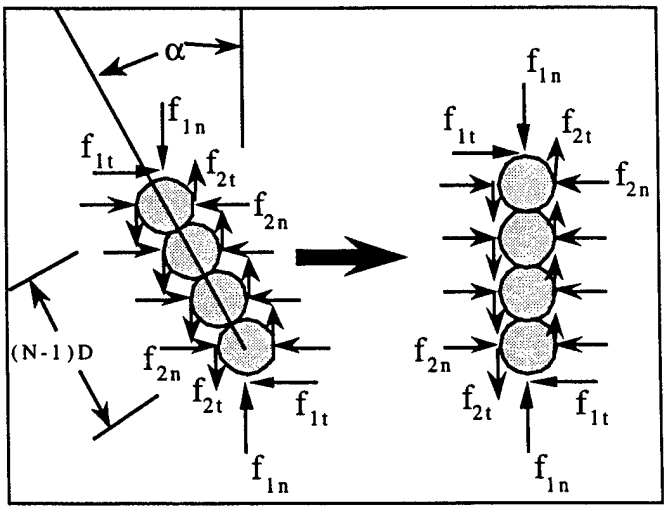

Figure 4-2 Isolated chain of particles. Forces shown are applied to the particle chain as it rotates from its initial position to the vertical position.

By considering the force and moment equilibrium of the particles shown in Figure 2, a relationship between f_{1n} and f_{1t} can be found (Jensen, 1998) such that

$$f_{1t} = \beta f_{1n} \qquad \text{where} \qquad \beta = \frac{(N-1)D\sin\alpha + ND\mu_p\kappa}{D[1+(N-1)D\cos\alpha]} \qquad (4)$$

and N is the number of particles in the chain, D is the particle diameter, μ_p is the interparticle friction coefficient, and κ is the ratio of the interparticle horizontal to the friction force in the interface region. The parameter β is somewhat analogous to a variable friction coefficient. This relationship is obtained when the lateral force (or pressure) in the interface region is related to the overall vertical force (or pressure) by

$$f_{2n} = \kappa f_{1n} \qquad (5)$$

The formulation of this relationship between the applied vertical stress in a mass to the lateral stress in the interface is the contributory portion of this paper. Its introduction is unique to our model. We are not aware of its use by any other researchers. At this time, the form that κ should have is not well understood. More work needs to be done to better characterize and understand its form and impact on interface behavior. Its presence seems to be demanded by physics and its values are related to the stress tensor supported by the soil, which is unknown. There is little reason to think it is a constant. It is most likely not a constant, but changes with deformation. In one simulation that gave good results, and will be reported later in this paper, κ was a function of α. However, the particular form of κ reported seems to be very specific to its application.

In determining the slip function and slip potential, the idea of a variable friction coefficient as given by equation **(4)** is used. The form of the slip function is similar to that of simple Coulomb friction except instead of μ_p, the parameter β is used. The slip function and slip potential are

$$F = |\sigma_t| + \beta\sigma_n \qquad \text{and} \qquad G = |s_n \sin\alpha + s_t \cos\alpha| \qquad (6)$$

By combining equations **(2)** and **(3)** with **(6)**, a constitutive equation relating increments stress to increments of relative displacement is obtained. The elastic-plastic stiffness, $\mathbf{E}^{ep}$, is non-linear and history-dependent.

4.3 Constitutive Law Performance

Paikowsky *et al.* (1998) performed a simple shear test of 2-D photoelastic discs and compared the results to that of a DEM simulation of the test. Using the dimensions and material properties used in the physical test and the DEM simulation of the test, an analytical solution was found using the constitutive relationship discussed previously. By taking the horizontal stress coefficient, κ, to be

$$\kappa = \kappa_o \sin\alpha \qquad (7)$$

remarkably close agreement was found to the physical test and numerical model. Figure 3 is the plot of shear force versus solid surface displacement of the physical test and DEM simulation. Superimposed over the top of these plots are the results from the analytical model. As can be seen from this figure, the analytical model closely replicated the behavior observed in the physical test as well as the DEM simulation. The plots of the vertical displacement versus solid surface displacement similarly showed close agreement between the physical test and the DEM simulation done by Paikowsky et al. (1998) and the analytical model (Jensen, 1998).

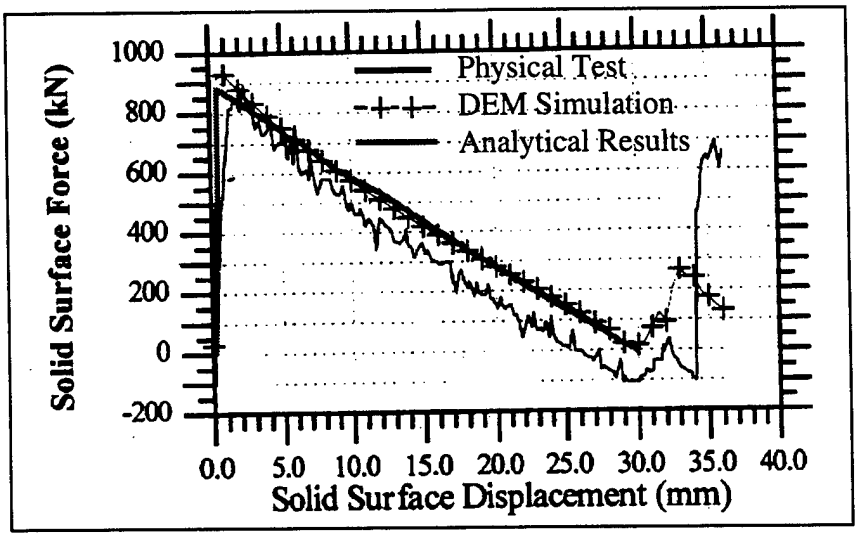

Figure 4-3 Graph of Shear Force vs. Shear Displacement of physical test and numerical simulation performed by Paikowsky et al. (1998). The results of the constitutive equation is superimposed on top of the graph.

4.4 Conclusion

A constitutive law for describing the interface behavior of a particulate media - structure interface has been presented. Macroscopically, the law is based on the idea that deformations at the interface are comprised of recoverable, or elastic, deformation and non-recoverable, or plastic, deformation. The changes in stress are associated with the recoverable deformation while frictional sliding and dilation are associated with the non-recoverable deformation. The microscopic features of the relationship are based upon the formation of chains of particles that rigidly rotate when shearing takes place. The other important feature of this relationship that has a large impact on interface behavior, is the introduction of a new variable, κ, that relates the vertical stress in a particulate media to the lateral stress in the interface region. The microstructural features that are captured by this constitutive relationship are particle size, shear zone thickness, dilation, and shear stress.

An example is presented. The example is a comparison of the results of the analytical model to the results of a physical test and DEM simulation performed by Paikowsky *et al.* (1998). The comparison showed that the analytical model replicates the behavior of the physical test and the DEM simulation remarkably well.

4.5 *Bibliography*

1987 Chen, Z. and H.L. Schreyer, "Simulation of Soil-Concrete Interfaces with Nonlocal Constitutive Models," J. eng. mech., 113, 1665-1677.

1978 Cundall, P. A. and Strack, O. D. L., The Distinct Element Method as a Tool for Research in Granular Media PART I, NSF Report Grant ENG76-20711.

1998 Jensen, R.P., Numerical and Analytical Modeling of the Microstructural Behavior of a Particulate Media-Structure Interface, Ph.D. Thesis, University of Wisconsin-Madison.

1998 Jensen, R. P., P. J. Bosscher, M. E. Plesha, and T. B. Edil, "DEM Simulation of Granular Media - Structure Interface: Effects of Surface Roughness and Particle Shape," Int. j. numer. anal. methods geomech., accepted for publication.

1997 Ligler, K., Soil/Structure Interaction in Direct Shear, Master's Thesis, University of Wisconsin-Madison.

1997 Oda, M., "A Micro Deformation Model for Dilatancy of Granular Materials," in Mechanics of Deformation and Flow of Particulate Materials, C. S. Chang et al., editors, published by ASCE.

1998 Paikowsky, S. G., J. M. Ting, F. Xi, and G. Mischel, "Numerical and Experimental Comparison of Shear Along Granular Material/Solid Interface," Int. j. numer. anal. methods geomech., accepted for publication..

1987 Plesha, M. E., "Constitutive Models for Rock Discontinuities with Dilatancy and Surface Degradation," Int. j. numer. anal. methods geomech., 11, 345-362.

1997 Williams, J. R. and N. Rege, "The Development of Circulation Cell Structures in Granular Materials Undergoing Compression," Powder technol., 90, 187-194.

5. Summary and Conclusions

The interface shear zone of a granular soil against a structural surface was successfully imaged, subsequently analyzed and finally modeled. The following conclusions result from this effort:

1. For simulated shallow and deep soil elements (constant stress and constant volume tests) the only factor that is significant to the interface shear zone behavior is the roughness of the structural surface. This effect is most pronounced when the surface being used is very smooth. The addition of even small ridges on this surface dramatically magnifies the measured response.
2. For a simulated shallow soil element (constant stress test), the factors that are significant to the strength response behavior of the soil are the normal load, surface roughness, and a combination of both.
3. For a simulated deep soil element (constant volume test), the factor that is significant to the strength response behavior of the soil is the surface roughness.

An enhancement to the discrete element method for modeling particulate media has been presented. It has been shown that particles of general shape are effectively modeled by combining several smaller circular particles into a cluster that acts as a single larger particle. The creation of clusters can be done within the framework of existing DEM programs and without the need for new contact detection or force algorithms.

Numerical "experiments" simulating ring shear tests were performed comparing the cluster particles to non-clustered particles. The "experiments" were conducted with varying normal loads, roughness of the shearing surface, and particle types (clusters versus non-clustered). Periodic boundaries were used in order to increase the computing efficiency and to remove any deleterious boundary effects. The simulations clearly demonstrated that the particle rotations were significantly reduced when cluster particles were used as compared to the non-clustered particles. As a result, the shear strength of the cluster particle assembly is increased when compared to the non-clustered particle assembly.

Overall behavior of the mass is qualitatively similar to those observed in experiments involving sands with round and angular particles. DEM revealed an intimate and detailed view of response at the particle level. In particular, the DEM simulations can be computer animated allowing enhanced visualization of all aspects of the particulate medium behavior.

Another feature of clustering is the opportunity to incorporate particle damage such as grain crushing, wear of roughness, etc. for more realistic simulation of particle medium.

A constitutive law for describing the interface behavior of a particulate media - structure interface has also been presented. Macroscopically, the law is based on the idea that deformations at the interface are comprised of recoverable, or elastic, deformation and non-recoverable, or plastic, deformation. The changes in stress are associated with the recoverable deformation while frictional sliding and dilation are associated with the non-recoverable deformation. The microscopic features of the relationship are based upon the formation of chains of particles that rigidly rotate when shearing takes place. The other important feature of this relationship that has a large impact on interface behavior, is the introduction of a new variable, κ, that relates the vertical stress in a particulate media to the

lateral stress in the interface region. The microstructural features that are captured by this constitutive relationship are particle size, shear zone thickness, dilation, and shear stress.